Investigation of local brain invasion by cerebral metastases and implications for clinical management

Thesis submitted in accordance with the
requirements of the University of Liverpool for the
degree of Doctor in Philosophy

by

Rasheed Zakaria MA, BM, BCh

May 2016

Table of Contents

Acknowledgments

The work presented in this thesis was funded by the Walton Centre NHS Foundation Trust, the Medical Research Council (UK) and the Royal College of Surgeons of England. I am grateful to Mr Michael Jenkinson, one of my co-supervisors, and Dr Carol Walker for formulating the initial post which enabled the project to start and their continued support and advice. The clinical neuroradiologists at the Walton Centre, Dr Kumar Das, Dr Mark Radon and Dr Maneesh Bhojak have provided invaluable assistance with MRI studies and interpretation, and the radiographers have been extremely tolerant in accommodating me during busy clinical schedules and allowing me to use hardware and software in the department. Dr Vanessa Sluming generously agreed to supervise MRI aspects despite not knowing what my needs and experience were and I hope we have both learnt a great deal in the process. The neuropathology department have been most helpful, Dr Daniel Crooks and Dr Nitika Rathi for their second opinions and expertise, Mr Syed Khaja and colleagues for their handling of clinical samples and support of the tissue bank. For laboratory work I am most grateful to Angela Platt-Higgins for her invaluable expertise in immunohistochemistry and my primary supervisor Professor Philip Rudland for experience, guidance, proof reading and good humour. In the neurosurgical department, Mr Andrew Brodbelt, Mr David Lawson, Mr Emmanuel Chavredakis and Professor Paul Eldridge are thanked for their patience in the operating theatre amidst busy lists. I am of course indebted to the many patients who contributed tumour samples to the programme over the years, without which no research would be possible.

This thesis is dedicated to my late father Dr Hisham Zakaria – an excellent scientist and successful engineer who always felt his time in research was the most rewarding period of his life.

Abstract

Brain metastases are common intracranial tumours which cause considerable morbidity and mortality. There are a variety of treatment modalities for brain metastases, including surgery, radiation and chemotherapy. There is, however, disagreement about the best combination of these therapies and prognostic scoring systems are not individualised. MRI is frequently obtained in the course of diagnosing these tumours and advanced MRI sequences, in particular diffusion MRI, which measures white matter disruption, may provide useful prognostic information which is patient and tumour specific. Finally, the interface between the brain metastasis and the surrounding brain has been poorly investigated compared to intrinsic brain tumours such as glioma, and may be a rich source of therapeutic targets and biomarkers. This thesis therefore aimed to derive biological and radiological markers of local brain metastasis invasion, intracranial progression and survival which may be used in clinical practice, whilst deepening scientific understanding of the brain-brain metastasis interface.

Expression of the metastasis-inducing protein S100A4 was identified as a possible predictor of metastasis recurrence post operatively and OPN as a possible marker of radiation response. Using diffusion MRI, the change in the change in the apparent diffusion coefficient (ADC) across the brain-brain metastasis boundary was found to be a reliable, repeatable measure on clinically obtained scans and independently associated with overall survival for operated brain metastases. Finally, using combined image-guided neurosurgical samples and diffusion tensor imaging, we have shown that the FA in the peritumoural region is a surrogate marker of the density of T cell infiltration there and that both increased CD3+ T cell infiltration and reduced FA (corresponding to more white matter tract disruption) are associated with prolonged overall survival after macroscopic resection.

These studies highlight the importance of studying the brain-brain metastasis interface both radiologically and biologically whilst offering truly novel avenues for further study in the field, including imaging, tissue biomarkers and potential therapeutic targets.

List of tables

List of figures

Abbreviations used

ADC	apparent diffusion coefficient
AGR2	anterior gradient protein 2
CBF	cerebral blood flow
CT	computed tomography
DSC	dynamic susceptibility contrast
DTI	diffusion tensor imaging
DWI	diffusion weighted imaging
ECM	extracellular matrix
EGFR	epidermal growth factor receptor
EMA	epithelial membrane antigen
EORTC	European Organization for Research and Treatment of Cancer
FA	fractional anisotropy
FLAIR	fluid attenuated inversion recovery
fMRI	functional magnetic resonance imaging
GPA	graded prognostic assessment
Gy	gray (unit)
HER2	human epidermal growth factor receptor 2
MD	mean diffusivity
MDT	multidisciplinary team

MRI	magnetic resonance imaging
MRS	magnetic resonance spectroscopy
NICE	National Institute of Clinical Excellence
OPN	osteopontin
OS	overall survival
PFS	progression free survival
RANO	Revised Assessment in Neuro-Oncology
rCBV	relative cerebral blood volume
ROI	region of interest
RPA	recursive partitioning analysis
RTOG	Radiation Therapy Oncology Group
SRS	stereotactic radiosurgery
TTF-1	thyroid transcription factor 1
WBRT	whole brain radiotherapy

Chapter 1: An introduction to cerebral metastases

Cerebral metastases are secondary brain tumours which have spread from an extracranial, primary cancer. Herein - as with the wider medical literature – "cancer" is taken to mean a solid organ primary cancer, thus excluding haematological malignancy such as lymphoma. The term brain metastasis is used interchangeably with cerebral metastasis.

1.1 Epidemiology

Cerebral metastases are common intracranial tumours, but estimates of incidence are inconsistent due to the variety of different sources of information. In the general population, studies from Europe and North America consistently find incidence rates of between 7 and 14 per 100,000 (Fox et al., 2011). By comparison, recent figures for other common brain tumours are 4.6 per 100,000 for glioblastoma (the most common primary malignant brain tumour) and 7.6 per 100,000 for meningioma (a generally benign tumour of the brain envelope or meninges) (Brodbelt et al., 2015, Ostrom et al., 2014). This population data encompasses the risks of cancer, however, since one cannot develop a brain metastasis without having a primary cancer, known or unknown (Barnholtz-Sloan et al., 2004). Hence studies in the "at risk" population of patients with a known solid organ cancer may be more useful. In such groups, the incidence of brain metastasis has been reported as high as 1 in 4 (25%) at post mortem (Posner and Chernik, 1978). Such rates are not seen in clinical practice, however, and in fact around 1 in 20 (6%) of newly diagnosed patients with cancer in a given year would be expected to develop a brain metastasis (Davis et al., 2012). This means the longer patients survive with their primary cancer, the greater the incidence of brain metastases should be; accordingly, improved imaging availability and better systemic treatments have coincided with increased numbers of these tumours, as **Figure 1.1** illustrates, and an increase in their scientific investigation (Owonikoko et al., 2014).

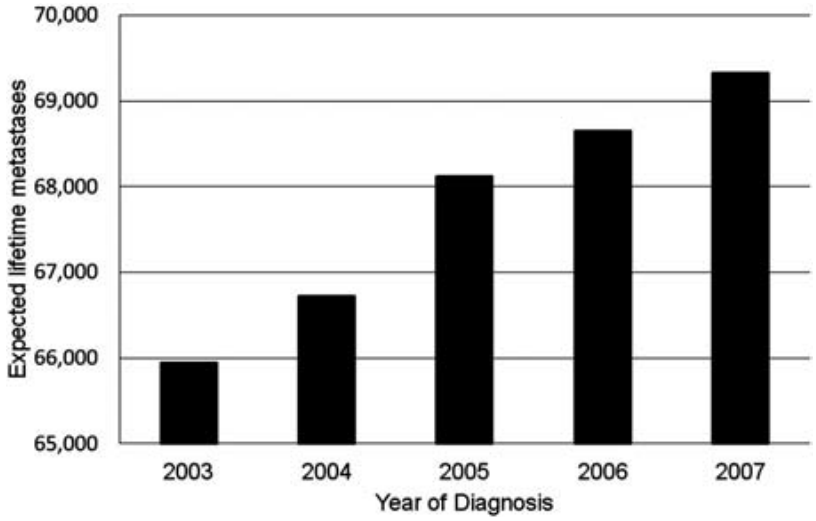

Figure 1.1: Bar chart showing the estimated lifetime metastases of the brain for selected primary cancer sites, by individual year of diagnosis in the United States, 2003– 2007 (Davis et al., 2012).

1.2 Aetiology

In keeping with Paget's seed and soil hypothesis of cancer spread (Paget, 1889), it has always been known that particular cancers (seed) have a higher than expected incidence of metastasis to the brain (soil). The most common sites of primary cancer for brain metastases are shown in **Figure 1.2 (**based on raw data from (Nussbaum et al., 1996)).

The processes by which tumour cells escape their primary site of origin, enter the circulation, survive there and finally seek out and populate a new site is extensively studied and referred to as the ***metastatic cascade*** (Winkler, 2015, Beasley and Toms, 2011, Svokos et al., 2014, Preusser et al., 2012, Rahmathulla et al., 2012). A number of steps comprise this cascade including:

- Proliferation and cellular heterogeneity in the primary site
- Epithelial-mesenchymal transition
- Interaction with tumour stroma
- Local invasion
- Migration
- Enter and exit the circulatory system
- Colonisation of the host site

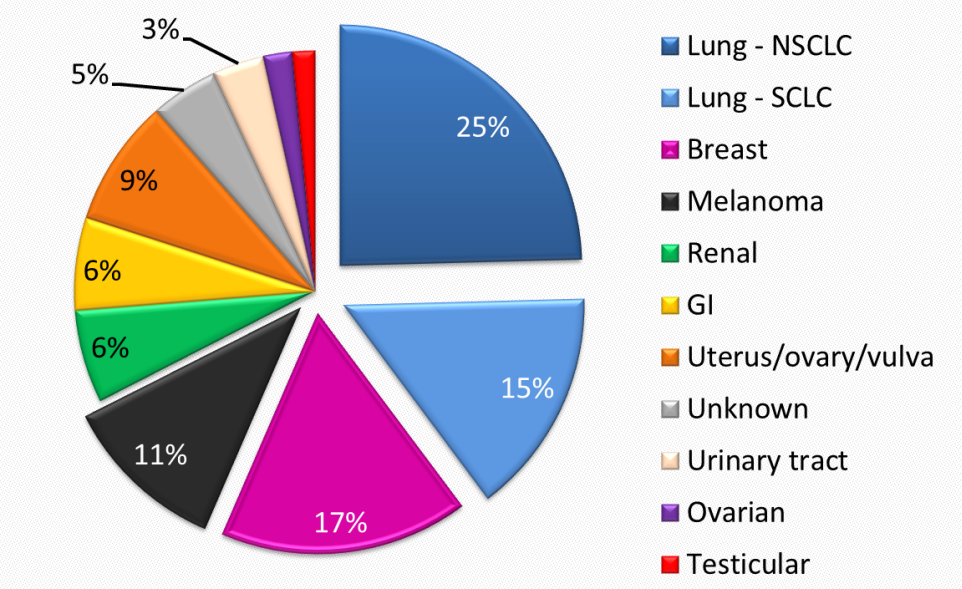

Figure 1.2: Summary of primary solid organ cancers causing metastasis to brain reproduced as a pie chart from an original series of 729 cases gathered over a 20 year period (Nussbaum et al., 1996). The exploded slices show that three sites – lung, breast and skin – account for the majority of cases. NSCLC = non-small cell lung cancer. SCLC = small cell lung cancer, GI = gastrointestinal tract.

Specific to brain metastases is the requirement to cross the blood brain barrier and survive in the unique microenvironment of the central nervous system. This process is now increasingly thought to rely on cell adhesion molecules (CAM) (Soto et al., 2014) with a process similar to inflammatory cell "rolling" adhesion and migration. Once across the blood brain barrier, metastatic cells occupy a niche in the perivascular region and either spread along this plane as described in **Section 1.3.2 Microscopic pathology** or induce angiogenesis to enable their continued growth (Kienast et al., 2010).

1.3 Pathology

1.3.1 Macroscopic

Brain metastases occur at areas of high cerebral blood flow because they derive from tumour cells carried in the circulation from the primary site. This explains historic observations that some 80% are distributed in the hemispheres, 15% in the cerebellum and 5% in the brainstem/basal ganglia and this has not been disproven by newer imaging modalities (Delattre et al., 1988, Fink and Fink, 2013). These tumours appear as solid, firm lesions at the grey-white matter interface (where narrow, branching blood vessels lead to tumour cell arrest and adhesion) with occasional

haemorrhage, especially in melanoma, renal cell and thyroid cancer types. They tend to be surrounded by intense vasogenic oedema. Around 1/3 are solitary (Norden et al., 2005) and the remainder oligo- or polymetastatic (the cut-off between these two arbitrarily taken to be 4 or 5 distinct lesions depending on the study). Metastases vary in size from what is termed "unmeasurable disease" of <5mm diameter to very large tumours and at present response is assessed using diameter, as if tumours were a perfect sphere (Lin et al., 2015). Whilst volume may be a useful measure of response in future, it is likely the *total* volume of disease (i.e. all the lesions in the brain) is more important (Kondziolka et al., 2014), although harder to measure in real time.

1.3.2 Microscopic: the brain-brain metastasis interface

Microscopically brain metastases tend to show characteristics of the primary cancer including architecture, such as mucin secreting glands. However, in cases of poorly differentiated metastases, staining for glial markers such as glial fibrillary acidic protein (GFAP), OLIG2, and SOX2 may be performed to help distinguish from glioma (Pekmezci and Perry, 2013). Historically, metastases were always said to be clearly delineated from the surrounding brain and the microscopic presence of a pseudocapsule - illustrated in **Figure 1.3** – may explain the often recounted neurosurgical description that they shell out like a pea from a pod.

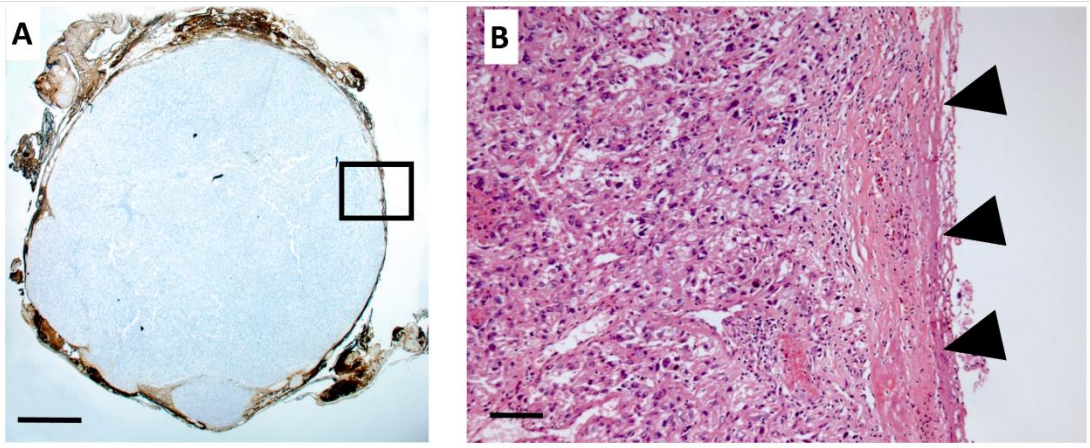

Figure 1.3: Photomicrographs of a renal cell carcinoma metastasis from the Walton Research Tissue Bank. Panel A. GFAP stain highlights the compressed glial component of the pseudocapsule around the resected tumour. 12.5x magnification, scale bar = 1mm. This is seen macroscopically by the operating neurosurgeon as a plane between tumour and brain. Panel B. shows this pseudocapsule at high power (arrowheads) with H&E staining, 200x magnification, scale bar = 50µm.

Recent evidence accumulated from post mortem and *in vivo* studies, however, has contradicted this understanding and the microscopic boundary between metastases and brain may be more complex than previously thought, with implications for both treatment and prognosis. A post mortem study of 57 cases within the Austrian brain tumour bank showed diffuse infiltration in around one third of cases with no association of growth pattern with a particular primary (Berghoff et al., 2013b). The remainder showed either well demarcated margins or co-opting of existing vessels in the peritumoural region, a well described growth pattern that has been observed in animal models (Carbonell et al., 2009) and in human studies (Pekmezci and Perry, 2013). A second autopsy study of 45 patients suggested fewer than half of metastases show a clear demarcation from brain, with 70% of lung cancer cases, particularly small cell lung cancers, showing infiltrative growth (Baumert et al., 2006). This association with lung cancer is well established with 26 of 66 cases of metastatic anaplastic small cell carcinoma showing poorly defined borders in an *in vivo* study, what the authors describe as a pseudogliomatous pattern (Neves et al., 2001). Finally, this infiltrative growth pattern has recently been shown to be associated with a worse prognosis compared to the well demarcated cases in a prospective series (Siam et al., 2015) receiving adjuvant treatments.

1.4 Symptoms and presentations

Common signs and symptoms follow from the pathological description above: almost half of patients present with seizures due to the location of metastases at the grey-white matter boundary and the remainder with headache and neurological compromise due to vasogenic oedema and compression of deep white matter tracts (Taillibert and Delattre, 2005). Synchronous presentation of metastases refers to patients with no previously identified primary cancer. Patients with no signs or symptoms of brain metastases are increasingly being screened by their oncologist; up to 15% of breast (Miller et al., 2003) and 40% of non-small cell lung cancer brain metastases may be asymptomatic yet detectable by conventional radiological studies (Ohana et al., 2014).

1.5 Investigation

1.5.1 Assessment

Patients are assessed with a thorough history - including of any prior cancer - followed by clinical examination, paying attention to neurological deficits and dysfunction as well as any extracranial signs of the primary tumour. Imaging is then used to assess both the brain and the extracranial disease. The primary cancer may be detected and staged by whole body CT scan (chest, abdomen and pelvis) or where available PET-CT.

1.5.2 The role of MRI

MRI is crucial in making the diagnosis, determining the best course of management, monitoring response to therapy and increasingly in trying to predict prognosis. Rather than reviewing each individual technique and its applications separately, as has been done elsewhere, the different clinical problems encountered in brain metastases are presented and the relevant MRI techniques which can be applied in each scenario addressed (Zakaria et al., 2014b).

1.5.2.1 How many brain metastases are present?

Accurately identifying the number, location and size of brain metastases is important to determine which interventions are most appropriate for that patient and multiple scoring systems which stratify outcomes of therapies take into account the number of lesions, for example, the Recursive Partitioning Analysis or RPA classification (Jenkinson et al., 2011, Nieder et al., 2009, Siu et al., 2011, Gaspar et al., 1997). With respect to detection, localisation and quantification, contrast enhanced MR has been widely demonstrated to be superior to both enhanced CT and non-enhanced MR (Yokoi et al., 1999, Schellinger et al., 1999, Kruger et al., 2011, Davis et al., 1991). The recommended gadolinium dose in this context is 0.1 mmol/kg and whilst double or triple dose administration has been suggested to increase the detection of small lesions, this causes increased false positives and a higher risk of nephrogenic systemic fibrosis, therefore it remains an “off label” use (Yuh et al., 1995, Sze et al., 1998, Schneider et al., 2001).

Could novel sequences and agents therefore increase detection without escalating the contrast dose? Different gadolinium based agents, all of which may have slightly differing relaxivity profiles, have been variously compared and these studies are summarised elsewhere, but at present gadobutrol appears to identify the greatest number of lesions with the greatest contrast to noise ratio, whilst having a lower risk of nephrogenic systemic fibrosis, along with the other "cyclic" structured gadolinium based agents (Anzalone et al., 2013). MR sequences are developing rapidly, but are not always explicitly evaluated against existing protocols. Magnetisation saturation transfer (MT) imaging has been directly compared to gradient echo T1 sequences and its addition reduced by half the standard dose of contrast needed for detection leading some to advocate it over ever increasing contrast doses (Ginsberg and Lang, 1998, Haba et al., 2001). More recently, 3D T1 weighted "spoiled gradient echo" (SPGR) and T2 weighted post contrast FLAIR sequences have been shown to detect sub-millimetre (<3mm) abnormalities and more sensitively assess leptomeningeal disease (Chen et al., 2012a, Kakeda et al., 2007).

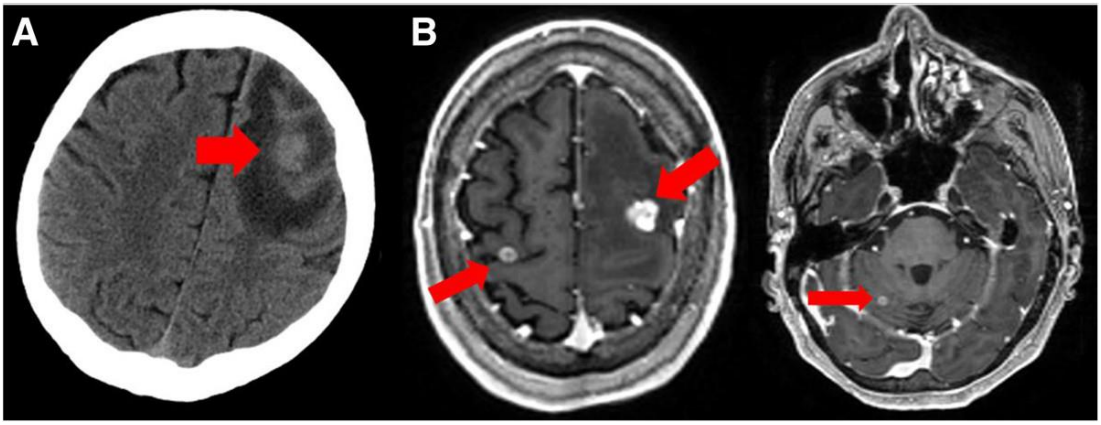

Figure 1.4: A patient known to have melanoma presents with a first seizure and (A) unenhanced CT brain (32-slice scanner, 10 mm slices) taken in the emergency department shows an abnormality in the left frontal lobe with surrounding oedema – they were referred for possible neurosurgical intervention. (B) T1 weighted MRI at 1.5 T with single dose (0.1 mmol/kg) gadolinium contrast detects this lesion but also delineates it further, allowing volume to be assessed accurately and in addition highlights two further areas of abnormality. After staging of the systemic disease and discussion with oncologists and surgeons, the patient was therefore treated with stereotactic radiosurgery to all three areas.

The spatial resolution of the acquisition differs depending on the indication for the scan and this has important implications for detection and management which need to be kept in mind. For example, if a treatment is decided upon with the multidisciplinary team and the patient but then a surgical or SRS "planning" scan of higher spatial resolution is obtained, the latter will be more sensitive for detection of metastases than a conventional diagnostic scan and multiple, previously unseen lesions may be identified which render that treatment inappropriate (Nagai et al., 2010).

1.5.2.2 Is this solitary lesion a metastasis, an abscess or a high grade glioma?

A patient presenting with no known primary cancer and a solitary ring enhancing brain lesion may be suspected to have a brain metastasis, a primary cerebral tumour such as glioblastoma or a cerebral abscess, and despite careful history and exam, misdiagnoses may still occur (Brodbelt, 2012). Distinguishing abscess from tumour is perhaps the most clinically relevant question and in this regard diffusion-weighted MRI (DWI) has been most useful. Diffusion-weighted images detect free water movement and allow a surrogate of diffusion to be calculated for each voxel to generate apparent diffusion coefficient (ADC) maps. A large number of observational studies have shown that for a solitary cystic or necrotic contrast enhancing lesion, restriction of diffusion on pre-operative MRI is predictive of abscess (Desprechins et al., 1999, Ebisu et al., 1996, Krabbe et al., 1997, Kim et al., 1998). Modifications to imaging protocols have increased sensitivity, including detection of early capsule formation during abscess development and even prediction of cellularity of abscesses at higher b-values and field strengths (Tomar et al., 2011, Fertikh et al., 2007). However, there are persistent cautions that some metastasis may show restricted diffusion and mimic the appearances of abscesses, for example two different studies have reported this for non-small cell lung carcinoma metastases and others have described it for lymphoma (Stadnik et al., 2001, Holtas et al., 2000, Duygulu et al., 2010, Hayashida et al., 2006).

Distinguishing metastases from high grade glioma has proven more difficult using DWI, although in theory the region of vasogenic oedema around metastases should show greater free diffusion than the more cellular, infiltrated region around a high

grade glioma. Studies have varied in their cut-off for distinguishing the two pathologies as well as the methodology of how to take the reading (does one use the lowest ADC value, the mean of multiple measurements and which areas should one sample in the peritumoural region?) and there is no agreement about reliability (Bulakbasi et al., 2005, Chiang et al., 2004, Lee et al., 2011, Wang et al., 2009, Calli et al., 2006). Diffusion tensor imaging (DTI) is an enhancement of DWI with more diffusion gradients and directions used during acquisition. This allows more advanced metrics than just the average diffusion coefficient to be calculated and disruption of white matter tracts to be visualised. Again, the theory that high grade glioma is an invasive tumour which infiltrates white matter tracts whereas a metastasis deforms them is supported, but not consistently repeated by studies examining DTI metrics such as fractional anisotropy and mean diffusivity which may be superior to ADC alone (Byrnes et al., 2011, Price and Gillard, 2011, Tsuchiya et al., 2005).

Further advanced techniques have therefore been combined with diffusion imaging in this context to try and increase sensitivity, most commonly MR spectroscopy (Bulakbasi et al., 2003). Single and multivoxel magnetic resonance spectroscopy (MRS) provides information about the metabolic profile of specific regions in and around a lesion (Pinker et al., 2012, van der Graaf, 2010). Proton MRS has previously shown discriminatory power between high grade glioma and metastasis by measurement of the choline/NAA ratio (Server et al., 2010, Wong et al., 2010). Novel spectroscopic markers continue to be investigated, including lipid and macromolecule concentrations by proton MRS (Crisi et al., 2013) and phosphate metabolites by 31P MRS (Ha et al., 2013).

Further information on physiological activity can be gathered by combining with MR perfusion studies. MRI perfusion permits the generation of maps of relative cerebral blood flow (rCBF) and volume (rCBV) which are measures of vascularity. High grade glioma pathologically shows neovascularisation and infiltration of surrounding brain, hence the peritumoural rCBV is higher than for a metastasis (Blasel et al., 2010, Law et al., 2002). Using the same dataset and different post processing

techniques, diffusion susceptibility contrast or DSC MRI allows prediction of tissue permeability, a measure of blood-brain barrier disruption and this accordingly increases around a metastasis, where there is increased capillary permeability and therefore vasogenic oedema (Lacerda and Law, 2009, Thompson et al., 2010).

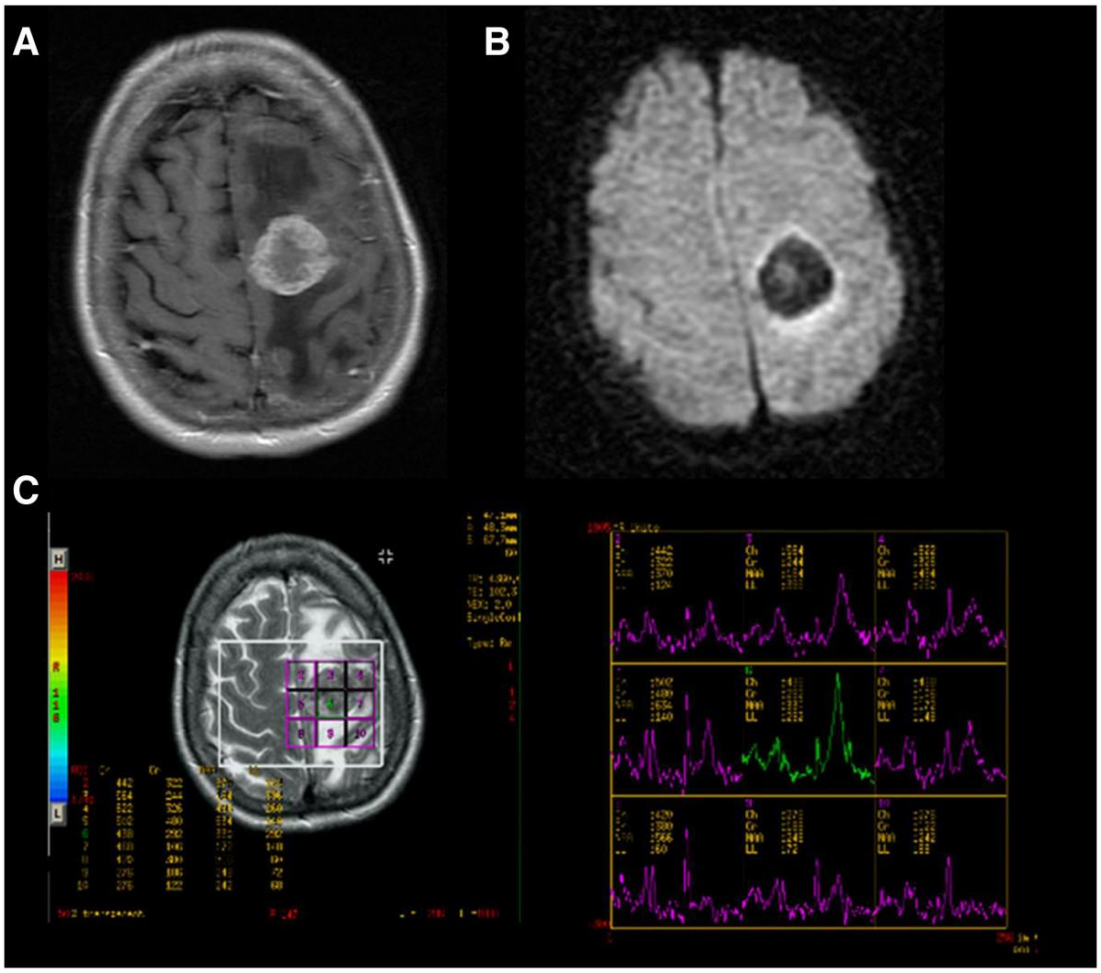

Figure 1.5: An elderly patient was referred with hemiparesis and suspected to have a stroke. MRI demonstrated a lesion in the left hemisphere which on (A) T1 weighted axial image post gadolinium at 1.5 T is shown to have a solid and ring enhancing portion. (B) The associated ADC map shows considerably reduced diffusion at the site of the solid portion of the lesion with increased diffusion due to vasogenic oedema in the white matter surrounding the mass. (C) Single voxel proton MRS of the lesion yields an abnormal spectrum with a large lipid and lactate peak, reduced NAA, reduced Cr and slightly elevated Cho. This pointed to a metastasis, glioma or lymphoma as opposed to an abscess. There was time to optimise the patient for surgery and begin steroid treatment before the lesion was resected and confirmed to be a renal cell carcinoma.

Summary: Multimodal MR used singly or in combination has improved our ability to distinguish metastases from primary cerebral tumours or abscesses. Despite the

application of these advanced MR techniques of diffusion, perfusion and spectroscopy to solve this clinical problem (Server et al., 2011) it remains a fact that for accessible, larger lesions surgery is often undertaken and tissue diagnosis obtained regardless in order to move forward treatment. The role and evidence for MRI in surgical planning is therefore the next area to consider.

1.5.2.3 Surgical planning

Image guided surgery allows the surgeon to plan the safest route to the tumour and intra-operatively to maximise safe resection. Conventional imaging post contrast T1 weighted images with thin slice protocols are generally acquired for image guidance software registration and the increased spatial resolution of such sequences compared to the usual diagnostic scans has been highlighted in the discussion of detection. Diffusion imaging allows images of white matter tracts and their relationship to tumour to be delineated. DTI acquisitions, in addition to generating quantitative parameters, can permit tractography by estimating the directionality of fibre tracts, permitting the tracking of fibre bundles in 3D space. The methodology for this post processing varies and a number of non-proprietary software solutions in addition to those supplied by manufacturers are available. Further refinements to the methodology, including use of higher order algorithms to resolve ambiguous directionality on voxels may further increase reliability (Farquharson et al., 2013). Functional MR detects changes in blood oxygen level or BOLD signal in metabolically more active areas during application of a stimulus or performance of a task. This is particularly useful to localise language areas or motor cortex. Few series have examined the role of fMRI in metastases resections alone, but in those that have, significant benefits in terms of motor recovery, preservation and therefore quality of life have been demonstrated (Walter et al., 2011). Modern software can integrate functional and tractography sequences into a single merged dataset for use in theatre. Whilst there are limitations on the accuracy of image guidance systems, ranging from the fidelity of the preoperative MRI scan to the type of image registration algorithms applied (Widmann et al., 2012) and the problems of brain shift (Kuhnt et al., 2012) where the pre-registered navigation is rendered inaccurate

once CSF is released, there are nonetheless improved outcomes reported for surgical series looking exclusively at metastases (Tan and Black, 2007, Paek et al., 2005).

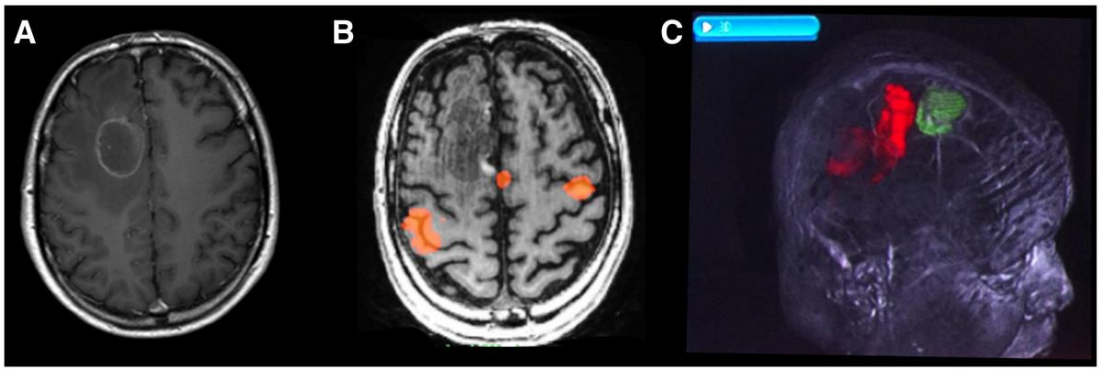

Figure 1.6: A patient known to have breast cancer with a manually dexterous job presented with intermittent left hand and arm weakness and was found (A) to have a solitary ring enhancing lesion in the premotor area on T1W MRI with gadolinium. (B) Functional MRI performing a hand tapping and gripping task determined the location of hand function and this was used as the "seed" region of interest on a DTI scan to produce a representation of the motor tracts. (C) These were used to generate a 3D object and fused with an anatomical planning scan (1 mm slices) using commercially available software (StealthViz™ with StealthDTI™ by Medtronic, running on an S7 workstation) to produce images that were used intraoperatively for image guided resection, avoiding the tracts (shown in red, with tumour rendered in green).

1.5.2.4 Predicting the primary cancer

In cases of multiple metastasis or solitary lesions with no known primary, MRI may give useful diagnostic clues as to the original tumour. Some primaries may have particular signal characteristics even on conventional MR. For example melanoma metastases may show high signal on non-enhanced T1 sequences due to the effect of melanin and mucinous metastases may show low T2 signal compared with the expected hyper-intensity on this sequence. The metabolic profile has been investigated for metastases of differing primary tumours as well as the surrounding brain, with no abnormal spectra reported outside of the lesion itself. Metabolic features on MRS have shown limited value in predicting primary type. However, raised mobile lipid content has been proposed as a weak sign of a colonic origin metastasis (Chernov et al., 2006). Others have tried to use the diffusion characteristics of particular metastases to distinguish the primary and, whilst it has

been shown that ADC values are higher in well differentiated adenocarcinoma metastases than poorly differentiated types, this may simply reflect cellularity and could not predict the primary, only suggest a narrower differential (Hayashida et al., 2006). Likewise in a series with a variety of primary cancers including lung and breast, restricted diffusion could not be correlated with any primary nor could ADC predict primary pathology (Duygulu et al., 2010). Spectroscopy was combined with perfusion MR to show that differences in choline-creatine ratios between metastases of lung and breast cancer correlated with differences in relative cerebral blood volume, but tissue was not available for comparison to look for a unifying pathological basis (Huang et al., 2010).

Summary: MRS may be used to distinguish primary tumour origin. However, more than one advanced MR metric may need to be combined in order to robustly generate models that differentiate the primary lesion and, though these studies would likely be retrospective, ideally some image guided correlation of regions of interest on the advanced MR with the final tissue samples is needed, as has been performed for glioma (Price and Gillard, 2011).

1.5.2.5 Monitoring response to treatment

Beyond diagnosis, MRI may be used to monitor response to treatment as part of clinical and radiological follow up. This may be immediate, as in post-operative MRI to determine if there has been a complete resection, or delayed, i.e. has the metastasis responded to chemo- or radio-therapy. In general, conventional sequences are utilized, but one area of particular clinical interest in following cases up is ongoing or increasing enhancement following stereotactic radiosurgery to a metastasis and whether this represents radio-necrosis or recurrence (Kang et al., 2009). Standard patterns of changes in brain metastases are seen on conventional MRI with peri-lesional oedema, central hypo-intensity on T2 weighted imaging at 2-6 months followed by blurring of the enhancement margin, reduction in enhancing volume over time and formation of a glial scar (Peterson et al., 1999, Lunsford et al., 1998, Friedman et al., 2001). Although attempts have been made to build discriminatory measures from conventional MRI (Dequesada et al., 2008) performance has proven disappointing (Stockham et al., 2012). Blood flow would be expected to differ

significantly between areas of necrosis and recurrence. MR perfusion has shown higher rCBV in recurrent metastases after radiosurgery compared to areas of radionecrosis and reduction in CBF over time for treated lesions (Hoefnagels et al., 2009, Barajas et al., 2009). Furthermore, the first reading of CBF following treatment was highly predictive of the final response, even though pre-operative readings could not predict this. Diffusion imaging may reflect cellularity and ADC readings from metastases treated with radiosurgery, taken immediately post treatment may be tracked to determine if the lesion is responding to therapy, manifest as increasing ADC, as compared to a recurring or necrotic lesion where the changes in ADC differ. The initial ADC value may also predict final response to the treatment (Goldman et al., 2006). In conjunction with perfusion MRI, this suggests the novel application of advanced MR readings, not just as diagnostic tools but as predictors of future treatment response or biological markers.

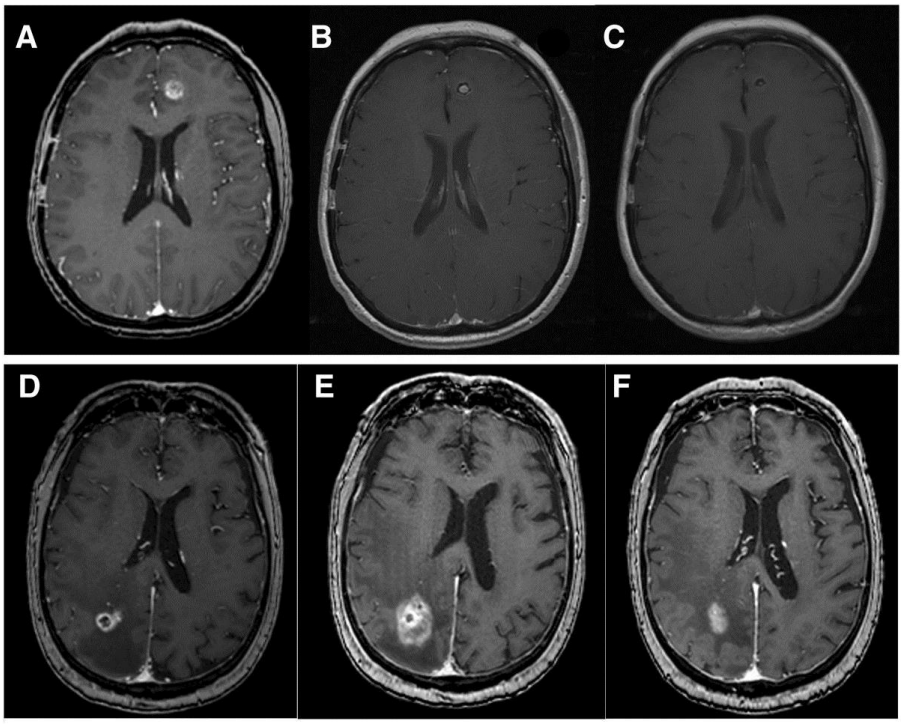

Figure 1.7: Monitoring of treatment response after stereotactic radiosurgery. A patient with known metastatic melanoma underwent treatment to a left frontal lesion (A) and at 3 months (B) the characteristic changes of a blurred margin and necrosis followed by formation of a glial scar at 6 months (C) are seen. However in a similar appearing patient (D) with a right parietal lesion from metastatic renal cell carcinoma, the lesion shows more florid changes at 3 months (E) with increased contrast enhancement at the margins and the possibility of progression, as opposed to radionecrosis is raised. Multi-modal techniques described in the text may show promise in deciding how to proceed at this stage. The patient was well and on monoclonal antibody chemotherapy, with observation the lesion eventually regressed at 6 months (F) and is currently stable.

1.5.2.6 Predicting survival

As described in many studies here, various metrics or measurements may be taken from the different advanced MR images described using the device workstation or non-proprietary software. A biological marker or "biomarker" is strictly any such reading which is used for diagnostic or prognostic purposes. Even conventional MR may provide such markers, and it has been shown that for solitary metastases in one series, the degree of oedema on the preoperative T2 weighted scan was related to the degree of angiogenesis, brain invasiveness and overall survival with reduced oedema surprisingly being a worse prognostic factor (Spanberger et al., 2013b). The role of ADC and CBF in predicting response of metastases to SRS has been discussed in the preceding section. Berghoff and colleagues took readings from preoperative DWI in single metastases which were subsequently resected. They found a reduced overall survival, irrespective of adjuvant treatments and denser reticulin (stromal) matrix in patients with low tumoural ADC compared to the group mean (Berghoff et al., 2013c). These measures could potentially be incorporated into the prognostic models mentioned such as the recursive partitioning score (RPA) or graded prognosis assessment (GPA) score; widely validated predictors of survival in brain metastases patients which combine clinical information such as age, status of the primary cancer and extracranial disease amongst others (Sperduto et al., 2008, Gaspar et al., 1997). Further standardisation of the post processing and measurement workflow is needed, however, before MRI metrics could be confidently used in clinical practice.

1.5.2.7 Future directions

As cancer diagnostics and therapeutics become increasingly related, three areas of emerging MR technology with practical applications to brain metastases stand out. Integration of cancer staging via PET-MR offers one potential means of incorporating further functional data in real time without losing all the knowledge already acquired about the behaviour and characteristics of metastases on MRI (Torigian et al., 2013). Novel contrast agents, including those that can identify molecular targets, are in development in animals and an agent based on iron oxide particles which bind to a vascular cell adhesion molecule common to human metastases has been used to visualise micro-metastases at MRI, suggesting the

possibility of diagnosing and possibly treating brain metastases long before they were previously even detected (Serres et al., 2012). Finally the application of MR as an intraoperative tool for guiding minimally invasive therapies such as laser coagulation or high intensity focused ultrasound is no longer conceptual, with several small series of treated tumours including metastases being reported (Jethwa et al., 2012, Ram et al., 2006). MR technology will continue to enhance diagnosis but is now being used to predict prognosis and being incorporated into the treatment of metastases too (Monteith et al., 2013).

1.5.3 Histopathology

Due to increasing concern regarding the adverse effects of radiotherapy treatment, more tailored chemotherapy regimens and the presence of common mimics such as lymphoma and glioma, imaging diagnosis alone for brain metastases is essentially insufficient, even with a persuasive clinical picture. In such situations tissue may be obtained by resection (if indicated clinically – see **Section 1.6.1**) or biopsy and analysed by a specialist neuropathologist for macroscopic features and microscopic morphology. This is supported by IHC, including, but not limited to, cytokeratins (CK7 for lung, breast origin versus CK20 for colorectal, pancreatic, urothelial), EMA (carcinoma), S-100 (melanoma, glioma), TTF-1 (small cell and lung adenocarcinoma) and Ki67 (marker of proliferation)(Pekmezci and Perry, 2013). Ancillary tests such as HER2 status for breast cancers or EGFR receptor status for lung adenocarcinomas may be added as required and primary tissue from any previously operated cancer is reviewed.

1.6 Treatment

Treatment of patients with brain metastases is not directed at curing the disease, but rather extending survival with as high a quality as possible. Patients may present late in the course of their systemic disease and be appropriate for palliation only, but for those patients with a good level of function (generally taken to mean they can care for themselves), brain metastases are treated by a combination of surgery, radiotherapy – either focal or to the whole brain – and chemotherapy. Management is

collaborative through a multidisciplinary team (MDT) of the relevant specialities including neurosurgery, oncology, radiology, pathology, nurses and therapists. There are a number of randomised controlled trials comparing these different treatments and their combinations, but guidelines in the United Kingdom, North America and Europe reflect deep uncertainty about which therapies to use and in which patients.

1.6.1 Surgery

Neurosurgical resection of brain metastases, usually performed for solitary tumours, provides tissue for diagnosis (see **Section 1.5.3**) and relieves mass effect. Neurosurgery followed by whole brain radiotherapy (WBRT) prolonged functional independence, local control and overall survival compared to biopsy and WBRT in a randomised controlled trial (Patchell et al., 1990) and compared to WBRT alone in a meta-analyses of randomised controlled trials (Hart et al., 2005). Local recurrence rates for solitary metastases after neurosurgery are approximately 15-20% across a variety of settings (Patel et al., 2010, Jenkinson et al., 2011) although more aggressive surgical resection of the metastasis margins in non-eloquent areas may reduce this (Yoo et al., 2009). Risks of neurosurgery include a general anaesthetic, risk to life, bleeding, infection and neurological impairment. The latter is reduced by the use of modern image guidance techniques (Tan and Black, 2007), as described in **Section 1.5.2**. Nonetheless, hemiparesis may occur more often than expected, even with intraoperative monitoring of motor cortical tract function, in keeping with these tumours being more locally invasive, or more gliomatous, than previously thought (Obermueller et al., 2015).

1.6.2 Radiotherapy

1.6.2.1 Stereotactic radiosurgery

Stereotactic radiosurgery (SRS) is the administration of high doses of radiation to a focal target sparing as much of the surrounding tissue as possible. This is delivered in a single dose (strictly this is the true definition of SRS) or in fewer than five doses for larger tumours (this is hypo-fractionated or stereotactic radiotherapy (SRT), but

often referred to as SRS and grouped under SRS in the medical literature). A variety of technologies or platforms are used to deliver SRS including Gamma Knife ®, Cyberknife ® and linear accelerators (LINAC).

SRS is therefore a focal treatment for brain metastases and can be performed in the outpatient setting or as a day case, without fixation on some devices and without anaesthesia, if tolerated. Although never compared directly to surgical resection in a trial setting, case series suggest SRS is non-inferior to surgery when both are combined with WBRT (Schöggl et al., 2000) and is certainly more cost effective (Mehta et al., 1997). In UK clinical practice, SRS is reserved for treating 1-3 smaller tumours (risk of radionecrosis increases with increasing size, so an upper limit of 20cc is used), where there is little oedema or mass effect, and the patient is expected to survive 6 months (NICE – reference NHSCB/ D05/P/d).

Neurosurgery	SRS
Significant mass effect	No midline shift or CSF pathway obstruction
Superficial or non-eloquent location	Deep seated or difficult to access
	Radiosensitive histology if already known
Large, solitary lesion	Small volume of tumour overall (e.g. under
Tissue needed for diagnosis, e.g.	30mm diameter) or small number of tumours in
cancer of unknown origin or no primary	older schemes (e.g. ≤ 3)
found after staging studies	Medically unfit or high risk for anaesthesia e.g.
Radio-resistant histology, if known	warfarin for metallic heart valve, restrictive lung
	disease

Table 1.1: Factors favouring neurosurgery or stereotactic radiosurgery (SRS) as the treatment of choice for brain metastases. CSF = cerebrospinal fluid, mm = millimetres.

Elsewhere, SRS is being increasingly used, both as an alternative to WBRT in patients with multiple metastases (Yamamoto et al., 2014), and in addition to neurosurgery as a "boost" (Ojerholm et al., 2014). Indeed a randomised trial of SRS to the cavity after neurosurgery is underway in North America (ClinicalTrials.gov Identifier: NCT01372774) and markers of local invasion and radiosensitivity will thus be urgently required to stratify patients for such treatments in the future.

1.6.2.2 Whole brain radiotherapy

Whole brain radiotherapy (WBRT) is usually delivered as 30Gy in 10 fractions as an adjunct to a local therapy or as a palliative measure on its own for those unsuitable for more aggressive treatments. Support for the former is well established with randomised trials showing reduced intracranial progression and fewer salvage therapies needed in those irradiated compared to those simply observed after either SRS (Kocher et al., 2011) or neurosurgery (Patchell et al., 1998). An improvement in overall survival was never proven and with recent evidence suggesting patients may get deleterious cognitive effects within months of WBRT (Chang et al., 2009), this result has been used to justify omitting WBRT after local treatments (Tsao et al., 2012). Even for those not receiving any active local therapy, a large study has suggested WBRT may be worse in terms of quality of survival than optimal palliative care (Langley et al., 2013). Despite these studies, WBRT remains easy to access and administer in most healthcare systems, whilst progressive disease - even if it does not affect survival - may cause just as many harmful cognitive effects as radiation; thus the balance of where this risk lies is not yet defined (Kondziolka et al., 2014). What will be needed are markers of local invasion, radiation response and intracranial progression to allow optimisation of therapy (i.e. the correct balance of risks and benefits) for individual patients.

1.6.3 Chemotherapy

All patients are routinely managed with dexamethasone or oral steroid equivalent at high dose, typically 8-16 mg in divided doses tapered off as quickly as tolerated over the course of treatment (Soffietti et al., 2006). Systemic chemotherapy for the primary cancer is generally continued during surgery or radiation therapy - if already instated - or administered once these treatments have finished if not, although from an oncological point of view, the central nervous system has been regarded as a sanctuary site with limited effectiveness of systemic chemotherapy.
Strategies (Puhalla et al., 2015) therefore include:

- facilitating passage of known systemic chemotherapy agents across the blood-brain or rather blood-tumour barrier (Connell et al., 2013)
- identifying anti-metastatic effects amongst agents already known to function in the brain (Abel et al., 2013)
- developing agents that may act systemically to prevent spread of metastatic cells in the systemic circulation into brain, for example by reducing circulating tumour cell load (Pierga et al., 2013)
- administering chemotherapy before surgery to alter the immune response or behaviour of the operated tumour (Jones et al., 2015)

1.6.4 Summary of treatment options

The evidence and treatment options are highly varied. Trials include patients with metastases from different primary cancers, hence there are a wide range of outcomes seen and it is difficult for clinicians to generalise even the more robust results to the individual patient with a particular primary tumour. In general, comparing WBRT alone to local therapies with WBRT, combined treatment seems to improve overall survival and control of brain disease. When considering whether to add WBRT or not after a local treatment, the addition of WBRT may result in improved control of brain disease and hence reduced death from neurological causes, but it does not necessarily improve the overall survival. This is especially true for oligometastatic disease compared to solitary metastases. There is conflicting data about the cognitive and quality of life effects of WBRT and any strategy which omits this treatment must show active monitoring for progression, which may itself cause these effects. In terms of local therapies, surgery is still the standard of care for large, solitary, accessible lesions with significant mass effect or oedema and adjuncts, such as image-guidance and extensive resection, may improve local control further. Detailed treatment information must therefore be taken into account and clear outcome measures used when studying patients with cerebral metastases.

1.7 Outcomes and their estimation

The wide variation in prognosis from brain metastases has led to a number of scoring systems which have been adopted into clinical practice in order to guide decision making and, in particular, select patients for aggressive treatment. All of these incorporate an assessment of functional impairment, scored using a set scale by a treating healthcare professional and encompassing the patient's ability to care for themselves (Schag et al., 1984, Karnofsky DA, 1949).

Able to carry on normal activity and to work; no special care needed.	**100**	**Normal, no complaints; no evidence of disease.**
	90	Able to carry on normal activity; minor signs or symptoms of disease.
	80	Normal activity with effort; some signs or symptoms of disease.
Unable to work; able to live at home and care for most personal needs; varying amount of assistance needed.	70	Cares for self; unable to carry on normal activity or to do active work.
	60	Requires occasional assistance, but is able to care for most of his personal needs.
	50	Requires considerable assistance and frequent medical care.
Unable to care for self; requires equivalent of institutional or hospital care; disease may be progressing rapidly.	40	Disabled; requires special care and assistance.
	30	Severely disabled; hospital admission is indicated although death not imminent.
	20	Very sick; hospital admission necessary; active supportive treatment necessary.
	10	Moribund; fatal processes progressing rapidly.
	0	Dead

Table 1.2: The Karnofsky performance scale (KPS) which is used to classify functional impairment in patients with cerebral metastases.

In the early Recursive Partitioning Analysis (RPA) score (Gaspar et al., 1997), data was pooled from approximately 1200 patients and they were assigned to one of three categories based on the Karnofsky performance scale (KPS), their age and the status of their primary cancer (whether it is controlled and without other metastases). This score was used to predict the overall survival time and has been widely validated in clinical practice, but criticised for not taking into account the number of cerebral metastases. Hence the Graded Prognostic Assessment (GPA) score which was based on an expanded database from the RTOG (Sperduto et al., 2008) and assesses age in

more categories and includes number of lesions. Most recently the idea that "all cerebral metastases are created equal" gave way to the disease specific GPA score (Sperduto et al., 2010), with different factors seen as being important for different types of tumour histology (reproduced in **Table 1.3**).

Non–small-cell and small-cell lung cancer

Prognostic Factor	GPA Scoring Criteria 0	0.5	1.0	Patient Score
Age, years	> 60	50-60	< 50	____
KPS	< 70	70-80	90-100	____
ECM	Present	—	Absent	____
No. of BM	> 3	2-3	1	____
Sum total				____

Median survival (months) by GPA: 0-1.0 = 3.0; 1.5-2.0 = 5.5; 2.5-3.0 = 9.4; 3.5-4.0 = 14.8

Melanoma

Prognostic Factor	GPA Scoring Criteria 0	1.0	2.0	Patient Score
KPS	< 70	70-80	90-100	____
No. of BM	> 3	2-3	1	____
Sum total				____

Median survival (months) by GPA: 0-1.0 = 3.4; 1.5-2.0 = 4.7; 2.5-3.0 = 8.8; 3.5-4.0 = 13.2

Breast cancer

Prognostic Factor	GPA Scoring Criteria 0	0.5	1.0	1.5	2.0	Patient Score
KPS	≤ 50	60	70-80	90-100	n/a	____
Subtype	Basal	n/a	LumA	HER2	LumB	____
Age, years	≥ 60	< 60	n/a	n/a	n/a	____
Sum total						____

Median survival (months) by GPA: 0-1.0 = 3.4; 1.5-2.0 = 7.7; 2.5-3.0 = 15.1; 3.5-4.0 = 25.3

Renal cell carcinoma

Prognostic Factor	GPA Scoring Criteria 0	1.0	2.0	Patient Score
KPS	< 70	70-80	90-100	____
No. of BM	> 3	2-3	1	____
Sum total				____

Median survival (months) by GPA: 0-1.0 = 3.3; 1.5-2.0 = 7.3; 2.5-3.0 = 11.3; 3.5-4.0 = 14.8

GI cancers

Prognostic Factor	GPA Scoring Criteria 0	1	2	3	4	Patient Score
KPS	< 70	70	80	90	100	____

Median survival (months) by GPA: 0-1.0 = 3.1; 2.0 = 4.4; 3.0 = 6.9; 4.0 = 13.5

Table 1.3: Scoring system to predict the overall survival of patients with cerebral metastases based on clinical and pathological features from (Sperduto et al., 2012).

These scores, though useful in trials and widely used by some oncologists, are still felt to be unsatisfactory in clinical practice. Clinicians are poor at estimating prognosis (Jakola et al., 2012, Zakaria and Jenkinson, 2015), there is too wide a variation within categories (Grossman and Ram, 2014) and scoring systems are based on cohorts treated with surgery, radiation and chemotherapy. Furthermore, there is no incorporation radiological data and little use of biological data in these scores and no systems for estimating time to intracranial progression nor radiation sensitivity, despite the importance of these features for patients and healthcare professionals.

1.8 Statement of the problem and outline of the thesis hypotheses

Cerebral metastases are increasingly common and cause significant morbidity, threatening to limit the gains made in treating common solid organ cancers. Despite this, there is a lack of consensus surrounding the best treatment strategies and, in particular, how to combine local treatments (surgery, SRS) with WBRT. Better understanding of the biological mechanisms of local brain invasion by these tumours is urgently needed, not only to inform these strategies but also to enable improved prediction of clinical outcomes such as intracranial progression.

The aim of this thesis is to derive biological and radiological markers of local brain metastasis invasion, intracranial progression and survival which may be used in clinical practice, whilst deepening scientific understanding of the brain-brain metastasis interface.

Chapter 2 describes the investigation of metastasis-inducing protein expression in a series of brain metastases and their clinical importance as possible biological markers of survival, recurrence and radiation sensitivity.
Hypotheses: Proteins which induce a metastatic phenotype in solid organ cancers are also involved in local invasion in brain metastases. Levels of expression of such proteins may be associated with clinical outcomes such as survival and progression for patients with brain metastases.

Chapter 3 describes the MRI analysis of the brain-brain metastasis interface. This is presented in the form of two published papers, one determining the methodology and the other the analysis itself.
Hypotheses: Measurements may be taken from diffusion weighted MRI brain scans of patients with brain metastases with high reliability on clinical grade hardware and software. These MRI measures may be associated with clinical outcomes such as survival and progression in patients with brain metastases. Specifically, the change in apparent diffusion coefficient at the brain-brain metastasis interface may be predictive of survival after resection of that brain metastasis.

Chapter 4 describes a prospective study in which the brain-brain metastases interface was examined using image-guided neurosurgical sampling alongside MRI analysis of the co-localised regions of interest to bring together the previous work in an integrated analysis of the tumour leading edge and peritumoural region.
Hypotheses: Differences between tumours in diffusion weighted MRI characteristics at the brain-brain metastasis interface reflect underlying differences in invasive growth pattern, metastasis inducing protein expression and markers of aggressive behaviour such as vascularity, cellularity and proliferation. This relation explains why the MRI measures are predictive of clinical outcomes.

Chapter 5 discusses the implications of the thesis findings, whether the hypotheses were proven and the future directions for study.

Chapter 2: Biological markers of local invasion

2.1 Abstract

Background: Understanding the factors that drive recurrence and radiosensitivity in brain metastases would improve prediction of outcomes, treatment planning and development of therapeutics. We investigated the expression of known Metastasis-Inducing Proteins in human brain metastases.

Methods: Immunohistochemistry on metastases removed at neurosurgery from 138 patients to determine the degree and pattern of expression of the proteins S100A4, S100P, AGR2, osteopontin (OPN) and the DNA repair marker FANCD2. Validation of significant findings in a separate prospective series with investigation of intra-tumoural heterogeneity using image-guided sampling. Assessment of S100A4 expression in brain metastatic and non-metastatic primary breast carcinomas.

Results: There was widespread staining for OPN, S100A4, S100P and AGR2 in human brain metastases. Positive staining for S100A4 was independently associated with a shorter time to intracranial progression after resection in multivariate analysis (hazard ratio for negative over positive staining = 0.17, 95% CI: 0.04 – 0.74, p=0.018). S100A4 was expressed at the leading edge of brain metastases in image guided sampling and overexpressed in brain-metastatic versus non-brain metastatic primary breast carcinomas. Staining for OPN was associated with a significant increase in survival time after postoperative whole brain radiotherapy in retrospective (OPN negative 3.43 months, 95% CI: 1.36 – 5.51 vs. OPN positive, 11.20 months 95% CI: 7.68 – 14.72, Log Rank test, $p<0.001$) and validation populations.

Conclusions: Proteins known to be involved in cellular adhesion and migration *in vitro* and metastasis *in vivo* are significantly expressed in human brain metastases and may be useful biomarkers of intracranial progression and radiosensitivity.

2.2 Introduction

Brain metastases (BMs) are common brain tumors in adults with a steeply rising incidence due to the increased use of brain imaging in asymptomatic patients and prolonged survival from solid organ cancers (Owonikoko et al., 2014). There are no known biological markers that are routinely used to predict patient outcomes in BMs. Clinical factors are combined to generate predictions of overall survival, but cannot predict intracranial progression and the various models are not individualised to each patient, even if different primary cancer types are assessed separately (Sperduto et al., 2010).

We have previously identified two groups of proteins in the rat mammary model system that can induce metastasis and are associated with clinical outcomes in patients with breast (de Silva Rudland et al., 2011) and other solid organ cancers. S100A4 and S100P are small calcium-dependent regulatory molecules that probably work by inducing cellular migration and invasion directly (Gross et al., 2014). S100A4 is active in the brain microenvironment (Dmytriyeva et al., 2012), elevated levels are associated with a metastatic phenotype, it cooperates with growth-inducing activated oncogenes to yield growing metastases and carcinomas in S100A4 knockout mice do not metastasise to brain.(Bresnick et al., 2015) The second group – osteopontin (OPN) and anterior gradient 2 (AGR2) - work primarily by inducing cellular adhesion to the ECM that then allows migration to take place (Moye et al., 2004, Liu et al., 2005). OPN binds the cell surface integrins $\alpha_V\beta_3$ / $\alpha_V\beta_5$ with the latter widely expressed in human BMs and their microenvironment (Schittenhelm et al., 2013, Berghoff et al., 2014). The integrin $\alpha_V\beta_3$ / $\alpha_V\beta_5$ inhibitor cilengitide induces cellular detachment and apoptosis, and reduces proliferation in a panel of brain metastatic breast cancer cell lines (Lautenschlaeger et al., 2013). AGR2 has been shown to be necessary and sufficient for migration *in vitro* in a glioblastoma cell line (Hong et al., 2013). Finally, the underlying change that is believed to result in selection for overexpression of these Metastasis-Inducing Proteins (MIPs) is a failure of ds DNA repair in a progenitor cell and in the breast this process is identified by immunohistochemical loss of FANCD2 (Rudland et al., 2010); the related proteins FANCA and FANCG have recently been shown to be overexpressed in BMs compared to the primary breast carcinoma in paired human samples (Woditschka et al., 2014).

2.3 Materials and methods

2.3.1 Patients and specimens

Patients with a diagnosis of brain metastasis were identified from histopathology records between 2005 and 2012 at a single institution and formalin-fixed, paraffin-embedded specimens were obtained in 138 cases. Full clinical information was gathered and is summarised in **Table 2.1**.

Age at surgery (median, range)		59.9 years (20.3 – 82.4)	
		Number	Percentage
Karnofsky performance status	< 70%	101	73.2%
	> 70%	37	26.8%
Location of operated metastasis	Posterior fossa	33	23.9%
	Supratentorial	105	76.1%
Number of brain metastases	Multiple	26	18.8%
	Solitary	112	81.2%
Size of operated metastasis (diameter)	< 30mm	56	40.6%
	> 30mm	82	59.4%
Primary cancer controlled?	No	29	29.9%
	Yes	68	70.1%
Extra-cranial metastases?	Absent	91	65.9%
	Present	47	34.1%
Synchronous presentation: primary and brain metastases?	No	97	70.3%
	Yes	41	29.7%
Primary cancer histology	Bladder	3	2.2%
	Breast	40	29%
	Endometrial	2	1.4%
	Colorectal	12	8.7%
	Renal	7	5.1%
	Melanoma	16	11.6%
	Non-small cell lung	38	27.5%
	Oesophagus	5	3.6%
	Ovarian	2	1.4%
	Pancreas	1	0.7%
	Prostate	2	1.4%
	Small cell lung	8	5.8%
	Squamous cell	2	1.4%
Type of operation	Biopsy	1	0.7%
	Gross total resection	127	92%
	Subtotal resection	10	7.2%
Whole brain radiotherapy after neurosurgery*	No	33	23.9%
	Yes	105	76.1%
Chemotherapy after neurosurgery	No	86	62.3%
	Yes	52	37.7%

Table 2.1: Summary of clinical and radiological characteristics of 138 patients with operated brain metastases and their treatment following neurosurgery.

For validation and investigation of intratumoral heterogeneity, 24 consecutive patients were included who underwent neurosurgical resection of a solitary supratentorial metastasis in non-eloquent brain by image-guided craniotomy as part of their standard care from 2014 - 2015. Clinical details are listed in **Table 2.2** and surgical, MRI techniques have been described previously (Zakaria and Jenkinson, 2014). Primary breast carcinoma specimens were obtained from partner tissue banks locally and ethical approval was granted within the Walton Research Tissue Bank (NRES 11/WNo03/2) and by the UK Health Research Authority (NRES 12/NW/0778).

Table 2.2: Clinical data for prospective series of 24 patients with resected supratentorial metastases.

Age at surgery	(median, range)	59.3 years	(23.9 – 76.0)
Gender	Female	13	54%
	Male	11	46%
Primary carcinoma	Non-small cell lung	12	50%
	Melanoma	4	17%
	Breast	3	13%
	Colorectal	2	8%
	Endometrial	1	4%
	Renal	1	4%
	Sarcoma	1	4%
Extracranial disease?	Absent	17	71%
	Present	7	29%
Controlled primary?	Synchronous presentation	8	33%
	Yes	16	67%
Adjuvant whole brain radiotherapy?	No	5	21%
	Yes, 30 Gray in 10#	19	79%
Adjuvant chemotherapy?	No	13	54%
	Yes	11	46%

2.3.2 Immunohistochemistry

Acknowledgement: This section was largely written by Mrs Angela Platt-Higgins BSc, scientist at the Institute of Integrative Biology.

Histological sections were cut at 4 µm on APES coated slides, dewaxed in xylene and rehydrated through graded ethanol to water. Firstly, endogenous peroxidase activity in the tissue sections was blocked by immersing the slides in 100% methanol containing 0.05% (v/v) H_20_2 for 20 min at room temperature. Sections were then incubated in a moisture chamber with antibodies diluted in phosphate-buffered saline (PBS) containing 1% (w/v) bovine serum albumen (BSA), pH 7.4.

Polyclonal affinity-purified anti-AGR2 (13) (#ARP42290, Aviva Systems Biology, San Diego, CA) was used at a dilution of 1:750 in phosphate-buffered saline (PBS) containing 2% (w/v) bovine serum albumen (BSA) pH7.4 and monoclonal anti-osteopontin (#MP111B10, Developmental Studies Hybridoma Bank, Iowa City, IA, USA) was used at 1:300 in 0.5% (w/v) BSA. Both were incubated on the sections overnight at 4^oC. Polyclonal anti-S100A4 (#A5114, Dako UK Ltd, Ely, Cambridgeshire) and monoclonal anti-S100P (#610307, BD Biosciences, Oxford Science Park, Oxford) were used at a dilution of 1:400 and 1:75 respectively and were incubated for 2hr at room temperature, following an initial pre-incubation with 2% (w/v) BSA in PBS for 30 min at room temperature on the sections. Polyclonal anti-FANCD2 (#H300; sc28194, Santa Cruz Biotechnology Inc., Dallas, Texas, USA) was used at a dilution of 1:300 and was incubated for 3hr at room temperature, again following a 30 minute pre-incubation with 2% (w/v) BSA on the sections. FANCD2 antibodies recognize both the non-monoubiquitylated and monoubiquitylated isoforms of FANCD2 (Wilson et al., 2008). Polyclonal anti-GFAP (#Z0334, Dako) and monoclonal anti-CD34 (#M7165, Dako) were used at a dilution of 1:2000 and 1:25 respectively and incubated on the sections for 1hr at room temperature. Prior to incubation, a 5 minute Proteinase K (Dako) digestion step was carried out by following the manufacturer's instructions. After all the above antibody incubations, sections were thoroughly washed in three changes of PBS.

Indirect immunohistochemical staining was carried out using an enhanced horseradish peroxidase (HRP) labelled polymer system, the *DAKO*

EnVision+System, peroxidase(DAB) (Heras A, 1995) with reagents prepared according to the manufacturer's instructions. After a final wash in running tap water, all sections were counterstained in Mayers' haemalum before being dehydrated through graded ethanol and xylene and mounted using DPX mountant (VWR, Lutterworth, Leicestershire).

For melanoma metastases a red coloured chromogen (AEC)(Dako) was used to avoid confusion with pigmented, brown/black melanin-containing cells. This is illustrated in **Figure 2.1**. In this case, the sections were mounted, without dehydration, using a water soluble mountant (Glycergel, Dako).

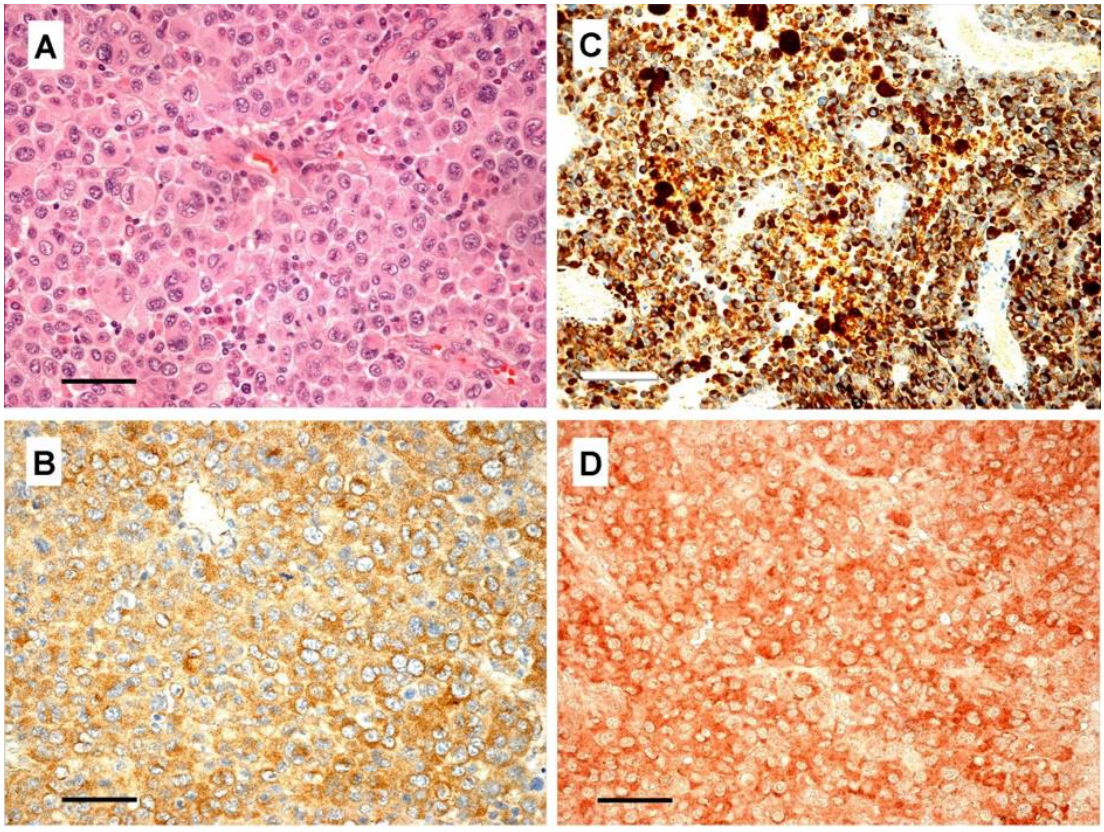

Figure 2.1: Immunohistochemical staining for the protein osteopontin in a 52 year old patient with metastatic melanoma who underwent craniotomy and resection. The H&E stained section (A) shows tumour cells with irregular, enlarged nuclei. Using standard antibody detection kits there seems to be evidence of protein expression in the cytoplasm predominantly (B), but the presence of brown and black melanocytes (C) makes it difficult to judge. Use of an alternative antibody detection kit with a red chromogen allows confirmation of staining (D) in tumour cells. Original magnification X 200. Bars= 100 µm.

Non immune sera consisting of mouse IgG (Abcam) for mouse monoclonal antibodies (OPN and S100P) and rabbit IgG (Abcam) for rabbit polyclonal antibodies (S100A4 & AGR2) were substituted for primary antibodies and were included in each staining run. Breast carcinoma sections that were known to express all the proteins were used as external positive controls. Antigen-blocked immune serum was prepared by prior incubation with the appropriate recombinant protein as in previous studies on S100A4 (de Silva Rudland et al., 2006), S100P (Wang et al., 2006) and FANCD2 (Rudland et al., 2010). Additionally AGR2 and OPN antibodies were blocked by pre-incubating it with the appropriate blocking peptides (# AAP42290 for AGR2and #AAP36677 for OPN, Aviva) in the ratio 100:1, Ag:Ab, with final antibody concentrations of 1:750 and 1:300 respectively. Blocking peptide pre-incubations were performed over 72hrs at 4°C. The control sera were then used in the immunohistochemical procedure as described above.

2.3.3 Assessment of staining

Slides were analysed independently by two observers using light microscopy and corroborated by a senior neuropathologist. The percentage of nuclear and/or cytoplasm stained tumor cells was recorded from well-separated sections of each specimen, 10 fields per section at ×200 magnification, at a minimum of 200 cells per field in a rigorous fashion as described previously (Wang et al., 2006). There was agreement on positive staining (1% or above of cells positively stained to any degree (de Silva Rudland et al., 2011)) in 94% of slides scored, with a kappa statistic of 0.884. Slides were photographed using a Leica DFC310FX camera attached to a DM2000 microscope with the LAS V3 software suite (Leica microsystems, 2014) with no additional filtering or post processing of images.

2.3.4 Statistical methods

Time from surgery to death was recorded as overall survival (OS) and non-cancer deaths or those lost to follow up censored at last recorded follow up. Progression free survival (PFS) was recorded as time from surgery to documented intracranial progression as assessed by neuroradiologists using standard (RANO) criteria(Quant

and Wen, 2011). Patients who died before this point were censored at the last date of follow up where there was no evidence of progression. Proportions were assessed using Fisher's two-sided exact test. Time to event comparisons were made using Kaplan-Meier survival analysis with Log Rank tests and multivariate analyses conducted using Cox's method. Data processing was performed using SPSS version 22.0 (IBM, Chicago, IL) and R version 3.10 (R Core (Team, 2013)).

2.4 Results

2.4.1 Exploratory immunohistochemical staining

Of 138 BMs assessed retrospectively, sixteen were negatively stained for OPN (11.6%) and 122 (88.4%) were positively stained in varying proportions and intensities. This staining was mainly cytoplasmic with a stippled pattern, although some nuclear staining was also noted (**Figure 2.2A**). For AGR2 38 (27.5%) BMs were negatively stained, whilst 100 (72.5%) showed cytoplasmic staining. BMs from the posterior fossa that included cerebellar cortex showed incidental positive staining of what appeared to be the granule cells, but this did not affect the tumour staining analysis (**Figure 2.2B**). Assessment for S100P staining was positive (nuclear and cytoplasmic) in 102 BM (73.9%) cases, negative in 36 (26.1%). In areas of white matter adjacent to tumour, occasional astrocytes were seen to stain with anti-S100P antibody (**Figure 2.2C**), however, morphology and staining of serial sections with GFAP clarified that these were not tumour cells, thus avoiding any false positives. Glial staining for the purposes of this study was not considered further. For S100A4, 32 BMs (23.2%) were negative and 106 (76.8%) stained to some degree (**Figure 2.2D**). Staining was both nuclear and cytoplasmic, however smooth muscle and endothelium were also seen to stain avidly with this antibody as noted previously. There was no staining of astrocytes nor peritumoural staining for S100A4 or OPN (**Figure 2.2 A,D**). The heterogeneity of tissue staining was better appreciated in lower power micrographs (**Figure 2.3**). There was no staining with antigen-blocked immune serum (**Figure 2.2**) or with non-immune serum (**Figure 2.4**) as negative controls. The majority of BMs (113 or 81.9%) showed no immunoreactivity for

FANCD2: only 25 (18.1%) showed weak cytoplasmic staining and there was no nuclear staining in any cases.

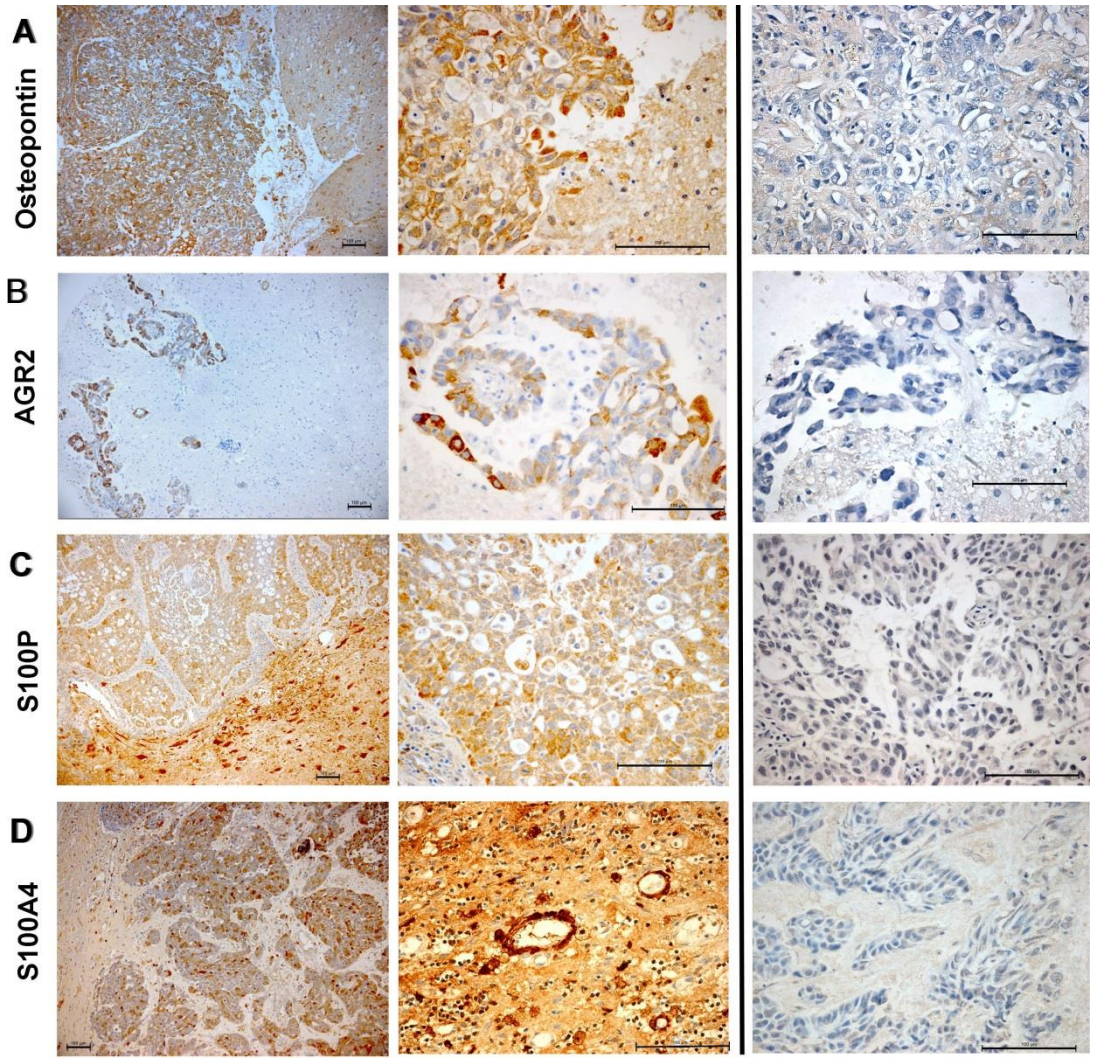

Figure 2.2: Staining for the Metastasis-Inducing Proteins in human brain metastases. A. Osteopontin in the tumour cytoplasm of a lung adenocarcinoma metastasis with some staining of the neuropial material in adjacent white matter. White matter and microglia, astrocytes were easily distinguished morphologically from tumour cells and their staining was not counted when scoring slides. B. AGR2 staining was seen mainly in the cytoplasm with no uptake in surrounding white matter as shown in this lung adenocarcinoma metastasis. C. S100P staining in a lung adenocarcinoma with adjacent white matter shown – this protein, as in previous studies, was overexpressed in connective tissue and smooth muscle. D. Nuclear and cytoplasmic staining for the protein S100A4 is shown in a brain metastasis from a breast carcinoma with avid staining of the endothelium also demonstrated. Taken at x100 and x400 magnification with scale bars shown (=100µm) and antigen-blocked immune serum controls given alongside.

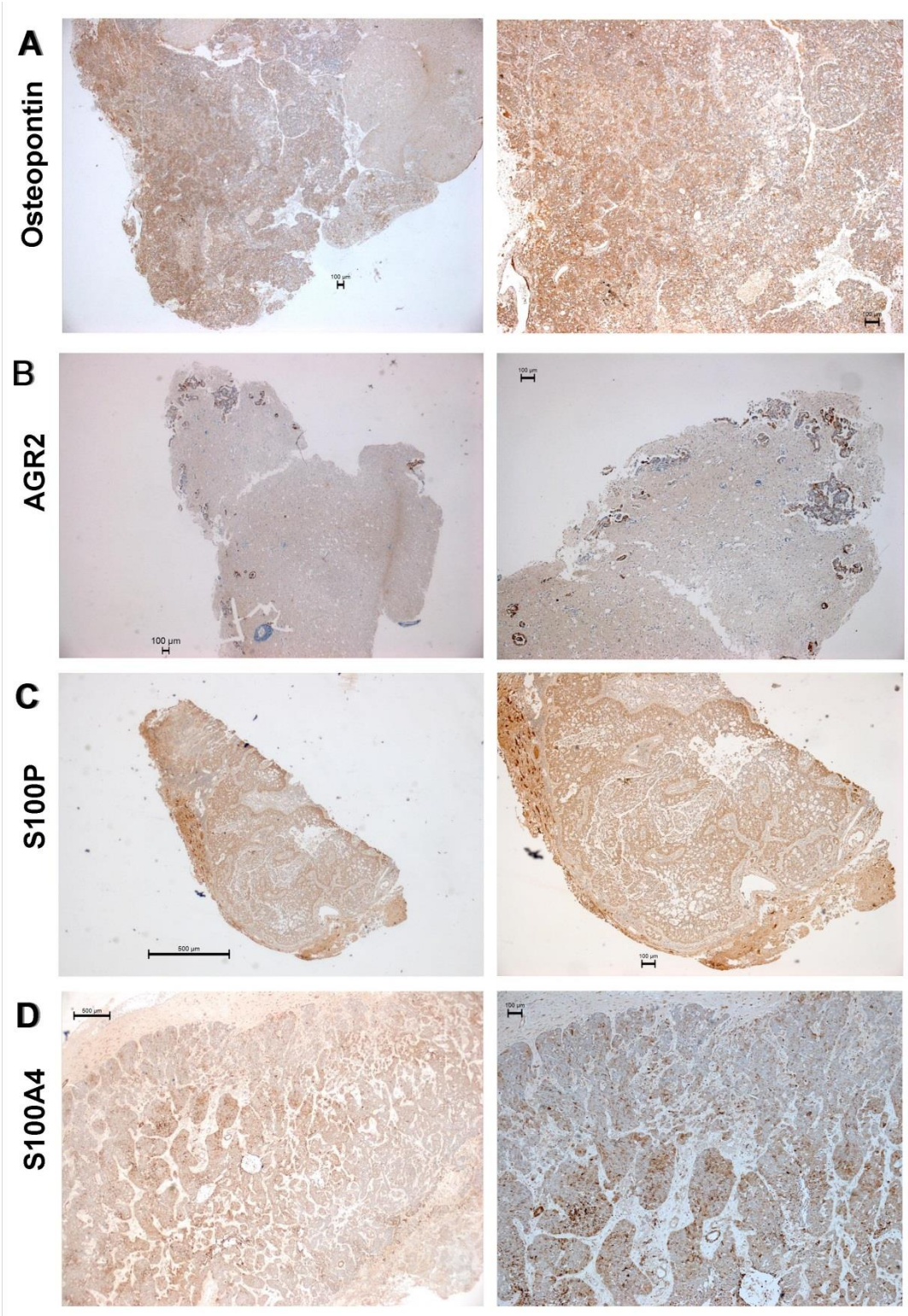

Figure 2.3: Photomicrographs at lower magnifications to demonstrate intratumoral heterogeneity of staining.

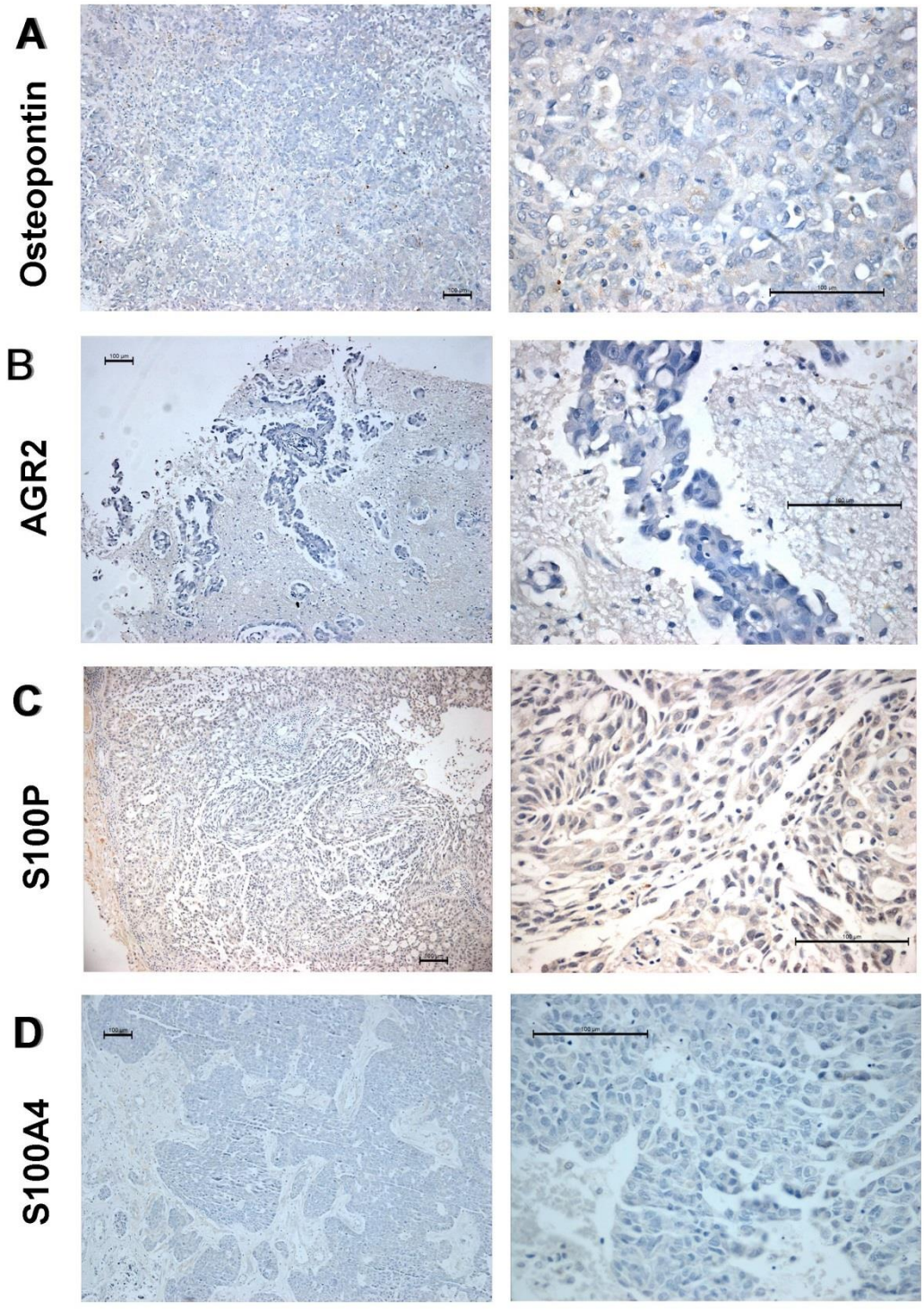

Figure 2.4: Negative controls: Non immune sera consisting of mouse IgG (Abcam) for mouse monoclonal antibodies (OPN & S100P) and rabbit IgG (Abcam) for rabbit polyclonal antibodies (S100A4 & AGR2) were substituted for primary antibodies and were included in each staining run.

2.4.2 Association between MIPs and primary cancer type, clinical features

Figure 2.5 and **Table 2.3** show positive BM staining for each MIP by primary cancer type. There was no significant variation in BM staining for the S100 proteins by primary cancer (Fisher's Exact test for S100P p=0.279, S100A4 p=0.135). There were significantly more AGR2 positive colorectal and non-small cell lung cancer BMs than expected ($p<0.001$) but fewer OPN positive lung cancer BMs of all types (p=0.033). Importantly, none of the clinical features which are traditionally used to determine prognosis in patients with BMs (Gaspar et al., 1997, Sperduto et al., 2008) were associated with positive staining for any of the MIPs (summarised in **Table 2.4**)

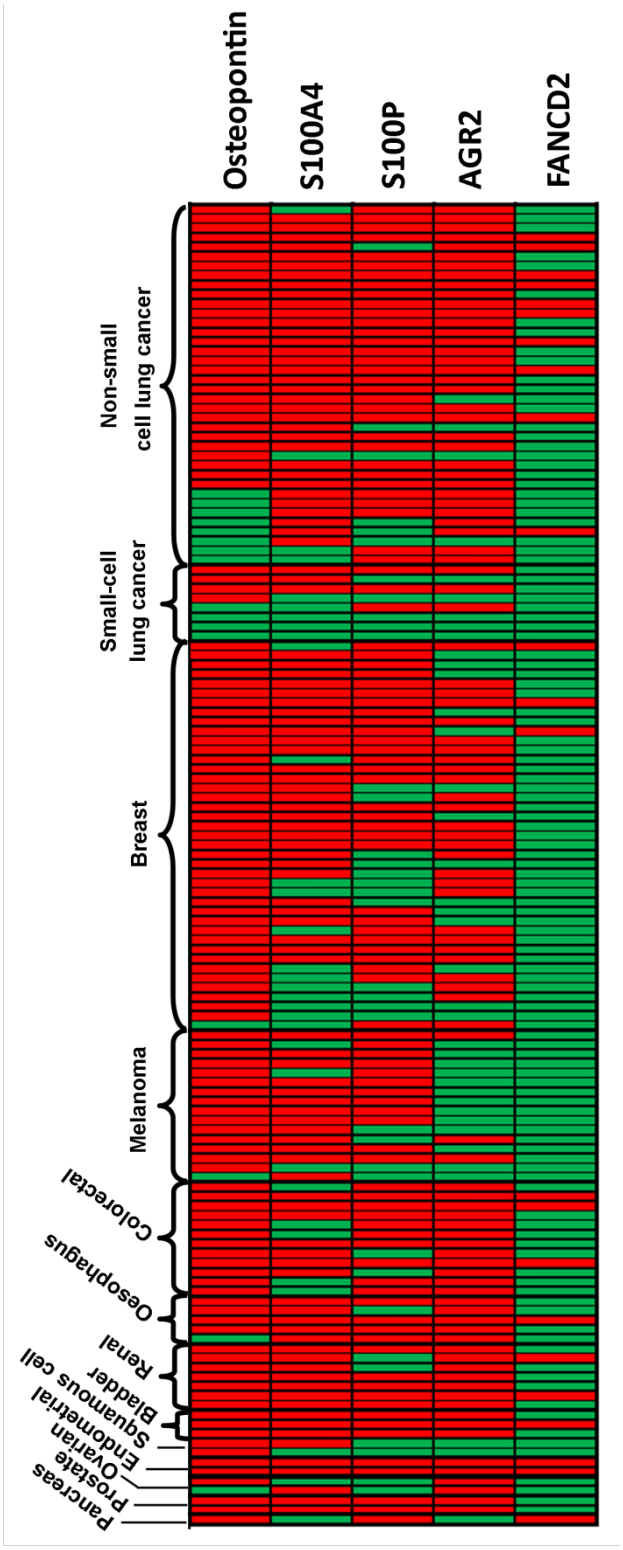

Figure 2.5: Binary heat map showing the immunohistochemical staining of 138 brain metastases removed at neurosurgery for the Metastases-Inducing Proteins osteopontin (OPN), S100A4, S100P, anterior gradient 2 (AGR2) and FANCD2. Brain metastases are grouped by the primary cancer of origin with red squares showing positive staining of any degree (≥1% carcinoma cells stained) and green squares indicating negative staining.

Table 2.3: Table showing the proportion of brain metastases from different primary cancers staining positively (1% or above of cells positively stained to any degree) for each Metastasis Inducing Protein.

Primary cancer and number of cases		Osteopontin		S100A4		S100P		AGR2	
		negative	positive	negative	positive	negative	positive	negative	positive
Breast	40	2%	98%	30%	70%	30%	70%	35%	65%
Non-small cell lung	38	21%	79%	11%	89%	16%	84%	11%	89%
Small cell lung	8	50%	50%	62%	38%	62%	38%	50%	50%
Melanoma	16	6%	94%	19%	81%	25%	75%	81%	19%
Colorectal	12	0%	100%	42%	58%	17%	83%	0%	100%
Renal	7	0%	100%	0%	100%	29%	71%	0%	100%
Oesophagus	5	20%	80%	0%	100%	20%	80%	0%	100%
Bladder	3	0%	100%	0%	100%	0%	100%	0%	100%
Squamous cell	2	0%	100%	50%	50%	100%	0%	100%	0%
Ovarian	2	50%	50%	50%	50%	100%	0%	0%	100%
Prostate	2	0%	100%	0%	100%	0%	100%	0%	100%
Endometrial	2	0%	100%	0%	100%	0%	100%	0%	100%
Pancreas	1	0%	100%	100%	0%	0%	100%	100%	0%

Table 2.4: Relation of clinical factors to positive staining for the Metastasis Inducing Proteins and cytoplasmic FANCD2 in 138 resected brain metastases cases.

Factor & level		Osteopontin		S100A4		S100P		AGR2		FANCD2	
		negative	positive	negative	positive	negative	positive	negative	positive	negative	positive
Metastasis location	Post fossa	9%	91%	18%	82%	36%	64%	18%	82%	76%	24%
	Supra-tentorial	12%	88%	25%	75%	23%	77%	30%	70%	84%	16%
Number of metastases	Multiple	4%	96%	23%	77%	27%	73%	35%	65%	88%	12%
	Solitary	13%	87%	23%	77%	26%	74%	26%	74%	80%	20%
Synchronous presentation	No	8%	92%	23%	77%	24%	76%	29%	71%	87%	13%
	Yes	20%	80%	24%	76%	32%	68%	24%	76%	71%	29%*
Controlled primary	No	10%	90%	21%	79%	17%	83%	24%	76%	90%	10%
	Yes	7%	93%	23%	77%	26%	74%	31%	69%	85%	15%
Extra-cranial metastases	No	14%	86%	22%	78%	25%	75%	23%	77%	78%	22%
	Yes	6%	94%	26%	74%	28%	72%	36%	64%	89%	11%
Performance status	>70%	11%	89%	24%	76%	26%	74%	33%	67%	86%	14%
	<70%	14%	86%	22%	78%	27%	73%	14%	86%*	70%	30%*

*indicates significantly different proportion positive:negative staining than expected, Fisher's exact test, 2-sided, $p<0.05$

2.4.3 Association of MIPs with patient outcomes

Median OS was 7.67 months (95% CI: 4.45 – 10.89) with 10 censored cases and only age < 60 years (HR= 0.56, 95% CI: 0.33 - 0.94, p=0.028) was found to be independently associated with prolonged OS. There was no relation between positive MIP staining and OS (**Figure 2.6A** & **Table 2.5**). Amongst patients receiving adjuvant WBRT, OS was 3.43 months (95% CI: 1.36 – 5.51) for OPN negative cases but 11.20 months (95% CI: 7.68 – 14.72) for positive cases, Log Rank test, p<0.001. There was no confounding difference in age (Student's t-test, p=0.118), performance status (p=0.331) nor other clinical factors such as radioresistant tumour types (e.g. renal cancer BMs) between the groups to explain this effect. Different cut-offs for positive staining were used to check if the percentage of tumour cells staining positive related to response to WBRT. There was a non-significant trend to prolonged median OS after WBRT with increasing percentage of positively OPN stained tumour cells: 11.2 months if > 5%, 13.9 months if >25% and 15.9 months if >50% positively stained.

Thirty solitary metastases that were completely resected showed intracranial progression at a median of 18.9 months from surgery (95% CI: 6.54 – 31.26). **Table 2.6** lists the clinical factors associated significantly with prolonged PFS alongside MIP staining. As illustrated in **Figure 2.6B**, negative staining for S100A4 in the resected BM was the only factor independently associated with a longer PFS (HR for intracranial progression = 0.17, 95% CI: 0.04 – 0.74, p=0.018). Tumour heterogeneity was assessed using different cut-offs for positive staining and there was no difference in clinical factors or outcomes when assessing tumours with >5%,>25%,or >50% of S100A4 positive staining cells, illustrated for PFS in **Figure 2.6C**.

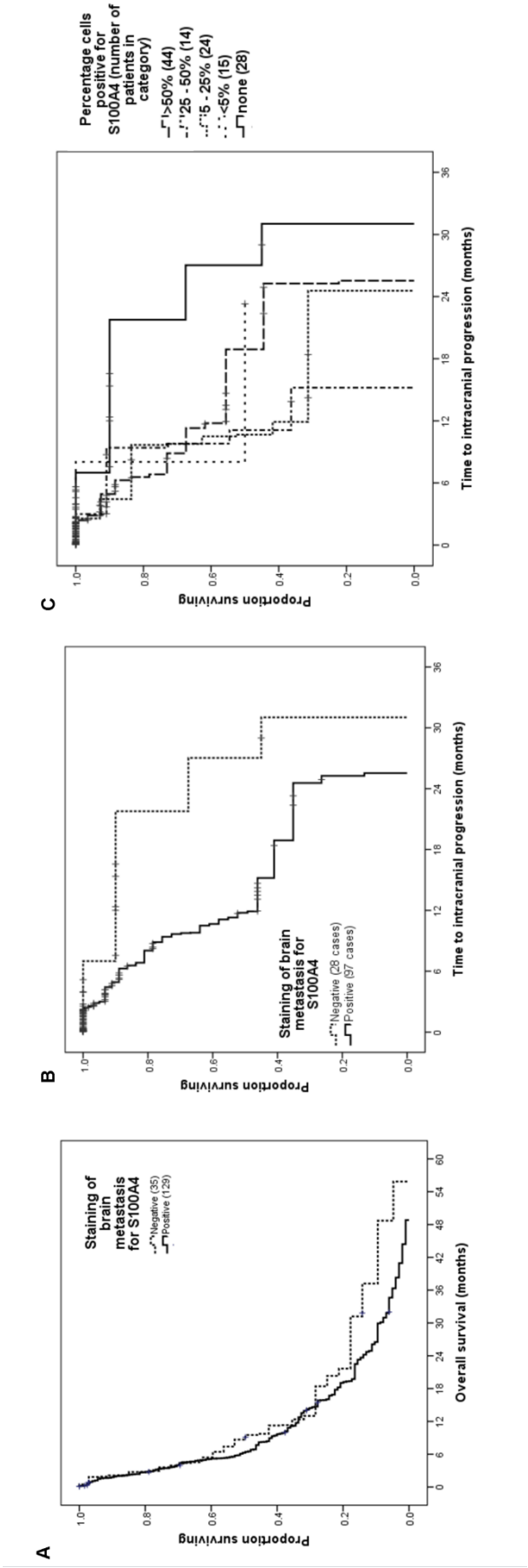

Figure 2.6: (A) Survival of patients with and (B,C) disease progression of 138 brain metastases from different primary sites. A. Proportion of patients surviving is plotted against overall survival time as Kaplan-Meier curves for positive (>1% carcinoma cells stained) and negative (<1% carcinoma cells stained) immunohistochemically stained brain metastases for S100A4. Survival time was not significantly associated with staining for S100A4 (Log rank test, p=0.222). B. Proportion of patients surviving without intracranial progression is plotted against time as Kaplan-Meier curves for positive and negative immunohistochemically stained brain metastasis for S100A4. These patients had a grossly resected tumour. Median time to progression was significantly shorter in cases staining positive for S100A4 (11.77 months, 95% CI: 7.07 – 16.47) versus negatively stained cases (27.03 months, 95% CI: 16.49 – 37.57), Log Rank test, p=0.007. This effect persisted in multivariate Cox analysis (HR 0.166, 95% CI: 0.04 – 0.74, p=0.018). C. S100A4 positive cases in B above are subdivided into categories by the proportion of carcinoma cells in the specimen staining to various degrees for the S100A4 protein (pooled Log-Rank test (4 df) = 9.806, p = 0.044). Ticks indicate censored data in all panels.

Table 2.5: Table showing the overall survival time for patients with a resected brain metastasis at different levels of common clinical factors and with positive or negative staining for the Metastasis Inducing Proteins and FANCD2. Log rank test statistics for comparison of survival (* = p<0.05) are given.

Factor	Median overall survival/ months	95% CI	Log rank & significance
Age			
<60 years	13.0	9.16 – 16.84	17.549
>60 years	3.77	2.48 – 5.06	p < .005*
Size of metastasis			
Diameter<30mm	9.43	3.34 – 15.53	2.883
Diameter>30mm	5.37	3.44 – 7.30	p =.09
Location of metastasis			
Supratentorial	9.30	5.99 – 12.61	1.302
Posterior fossa	4.90	3.05 – 6.80	p=.254
Number of metastases			
Solitary	7.67	0 – 15.95	0.23
Multiple	5.77	4.40 – 10.93	p=.879
Synchronous presentation			
Yes	4.93	1.55 – 8.31	5.627
No	9.73	5.27 – 14.20	p=.018*
Neurosurgery procedure			
Gross total resection vs.	8.27	4.79 – 11.74	9.131
Subtotal resection	2.93	0 – 6.08	p=.01*
Controlled primary disease			
Yes	13.97	10.24 – 17.7	6.753
No	4.53	3.84 – 5.22	p=.009*
Extra-cranial metastases			
Present	7.67	3.11 – 12.22	.159
Absent	6.83	2.88 – 10.79	p=.69
Performance status			
KPS<70%	3.93	2.07 – 5.79	19.21
KPS>70%	10.83	8.32 – 13.35	p=.000*
Adjuvant WBRT			
Yes	9.90	7.58 – 12.22	20.861
No	2.73	2.40 – 3.07	P<.005*
Adjuvant chemotherapy			
Yes	18.23	13.00 – 23.46	28.117
No	4.03	2.85 – 5.22	P<.005*
Primary			
Breast cancer vs.	14.23	9.21 – 19.26	
Non-small cell lung cancer	6.43	3.45 – 9.41	9.659
or melanoma	5.53	0 – 16.90	p=.022*
S100A4 staining			
Positive	6.83	5.59 – 13.41	1.21
Negative	9.50	3.51 – 10.16	p=.271
S100P staining			
Positive	7.40	3.07 – 11.73	1.652
Negative	8.37	3.63 – 13.10	p=.199
AGR2 staining			
Positive	6.83	3.93 – 9.74	.326
Negative	9.43	3.62 – 15.25	p=.568
OPN staining			
Positive	9.30	6.29 – 12.31	6.861
Negative	3.37	2.06 – 4.67	p=0.09
FANCD2 cytoplasmic staining			
Positive	6.83	2.37 – 11.29	.012
Negative	8.23	4.94 – 11.52	p=.912

Factor (events / total)	Median PFS / months (95% CI)	Log rank comparison & significance	HR (95% CI) & significance in Cox regression
Age			
<60 years (26 / 63)	11.3 (3.49 – 19.1)	4.813, p= 0.028*	0.97 (0.94 – 1.01), p=0.059
>60 years (4 / 62)	Not reached		
Performance status			
KPS>70% (30 / 90)	18.9 (6.54 – 31.26)	3.245, p=0.072	
KPS<70% (0 / 35)	Not reached		
S100A4 staining			
Positive (26 / 97)	11.77 (7.07 – 16.47)	7.295, p=0.007*	0.17 (0.04 – 0.74), p=0.018*
Negative (4 / 28)	27.03 (16.49 – 37.57)		
S100P staining			
Positive (24 / 95)	15.2 (6.16 – 24.25)	0.623, p=0.43	
Negative (6 / 30)	24.57 (0 – 49.5)		
AGR2 staining			
Positive (20 / 95)	21.77 (10.85 – 32.69)	1.117, p=0.291	
Negative (10 / 30)	11.10 (8.06 – 14.14)		
OPN staining			
Positive (28 / 110)	19.9 (6.25 – 31.5)	0.035, p=0.851	
Negative (2 / 15)	15.2 (NA)		
FANCD2 cytoplasmic staining			
Positive (4 / 23)	21.77 (6.88 – 36.66)	0.113, p=0.737	
Negative (26 / 102)	15.20 (4.96 – 25.44)		

Table 2.6. Clinical and biological factors associated with prolonged progression free survival time from resection to first brain progression. Significant relations highlighted (*).

2.4.4 Subtypes of BMs from common primaries

Forty patients with breast cancer were assessed separately and staining by subtype of breast carcinoma is shown in **Table 2.7**. The median OS was 14.23 months (95% CI 9.21 – 19.26) and negative staining for S100A4 was independently associated with longer OS (HR for death = 0.26, 95% CI: 0.08 - 0.80, p=0.019, **Figure 2.7A**) along with age <60 years (HR = 0.3, 95% CI: 0.11 - 0.81, p=0.017) and post-operative chemotherapy (HR = 0.12, 95% CI: 0.02 – 0.61, p=0.010). As an additional check, when the disease specific- graded prognostic assessment (DS-GPA) factors (Sperduto et al., 2010) for breast BMs (age, subtype of carcinoma and performance status) were combined in a model, the predictive value of staining for the protein

persisted (HR for death in S100A4 negative cases = 0.58, 95% CI: 0.35 - 0.96, p= 0.033). Intracranial progression occurred in 15/ 40 breast carcinoma patients and the 11 / 15 S100A4 positive cases showed significantly earlier intracranial progression (median 9.77 months, 95% CI: 8.28 – 11.25) than the 4 /15 negatively stained cases (median 27.03 months, 95% CI: 18.46 – 35.60, Log Rank test, p=0.023) (**Figure 2.7B**).

Breast Cancer Subtype (number)	**Osteopontin**		**S100A4**		**S100P**		**AGR2**		**FANCD2**	
	negative	positive	negative	positive	negative	positive	negative	positive	negative	positive
HER2 (18)	0%	100%	22%	78%	22%	78%	17%	83%	89%	11%
Triple negative (12)	0%	100%	33%	67%	50%	50%	67%	33%	92%	8%
Luminal (8)	0%	100%	38%	63%	25%	75%	25%	75%	100%	0%
Not specified (2)	50%	50%	50%	50%	0%	100%	50%	50%	100%	0%

Table 2.7: Staining of brain metastases for Metastasis Inducing Proteins and FANCD2 in patients with primary breast carcinomas by subtype.

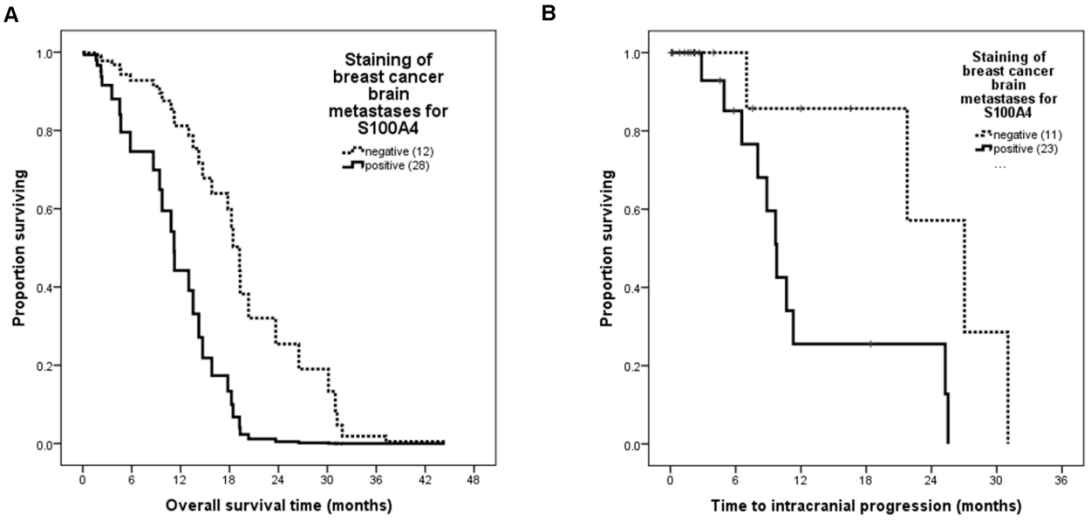

Figure 2.7: (A) Survival of patients with and (B) disease progression of 40 brain metastases from primary breast cancer stained for S100A4. A. Proportion of patients surviving is plotted against overall survival time as Kaplan-Meier curves for positive (>1% carcinoma cells

stained) and negative (<1% carcinoma cells stained) immunohistochemically stained brain metastases for S100A4. Positive staining in the brain metastasis was significantly associated with shorter overall survival in multivariate (Cox) analysis (HR of 0.26, 95% CI: 0.08 to 0.80, p=0.019) adjusted for age using the average covariate method (Makuch, 1982). B. Proportion of patients surviving without intracranial progression is plotted against time to intracranial progression as Kaplan-Meier curves for positive and negative immunohistochemically stained brain metastases for S100A4. Fifteen out of the 40 developed intracranial progression and of these, 11/15 cases which were positively stained for S100A4 showed significantly earlier progression (median 9.77 months, 95% CI: 8.28 – 11.25) than the 4 negatively stained cases (median 27.03 months, 95% CI: 18.46 – 35.60, Log Rank test, p=0.023). Ticks indicate censored data in all panels.

Non-small cell lung cancer patients had a median OS of 6.43 months (95% CI: 3.45 – 9.43) and 27 out of 38 received WBRT, this being the only factor associated with increased OS (HR of death if WBRT omitted = 3.07, 95% CI: 1.08 – 8.69, p=0.035) regardless of incorporating MIP staining or the DS-GPA factors. Only five of 38 patients developed intracranial progression - reflecting the burden of systemic disease on survival in these cases – but notably all of those BMs stained positively for S100A4.

There were 16 malignant melanoma cases and their median OS was 5.53 months (95% CI: 0.1 – 16.9). Incorporating the DS-GPA factors (number of BMs and performance status) with MIP staining showed that positive staining for S100A4 in the BM (13/16 cases) was the only factor independently associated with decreased OS (HR for death in negatively stained cases = 0.09, 95% CI:0.01 - 0.97, p=0.047). Only 5/ 16 patients developed intracranial progression, and notably all of the S100A4 positive BMs progressed.

2.4.5 Validation and investigation of intra-tumoural heterogeneity

Unselected BM samples from 24 prospectively treated patients were analysed, taking 1% as the cut-off for positive staining; 88% were S100A4 positive and 83% were OPN positive. This prospective validation cohort showed no significant differences from the retrospective cases in patient age, gender, size of operated metastasis, control of systemic disease, extracranial metastases or use of adjuvant chemo- and

radiotherapy. 19 / 24 patients received adjuvant WBRT and, as in the retrospective series, this conferred a survival advantage in OPN positive (6.3 months if irradiated vs 2.7 months if not, Log Rank test, p=0.001) but not in OPN negative cases (p=0.08). In total 9 of 24 cases showed intracranial progression and all of these were S100A4 positive (**Figure 2.8**). In the course of resection additional samples were obtained using image guidance at the leading edge of the BMs and all the MIPs showed a non-significant trend to a higher percentage of cells positive at the leading edge (Wilcoxon matched pairs analysis, p>0.05 for each MIP). S100A4 showed the greatest difference between percentage of positively staining cells at the edge and in the interior (ratio of 4.3 vs. 1.7 for OPN, 2.5 for AGR2, 3.2 for S100P) although this ratio was not associated with any clinical outcome, nor was it related to primary tumour type.

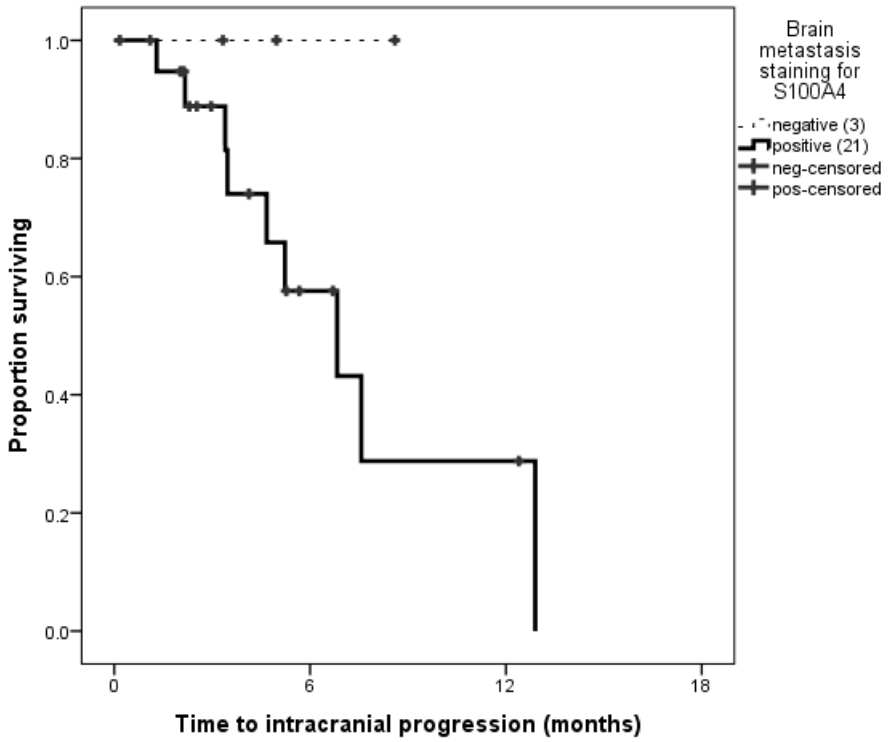

Figure 2.8: Kaplan-Meier plots showing time to intracranial progression for prospectively-analysed brain metastases of patients undergoing resection. All 21 cases with progression up to 13 months had stained positively for S100A4 although there was no significant difference in survival by the Log rank test (= 1.62, p = 0.203) compared to the 3 negatively stained cases.

2.4.6 Relationship of S100A4 staining to development of brain metastases

Given the relation of S100A4 overexpression to progression, the association of S100A4 with *risk* of BMs in patients with known cancer was investigated. In a series of breast cancer patients with BMs, 22 / 27 of primary tumours (81%) were S100A4 positive compared to 18/117 (15%) in a group with known non-metastatic breast cancer (Rudland et al., 2000, de Silva Rudland et al., 2011) as shown in **Figure 2.9** (Fisher's Exact test, $p<0.0001$). The median time until development of BMs after diagnosis of breast cancer was 25.5 months (95% CI: 20.1 – 30.9) and was no shorter in the S100A4 positive cases (Log Rank test $p=0.67$).

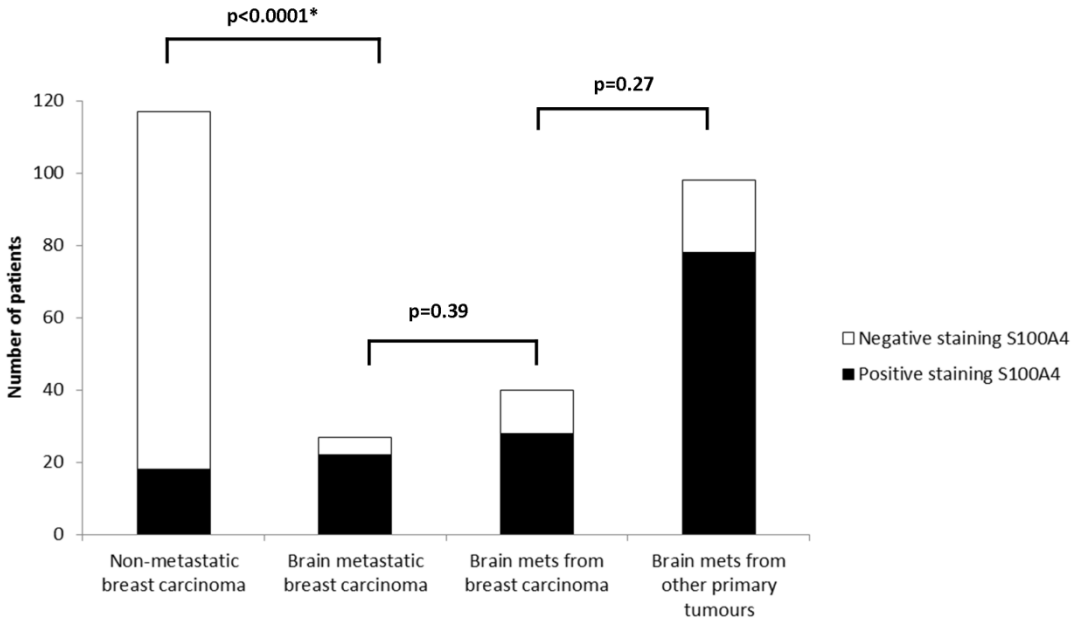

Figure 2.9: Comparison of staining for S100A4 in non-metastatic and brain metastatic breast cancers. The proportion of primary tumours staining positively for S100A4 in a group of previously reported patients with non-metastatic breast carcinoma surviving over 20 years was found to be significantly different from that of a group of breast carcinoma cases known to be brain metastatic (Fisher's Exact test, $p<0.0001$). There was no significant increase in S100A4 positivity in the breast BMs themselves compared to the primary breast tumours nor in the proportion of S100A4 positive staining in BMs from other primaries compared to those from primary breast cancer (Fisher's Exact test, $p=0.39$, $p=0.27$ respectively).

2.5 Discussion

We have shown for the first time that proteins which are (i) mechanistically proven to be involved in extracellular matrix adhesion and cell migration *in vitro*, (ii) convey a metastatic phenotype - including to brain - when overexpressed in animal models and (iii) are predictive of clinical outcomes in a variety of solid organ cancer cohorts, are *also* highly expressed at the protein level in human BMs and associate with important clinical outcomes. Previous publications have shown that the degree of immunohistochemical staining of carcinoma cells for the proteins described, OPN (Rudland et al., 2002), S100A4 (Rudland et al., 2000), S100P (Wang et al., 2006), AGR2 (Barraclough et al., 2009) and FANCD2 (Rudland et al., 2010) reflect the level of each particular protein in the specimens.

2.5.1 Association of S100A4 with patient outcomes and possible clinical applications

We found comparable OS to other large, multicentre series of BM patients with age and performance status again shown to be strong predictors of outcomes (Sperduto et al., 2008, Gaspar et al., 1997). Additionally, we find that S100A4 was expressed in all progressing melanoma and non-small cell lung cancer BMs as well as being independently associated with time to intracranial progression in breast cancer - where patients had the longest overall survival time - but not in lung cancer, where patients were less likely to die from their brain disease. This result holds true even when known clinical predictors for each tumor type are incorporated into multivariate models (Sperduto et al., 2008) and suggests that S100A4 has some role in spreading in the brain microenvironment; in support of this suggestion the protein was seen to be expressed at the leading edge of BMs in image-guided samples. It is known that S100A4 can reduce the formation of focal adhesions between cellular filopodia and the extracellular matrix via myosin heavy chain IIA to cause cell migration, invasion and metastasis (Gross et al., 2014) and thus it may represent a novel biological marker or a potential drug target. There is already interest in this protein as a monocloncal antibody target in metastatic melanoma and pancreatic cancer, following evidence that this family of proteins is a marker of aggressive, advanced tumours (Weide et al., 2013) (Hernandez et al., 2013).

2.5.2 Relationship of different proteins to BM development

Although staining for three MIPs is somewhat elevated in these BMs, only that for S100A4 show a significant association with clinical outcomes in the form of time to intracranial progression in all BMs, and OS in breast cancer and melanoma BMs. Since positive staining for S100A4 occurs more often in advanced rather than in early breast cancers in contrast to the other three MIPs (de Silva Rudland et al., 2011, Winstanley et al., 2013), it may be that only S100A4 plays a role in the subsequent progression of those patients with BMs, whilst the other three MIPs stimulate earlier and different steps in the metastatic pathways.

2.5.3 OPN as a marker of radiosensitivity

Although WBRT remains a pragmatic and readily available adjuvant treatment for BMs, there is concern regarding the cognitive effects in survivors and alternative post-operative management strategies are proposed. Using a simple BM marker to stratify patients as good or poor radiation responders would therefore be an extremely useful clinical tool. Regarding therapeutics, cilengitide, an αvβ3/αvβ5 integrin inhibitor known to have efficacy in the brain microenvironment, appears to enhance radiation response in preclinical breast cancer BM models (Lautenschlaeger et al., 2013). It is therefore logical that negative expression of OPN, an αvβ3/αvβ5 integrin ligand, may predict reduced OS from adjuvant WBRT compared to OPN positive cases and this result merits further investigation.

2.5.4 Limitations

Although retrospective data, particularly for performance status is undesirable, a wide range of different tumor types are represented in sufficient numbers to allow lung, breast and melanoma to be explored separately and there were no missing data fields. To validate either protein as a clinical biomarker, a larger prospective study would be required recording tumour and possible also serum IHC levels of S100A4 and OPN alongside clinical outcomes (Dancey et al., 2010). MRI of asymptomatic patients at regular, e.g. 2 monthly follow up, would have captured more detail on

intracranial progression, reducing censored data in this category and clarifying if this were at the site of surgery, distant or leptomeningeal (an under-recognised phenomenon).

2.6 Acknowledgments

With thanks to Brain Tumour North West, Dr Carol Walker, Dr Helen Wong and Mrs Linda Roberts for assistance in obtaining clinical data and specimens.

Chapter 3: MRI markers of local invasion

3.1 The reliability of routine clinical post processing software in assessing potential diffusion weighted MRI biomarkers in brain metastases

3.1.1 Abstract

Background & purpose: Diffusion MRI characteristics have been used as biomarkers to guide prognosis in cerebral pathologies including brain metastases. The measurement of ADC is often described poorly in clinical and research studies, with little detail given to the practical considerations of where to place ROIs, which post processing software package to use and how reproducible the resulting metrics will be.

Method: We investigated a series of 12 patients with brain metastases and preoperative DWI. Three post processing platforms were used and ROI were placed over the tumour, peritumoural region and brain-tumour interface. These recordings were made by a neurosurgeon and a neuroradiologist. Inter- and intra-observer variability was assessed using Bland-Altman analysis.

Results: There was excellent correlation between the software packages used for all measures including assessing the whole tumour, selective regions with lowest ADC, the change of ADC across the brain-tumour interface and the relation of the tumour ADC to peritumoural regions and the normal white matter. There was no significant inter- or intra-observer variability for repeated readings. There were significant differences in the mean values obtained using different methodologies.

Conclusion: Diffusion weighted MRI metrics offer promise as potential non-invasive biomarkers in brain metastases and a variety of metrics have been shown to be reliably measured using differing platforms and observers.

3.1.2 Introduction

As discussed in the first chapter, diffusion weighted magnetic resonance imaging (DWI) has traditionally been applied to a variety of practical clinical problems relating to brain metastases such as differentiation from an intracerebral abscess, but more recently parameters such as the tumour ADC have been shown to correlate with survival from brain metastases independently of other factors as well as predicting grade, invasiveness and survival in a variety of other adult and paediatric brain tumours (Berghoff et al., 2013c, Price and Gillard, 2011, Barajas Jr et al., 2010, Porto et al., 2013). These metrics have therefore been recommended as "imaging biomarkers" which could be integrated with traditional, widely validated tools for predicting prognosis and deciding which patients with brain metastases should receive treatments such as the recursive partitioning (RPA) or graded prognostic assessment (GPA) classifications (Gaspar et al., 1997, Sperduto et al., 2010). If these radiological metrics are to be used in routine clinical practice more information is urgently needed on how they are practically taken and whether comparable values are obtained on different post processing platforms. This information is often lacking from studies or, if included, is prohibitively complicated for use outside the research setting. Therefore a multidisciplinary group consisting of neurosurgeons, neuroradiologists, MR physicist and oncology researchers have retrospectively examined a series patients with brain metastases to measure a comprehensive range of DWI metrics on different software platforms – including two of the most widely available commercial solutions - so that performance and reliability could be formally assessed as a prelude to investigation of the diagnostic and prognostic impact of DWI in a larger clinical cohort.

3.1.3 Materials and methods

3.1.3.1 Clinical series

Twelve patients who had undergone DWI preoperatively followed by resection of a brain metastasis were identified from a database of histological samples at our institution spanning the period 2007 – 2012. The age at presentation, primary tumour type, size of resected lesion, RPA and GPA class of patients are detailed in **Table**

3.1. Of note, 11 of 12 patients had solitary metastases; case #10 had a small 2-3mm deposit in addition to the main lesion. All patients were recorded in the operating notes by the surgeon and on post-operative imaging to have undergone gross total resection. All patients underwent post-operative whole brain radiotherapy (30 Gray in 10 fractions) according to our local protocol and adjuvant chemotherapy for the primary tumour in all cases as determined by the treating oncologist. As seen in **Table 3.1** half of all cases showed local recurrence, at which point two had further treatment (case #1 had stereotactic radiosurgery and case #8 underwent repeat cranial surgery) and the remainder were managed palliatively. Eleven patients died and one had incomplete follow up.

Table 3.1: Clinical characteristics and outcomes for 12 patients studied, all of whom underwent MR brain including diffusion weighted MRI before surgical resection at a single centre.

Case #	Age/yrs	GPA score	RPA class	Primary cancer	Volume/cc	Necrosis/%	Overall survival/months	Time to local recurrence/months
1	48.4	4.0	1	Lung non small cell	4.5	50	34.77	15.87
2	38.0	4.0	1	Breast	6.9	56	9.90	3.80
3	61.9	3.0	1	Breast	5.8	45	21.47	13.13
4	58.5	3.5	1	Breast	21.0	42	11.13	6.87
5	76.2	2.0	2	Lung non small cell	10.6	29	16.73	16.10
6	50.0	3.5	1	Lung small cell	55.4	42	4.33	0.30
7	56.7	2.0	2	Melanoma	7.4	44	11.70	7.40
8	70.3	3.0	2	Lung non small cell	40.8	73	10.60	7.77
9	35.9	4.0	2	Lung non small cell	16.0	44	14.60	13.30
10	54.8	3.0	1	Ovarian	4.8	50	18.67*	18.67*
11	70.8	2.5	2	Ovarian	2.4	0	4.80	4.43
12	57.9	3.0	1	Melanoma	6.3	42	4.50	3.93

yrs = years, GPA = graded prognostic assessment, RPA = recursive partitioning analysis, cc = cubic centimetres.
* Censored data as patient moved out of region upon recurrence and was not followed up locally.

3.1.3.2 Imaging acquisition and analysis

All patients underwent MRI brain scans on a variety of 1.5T Philips whole body systems with single channel head coil at different local institutions before transfer to the Regional Neuroscience Centre. The imaging included DW images using one acquisition over 90 seconds through single-shot echo planar imaging with 2 b values of 0 and 1000 second/mm^2 in all cases as well as other sequences, as determined by the local institution's protocol. MR parameters differed between institutions, but were in the following range: slice thickness 6mm for all, TR 2515 - 3513 msec, TE 71-94 msec; FOV 128x128mm (n=5) or 256x256mm (n=7). Isotropic DW maps and ADC maps were calculated and subsequent readings taken using three different post processing software packages: GE FuncTool version 4.5.5 (General Electric Co., Maryland, USA), Philips Extended MR workspace (EWS) version 2.6.3.1 (Philips

Medical Systems, Netherlands) and DTI Studio version 3.0.3 (H Jiang & S Mori, Johns Hopkins University, Baltimore, USA) running on a Windows platform. The first observer, a clinical research fellow in neurosurgery with no higher radiological training took the readings described below and shown in **Figure 3.1**. A second observer with 10 years specialised training in neuroradiology took repeat readings of all metrics for all patients. Before any analysis of results, at a delay of 6-8 weeks from initial recording, the first observer then took repeat observations on the same platform of all metrics for all patients.

Figure 3.1 demonstrates the position of regions of interest (ROI) for recording each metric:

- **Whole tumour ADC**: The axial slice with the largest area of tumour is identified and a freehand ROI is created using the tumour border. Average values were obtained and repeated on the slices immediately above and below using the same method, the mean of the three being the "whole tumour ADC". This method generates a maximum and minimum reading for the given ROI and the minimum ADC was also recorded and averaged over 3 slices, to give the **ADCmin.**
- **ADCmean**: Next an alternative method for taking the ADC within each tumour was ascertained by placing as many 50mm^2 regions of interest (ROI) as could be accommodated within the borders of the tumour on each axial slice, avoiding areas of cyst, necrosis or haemorrhage, and taking the mean (the ADCmean). Cases with extensive (>25%) haemorrhage were excluded as diffusion analysis would have been meaningless. Up to four control readings were also taken from the unaffected contralateral white matter so that ADCmean values could be adjusted to this (**ADC normalised**).
- **Peri-tumoural region**: Readings (up to 3 on contiguous slices) of the near and far peritumoural region were taken, defining the "peri-tumoural region" as the extent of signal abnormality on the T2-weighted sequence and "near" as <1cm from the tumour edge.
- **ATC**: Finally to assess the tumour-brain interface, the gradient of change of the ADC across the tumour edge and into brain, the "ADC Transition Coefficient" or ATC was calculated as previously described (9).

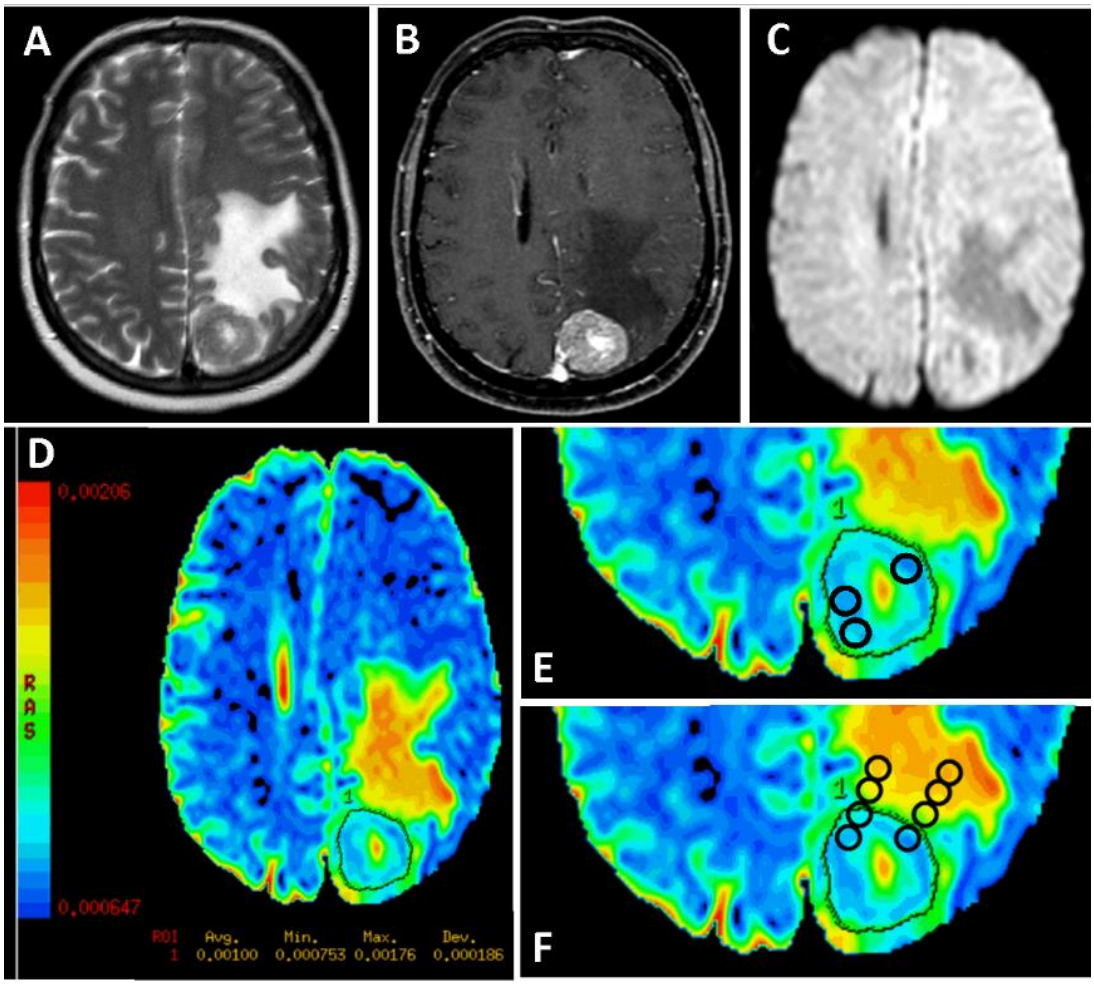

Figure 3.1: Method of recording metrics for use as potential biomarkers from an ADC map.
A. T2 weighted MRI brain showing a solitary occipital mass and surrounding oedema in a patient with known breast cancer presenting with headache & visual disturbance.
B. The lesion shows enhancement with an area of central lower signal, possibly necrosis, on T1 weighted sequence after administration of gadolinium contrast medium.
C. Diffusion weighted image of the same slice showing the mean of three gradients at B=1000.
D. This is used to generate an ADC map as described and the whole tumour is encircled with a freehand region of interest (ROI) to record the "whole tumour ADC" and minimum ADC (ADCmin) of the lesion.
E. Multiple ROI are placed inside the tumour avoiding cystic, necrotic and haemorrhagic areas and the values averaged to give the ADCmean.
F. Regions of interest are placed across the brain-tumour boundary and the gradient of change of ADC calculated in up to 3 directions on up to 3 slices and the mean taken to yield the ADC transition coefficient, or ATC.

3.1.3.3 Statistical methods

Data were analysed and graphs generated using standard methods on Statistica version 6 (StatSoft, Inc. 2003) and GraphPad Prism version 6.02 (GraphPad

Software, California USA). The level of significance was set at 95% to reject the null hypothesis and all p-values are stated in R**esults.** Intra-class correlation coefficients were plotted to determine if readings for a given metric but different platforms were from the same population and individual r values for each comparison are listed. Bland-Altman plots of the mean versus the difference for intra- and inter- observer reliability comparisons are shown with confidence intervals (95%) or bias is shown in tables. Group means for each metric are compared with student t-tests and tests for normality and variance stated where applied.

3.1.4 Results

3.1.4.1 Measures of tumour ADC

Whole tumour ADC varied between 0.68 and 1.307 10^{-3} mm^2 /s with values for each individual case are shown in **Figure 3.2** along with measures of correlation between the three platforms and Bland-Altman analysis for both intra- and inter-observer reliability. This method, which used a single freehand ROI drawn around the whole tumour, produced consistent readings across platforms and observers. The same analysis was applied to the ADCmin, ADCmean and normalised ADC metrics with similar agreement between platforms (shown in **Table 3.2**) and between observers (**Table 3.3**). Finally the different measures of tumour ADC (whole tumour ADC, ADCmin & ADCmean) were compared to one another. Significant differences were found between the group means for each metric, as shown in **Figure 3.3**, despite a strong correlation between whole tumour ADC and ADCmean ($r=0.8855$, $p<0.05$). The normalised ADC is a ratio of ADCmean to contralateral white matter and has no units but showed significant correlation with both ADCmean ($r=0.98$, $p<0.01$) and whole tumour ADC ($r=.8746$, $p<0.05$).

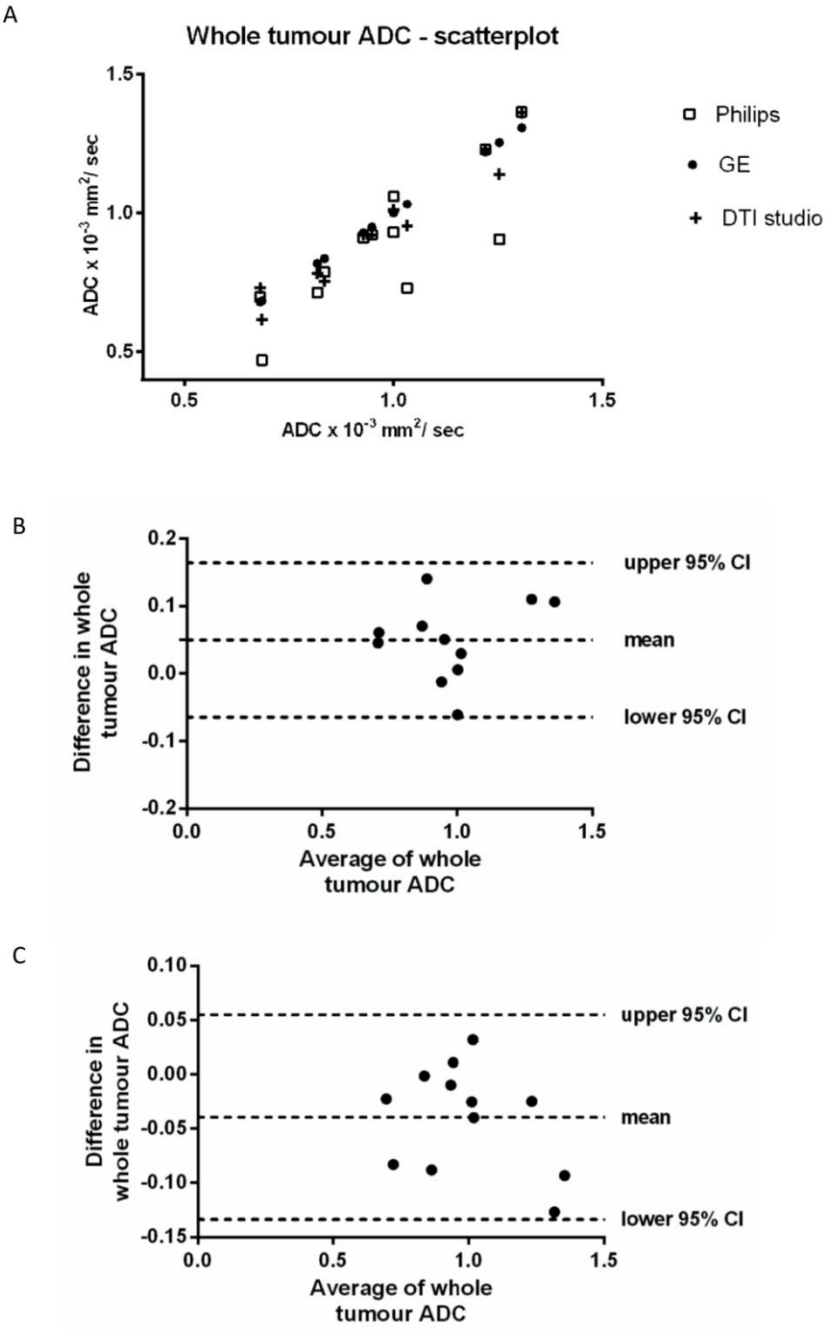

Figure 3.2: Analysing a metric as a potential biomarker. Three different post processing platforms are used to construct an ADC map from baseline DWI sequences and take readings.

A. Whole tumour ADC readings using Philips EWS and DTI studio software are plotted against those taken on the GE FuncTool software and Pearson correlation coefficients calculated, indicating highly significant correlation with r = 0.82 (P<0.01, 95% CI: 0.48 – 0.95) for Philips EWS vs. GE FuncTool and r = 0.96 (P<0.01, 95% CI: 0.89 – 0.99) for DTIstudio vs. GE FuncTool.

B. Bland-Altman plots of mean and difference of whole tumour ADC readings for a second observer with the 95% confidence intervals and the mean (bias) shown.

C. The same analysis is conducted for repeat readings taken by the original observer, indicating again that there is good agreement with all points within the 95% confidence intervals shown in dashed lines.

	Intraclass correlation coefficient		
Reading	GE Functool vs. DTI studio	GE Functool vs. Philips EWS	DTI studio vs. Philips EWS
Whole tumour ADC	0.986	0.945	0.968
ADC mean	0.964	0.973	0.954
ADC min	0.943	0.963	0.958
ATC	0.870	0.909	0.736
Normalised ADC	0.968	0.949	0.968
Near peritumoural ratio	0.938	0.912	0.846
Far peritumoural ratio	0.815	0.807	0.717

Table 3.2: Starting with the same DWI base data, each metric was derived using three different software packages for each of 12 cases and the readings compared. All relations were highly significant with F test compared to True Value 0, $p<0.05$, ADC = apparent diffusion coefficient, ATC = ADC transition coefficient

Metric studied	Intra-observer reliability Bias (95% confidence interval)	Inter-observer reliability Bias (95% confidence interval)
Whole tumour ADC	−0.0394 (−0.1340 to 0.0548)	0.0498 (−0.0646 to 0.164)
ADC mean	−0.0167 (− 0.1743 to 0.1409)	−0.0284 (− 0.2013 to 0.1445)
ADC min	−0.0065 (− 0.1406 to 0.1275)	0.0121 (−0.1259 to 0.1501)
ATC	−0.0509 (− 0.1470 to 0.0457)	−0.0153 (− 0.1200 to 0.0896)
Normalised ADC	−0.0260 (− 0.2912 to 0.2392)	−0.0322 (− 0.2288 to 0.1644)
Near peritumoral	0.0126 (− 0.2260 to 0.2513)	0.0618 (− 0.1679 to 0.2916)
Far peritumoral	0.0137 (−0.2074 to 0.2348)	−0.0109 (− 0.1213 to 0.0996)

Table 3.3: Bland-Altman analysis was performed on pairs of readings for each metric to investigate the variation between the same observer and between two independent observers. Bias (the mean difference) and confidence intervals are shown for each metric and each comparison.

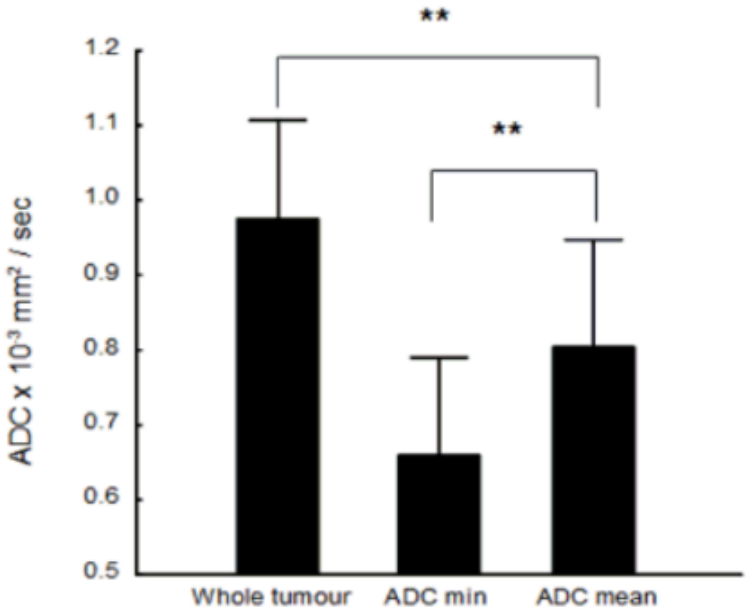

Figure 3.3: The ADC values for the 12 cases are demonstrated, as measured by 3 different methods. The whole tumour ADC is derived by drawing a single freehand region of interest around the tumour border on the axial slice with the largest area and repeating for the slices above and below. The ADCmin is the lowest value recorded within this region. The ADCmean is obtained by placing multiple (up to 4) regions of interest of 50mm^2 within the tumour avoiding cystic, haemorrhagic and necrotic regions. The ** indicates highly significant differences as assessed by the student t-test for dependent samples, with $p < 0.01$.

3.1.4.2 Assessment of the peritumoural region and brain-tumour interface

The ATC measured the rate of change of ADC across the interface from tumour into brain and was reliably measured by all three platforms, with correlations shown in **table 3.2**. It was noted that the correlation was not as strong as for other metrics which were directly measured rather than derived but nonetheless still significant. Ratios of the tumour to the near and far peritumoural region may reflect the intensity of surrounding peritumoural oedema and these measures were reliably measured by all three platforms with high intra- and inter-observer reliability as indicated in **tables 3.2** & **3.3**. The ratio of the far peritumoural region:tumour was significantly higher than that of the near region:tumour ratio for the group (t-test for dependent samples = 2.37, $p < .05$ having confirmed that both samples were normally distributed).

3.1.5. Discussion

3.1.5.1 Main findings and implications

The measurement of ADC is often described poorly in clinical and research studies, with little regard given to the practical considerations of where to place regions of interest, which post processing software package to use and how reproducible the resulting metrics will be. We have shown that using three widely available platforms, a number of metrics can be derived from DWI with minimal inter- and intra-observer variability and good agreement between software packages.

The way in which these metrics are taken (average readings, whole tumour readings, and minimum readings) does have an impact, as although the trends within the group correlated for each measure, the means obtained differ significantly in a given case. For example, we found lower mean ADC readings obtained when placing multiple ROI as compared to drawing a freehand ROI around the whole tumour outline, because the latter samples the central necrotic area of the mass in many cases (as demonstrated in **Figure 3.1**). Likewise we found no value in normalising to white matter *per se* in this case, although this is widely described in the literature and seems scientifically justified. This implies more clear definition of what method is

being used to measure "tumour ADC" and why, is required in studies reported in the literature.

3.1.5.2 Relation to existing studies of similar nature

Other researchers have examined the DWI characteristics of brain metastases. A study assessing the incidence of restricted diffusion in brain metastases of various primaries found similar readings to ours using a method of placing ROIs on the solid part of the tumour with the lowest ADC signal (Berghoff et al., 2013c). The authors could not find a relationship between histopathology and the ADC values in cases of restricted diffusion. Another retrospective series took ADC readings by averaging multiple ROI within tumour and found a similar range to ours (median 0.969 x 10^{-3} mm^2 /s) in 32 patients but also an association of higher ADC with prolonged overall survival (Duygulu et al., 2010). A further study compared the post-operative histology to preoperative DWI readings and found a correlation of various measures of ADC with cellularity but not specific primaries for a group of 13 operated cases (Hayashida et al., 2006). All these studies employed different methods to measure "tumour ADC" with little detailed explanation as to the rationale, exact methodology or post processing software used. Recent evidence supports the notion that small differences in methodology may cause variations in diffusion-based (ADC, tractography) metrics for healthy individuals (Bilgili and Unal, 2004, Urger et al., 2013, Ozturk et al., 2008) and there has been recent discussion about the reproducibility of perfusion MR parameters (Heye et al., 2013, Goh et al., 2013).

Other specialities which are utilising DWI metrics as biomarkers have begun to address these practical considerations. ADC readings from liver lesions in 48 patients taken using a "PACS" desktop system were compared with Philips and Siemens MR workstations to show there were no significant differences and the authors concluded that this should allow wider dissemination and use of such readings in patient care (El Kady et al., 2011). For colorectal cancer, the effects of ROI size and placement on reliability has been investigated, as well as the important question of how these metrics change in a given patient or tumour over time and during therapy (Lambregts

et al., 2011b). It has been shown that for healthy volunteers variations in voxel size do not affect ADC values (Oouchi et al., 2007).

3.1.5.3 Limitations

In order to determine whether the values obtained are inherent to the lesion, one would have imaged the same patient on different MRI machines (for example GE and Philips or 1.5T and 3T) and processed the baseline diffusion weighted sequences on both sets of software. In practice patients are at a late stage in systemic cancer treatment and are undergoing a second scan in order to obtain anatomical, fine cut sequences for use on image guidance software packages for surgical planning. A further MRI scan preoperatively simply to compare the platforms is unlikely to be ethically justifiable or acceptable to patients and this is, therefore, the best type of comparison one may be able to make. Patients were taking dexamethasone at the time of MRI scan and surgery so any effect on tumour or peritumoural regions should be comparable.

3.1.6 Conclusions

Diffusion weighted MRI may potentially provide non-invasive and widely available biomarkers of invasion and survival in brain metastases. This study confirms that reliable measurements can be obtained on clinically available software packages with minimal intra- and inter-observer variability. However, careful definition of how regions of interest are placed and what is being measured are needed in order to move forward.

3.1.7 Further study

Having shown that diffusion MRI measurements can be reliably taken using clinical data and platforms and investigated the methodology, a larger study was conducted to investigate the relation of these measurements to clinical outcomes in brain metastasis patients.

3.2 Diffusion weighted MRI characteristics of the cerebral metastasis to brain boundary predicts patient outcomes

3.2.1 Abstract

Background: Diffusion MRI has been used in neurological and neurosurgical practice mainly to distinguish cerebral metastases from abscess and glioma. There is evidence from other organs and disciplines that diffusion MRI may be used as a biomarker in various conditions. We therefore investigated diffusion weighted MRI characteristics of cerebral metastases and their peritumoural region recorded pre-operatively and related these to patient outcomes.

Methods: Retrospective analysis of data from 76 cases operated upon at a single institution. Diffusion weighted MRI was performed pre-operatively at 1.5T and maps of apparent diffusion coefficient (ADC) generated using standard protocols. Readings were taken from the tumour, peritumoural region, across the brain-tumour interface and in normal white matter. Patient outcomes were overall survival and time to local recurrence.

Results: Metastases from different primary cancers appeared to have different diffusion characteristics. These diffusion characteristics were strongly related to the cellularity of the metastases in a sample of cases that were analysed histologically. Patients having a metastasis with a higher ADC value preoperatively tended to survive longer and have better local control rates after surgery regardless of adjuvant therapies. This was not simply due to differences between the types of primary cancer, because the effect was observed even in a subgroup of 36 patients with the same primary, non-small cell lung cancer. For metastases of certain primary cancers, diffusion appeared to vary between near and far peritumoural regions, but these differences were not associated with patient outcomes. The change in diffusion across the tumour border and into peritumoural brain was more strongly predictive than ADC readings alone and metastases with a sharp change in diffusion across this border (measured by the "ADC transition coefficient" or ATC) had a significantly shorter overall survival and shorter time to local recurrence compared to those with a more diffuse edge. The ATC was the only imaging measurement which independently predicted overall survival in multivariate analysis suggesting this is a

powerful predictive measure even in a heterogeneous disease such as brain metastases.

Conclusions: Diffusion weighted MRI demonstrates changes in the tumour, across the tumour edge and in the peritumoural region which may not be visible on conventional MRI and this may be useful in predicting patient outcomes for cerebral metastases.

3.2.2 Background

As described in Chapter 1, when comparing cerebral metastases to glioma considerable attention has focused on the peritumoural region around the lesion (Wang et al., 2009, Tsuchiya et al., 2005, Toh et al., 2011, Stadnik et al., 2001, Lu et al., 2004, Lee et al., 2011, Chen et al., 2012b, Byrnes et al., 2011). A number of metrics from DWI including ADC values have been directly measured in this region and the "normal" range of values for a metastasis determined (Sternberg et al., 2013). The interaction of cerebral metastases and the surrounding brain tissue would be expected to be crucial to the development of therapies aimed at preventing further spread and invasion. Work on different methods of invasion - either co-opting existing blood vessels or inducing new blood vessel formation - has already led to anti-angiogenesis drugs for certain cerebral metastases (Kienast et al., 2010, Leenders et al., 2004). Furthermore, the degree of invasion of metastases may affect the margin used in existing treatments such as surgery and radiosurgery. Despite this potential clinical importance little has been done to investigate the invasiveness of cerebral metastases using MRI and nobody has compared the tumor and peritumoural ADC readings *within* a group of metastases. We therefore examined the MRI characteristics of the tumor, tumor boundary and peritumoural region for a series of patients with cerebral metastases who had undergone pre-operative MRI with DWI followed by surgery. We investigate whether patient outcomes such as survival and recurrence may be predicted by different DWI metrics.

3.2.3 Materials and methods

3.2.3.1 Patients

Patients with a diagnosis of cerebral metastasis were identified from a histopathology archive spanning the period 2007 – 2012 at a single institution. Records were searched and cases with a diffusion weighted MRI scan of the brain prior to first neurosurgical intervention were selected. Post-operative clinical course and oncology care including administration of whole brain radiotherapy (WBRT) or the use of adjuvant systemic chemotherapy were recorded from tumour board and patient notes as these were potential confounding factors. This study was conducted in accordance with the principles of the declaration of Helsinki. Ethical approval was granted as an internal project within the institution's research tissue bank (National Research Ethics Service # 11/WNo03/2) for which patients have to give written informed consent for inclusion.

3.2.3.2 Histological analysis

All cases had been reviewed by a consultant neuropathologist in the course of routine clinical care. A histological diagnosis of metastasis was made and primary tumour type suggested by review of H&E sections, tumour specific immuno-histo-cytochemistry and clinical correlation. Where original material was available an additional automated assessment of cellularity was then made "blind" to the clinical and imaging data. Five separate 200x magnification fields were photographed avoiding gross haemorrhage or necrotic material on the H&E slide. Using Image J software (U. S. National Institutes of Health, Bethesda, Maryland, USA 2007-2012) with no additional plugins the percentage area occupied by nucleus versus cytoplasm was determined using the measure function. A second independent observer, a cellular pathology researcher of 30 years' experience then repeated this analysis using a grid and microscopy alone.

3.2.3.3 Image analysis

MRI parameters and methodology have been described in **Section 3.1**. A number of different assessments of diffusion were made for each metastasis from the DWI scan and resulting ADC map and these are summarised once again in **Figure 3.4**.

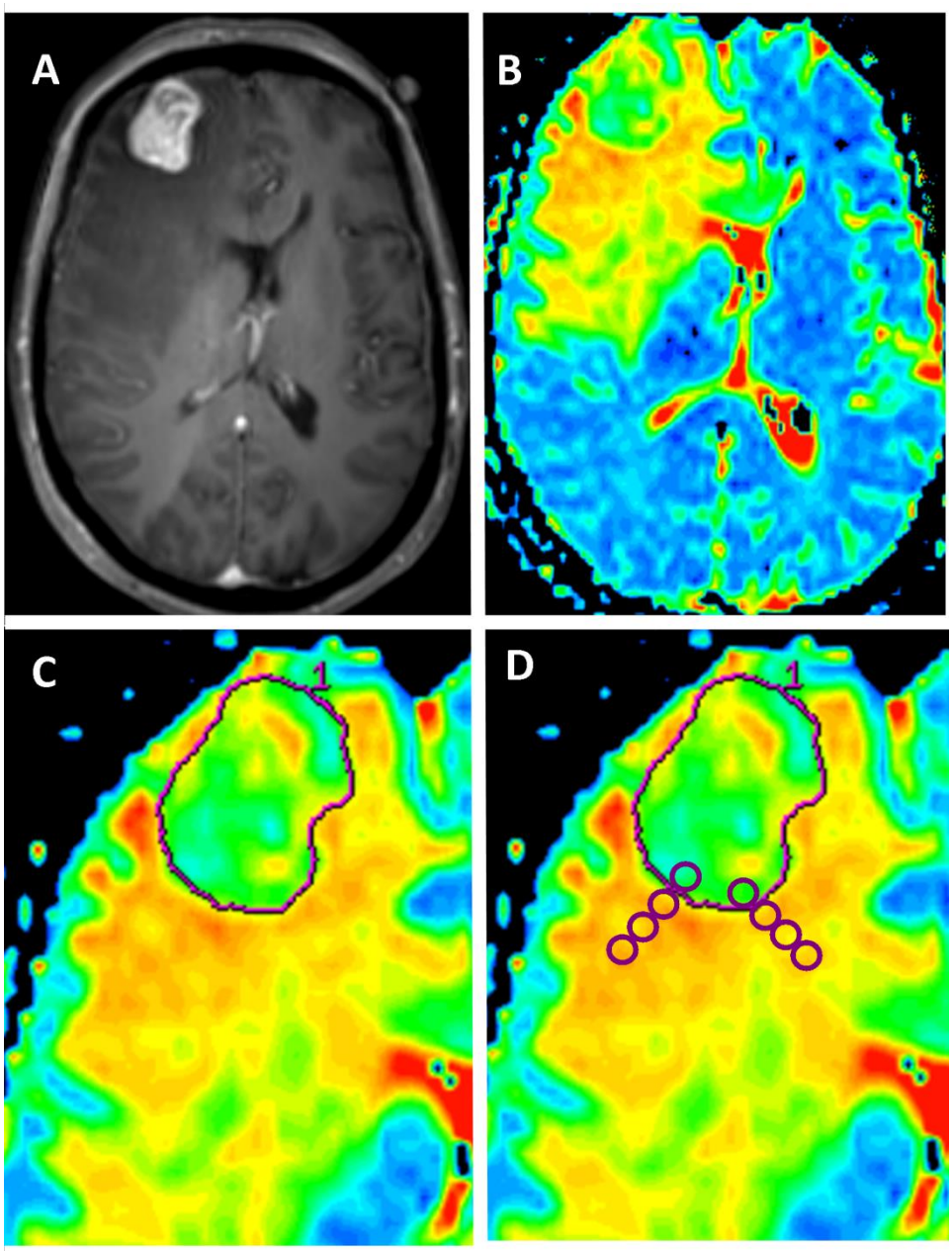

Figure 3.4: Measurement of ADC metrics from brain metastases on diffusion MRI scans. A patient with a history of lung adenocarcinoma presents with headache and focal neurological deficit. A. T1 weighted MRI with gadolinium demonstrates a right frontal lesion, which was confirmed as a metastasis after excision. B. An ADC map is generated from B=0,1000 images using post processing software. On this colour map, blue areas represent low ADC and red higher ADC. C. A freehand region of interest is traced around the tumour border using the T1+gadolinium scan as reference on the axial slice with the largest tumour area and those immediately above and below. The ADCmin is the lowest bin of a histogram of ADC values for all pixels contained within this ROI, averaged over these three slices. Three ROI are placed within the tumour on the axial slice with the largest area, avoiding necrosis, haemorrhage, cyst and the mean taken to give ADCmean. D. To assess change of ADC across the tumour border, four ROI are placed starting just inside the tumour border and extending out into the peritumoural region. The slope of the four ADC values is taken as the "ADC transition coefficient" or ATC. This is repeated in 3 orthogonal directions, avoiding structures such as ventricle or falx and then repeated on two slices above and below, with the ATC being the mean of the 9 readings.

3.2.3.4 Follow up & statistical methods

Patients were followed up in regional oncology clinics and repeat MRI brain taken only if symptoms were present. Local recurrence or progression was defined as demonstrable brain disease on a post-operative MRI with appropriate clinical correlation and management; patients dying before that point were censored at the last clear brain scan (CT or MRI) or last clinical appointment when neurologically well. Patients who could not be confirmed deceased were censored at the last clinic appointment that had been recorded.

Data were analysed and graphs generated using Statistica version 6 (StatSoft, Inc. 2003) and SPSS version 20.0 (IBM co., 2011). For analysis of survival, the Kaplan-Meier product limit method was used and life tables with survival curves plotted. Log rank tests were applied to detect differences between paired groups and Wilcoxon modification (the Breslow Chi square test) used in cases where hazard did not appear to be proportional. For multivariate analysis Cox regression was used. Standard tests were used for comparisons of means and analysis of variance and descriptive statistics, distributions were plotted for all variables to check assumptions. The level of significance was set at 95% to reject the null hypothesis and all p-values and confidence intervals are stated**.**

3.2.4 Results & Discussion

3.2.4.1 Clinical outcomes

The demographic details of the cohort of 76 patients are summarised in **Table 3.4**. The median survival from first diagnosis of cerebral metastasis to death was 9.3 months (range 0.9 – 34.3 months). 11 cases were censored, mainly due to death by other causes or loss of follow up suggesting the length of the follow up period was adequate. It was not appropriate to analyse local recurrence where the tumour was not fully resected; in the 66 cases where gross total resection was performed, local recurrence occurred in 16 patients (24%) at a median of 17.7 months from presentation (95% CI 10.9 – 24.6). The factors associated with overall and progression free survival, including standard MRI measures such as tumour size, volume and number, are summarised in **Table 3.5**.

Age at diagnosis / years (mean & range)	60.6 (35.9 – 81.4)	
Gender	36 male : 40 female	
Disease information	number	%
Primary cancer type Non-small cell lung Small cell lung Breast Melanoma Gastrointestinal Urogenital Ovarian Squamous cell tonsil Unknown primary	 36 6 10 5 5 4 4 1 5	 47.4 7.9 13.7 6.6 6.6 5.3 5.3 1.3 6.6
Size of operated lesion (median & range)	27 (9 – 70) 8.9 (0.3 – 130)	Diameter / mm Volume / cc
Location operated lesion Supratentorial Infratentorial	 64 12	 84.2 15.8
Number of brain mets Solitary 2 lesions >2 lesions	 56 11 9	 73.7 14.5 11.8
RPA class I II III	 19 51 6	 25 67.1 7.9
GPA score <1.0 1.5-2 2.5-3.0 >3.0	 6 20 39 11	 7.9 26.3 51.3 14.5
Neurosurgery Gross total resection Partial resection / Biopsy	 67 9	 88.2 11.8
Adjuvant chemotherapy for systemic cancer	45	59.2
Adjuvant whole brain radiotherapy	56	73.7

Table 3.4: Demographics and treatment summary for the series (76 patients)

Factor	Overall survival Median / months	95% CI	Sig. on univariate analysis	Progression free survival Median / months	95% CI	Sig. on univariate analysis
GPA score						
<1.0	5.3	0.4 – 10.2		not reached		
1.5-2	6.8	0 – 14.0	0.306	18.4	-	0.936
2.5-3.0	9.3	8.0 – 10.6		17.8	6.1 – 29.4	
>3.0	9.8	7.8 – 11.7		13.1	9.0 – 17.2	
RPA class						
I	14.0	6.1 – 22.0	0.030*	17.7	14.6 – 20.9	0.636
II	8.4	5.1 – 11.8		13.1	9.7 – 16.6	
III	2.0	0 – 6.2		not reached		
Primary cancer						
Lung non-small cell	9.2	2.0 – 19.8		not reached		(too many censored in each category cases for analysis)
Lung small cell	4.5	1.0 – 28.9		10.5	-	
Breast	10.4	0.9 – 21.2		9.2	5.6 – 12.9	
Colorectal	6.8	5.3 – 12.3	0.061	not reached		
Melanoma	11.5	2.4 – 14.7		7.3	4.9 – 9.7	
Urological	4.0	1.1 – 9.6		not reached		
Ovarian	11.2	4.7 – 30		17.8	-	
Unknown	5.6	1.5 – 22.8		18.4	-	
Location						
Supratentorial	9.6	8.2 – 11.1	0.070	17.7	10.8 – 24.6	0.872
Infratentorial	4.4	0 – 10.1		not reached		
Surgery						
Biopsy	5.9	0 – 16.4	0.091			
Resection	9.6	8.1 – 11.0				
Adjuvant WBRT						
Yes	10.5	8.9 - 12	0.000*	17.7	10.9 – 24.6	0.000*
No	2.4	1.5 – 3.3		not reached		
Adjuvant chemo						
Yes	10.5	8.2 – 12.7	0.001*	15.7	10.7 – 20.6	0.240
no	5.3	3.0 – 7.6		not reached		
DWI metrics						
ADCmin>919 $x10^{-6}mm^2/s$	9.7	8.5 – 11.0	0.049*	18.4	13.2 – 23.6	0.087
ADCmin<919 $x10^{-6}mm^2/s$	6.2	3.7 – 8.8		11.3	8.4 – 14.3	
ADCmean>1148 $x10^{-6}mm^2/s$	9.7	7.9 – 11.5	0.093	18.4	11.6 – 25.1	0.039*
ADCmean<1148 $x10^{-6}mm^2/s$	6.7	4.9 – 8.5		11.3	5.8 – 16.8	
ATC>0.279	6.8	5.3 – 8.4	0.041*	11.3	8.2 – 14.4	0.072
ATC<0.279	11.2	8.3 – 14.0		not reached		
MRI metrics						
diameter>30mm	6.7	2.4 – 11.0	0.246	13.1	9.7 – 16.6	0.551
diameter<30mm	9.6	8.8 – 10.4		17.8	14.7 – 20.1	
volume > 8.9 cc	6.7	1.9 – 11.5	0.077	13.1	9.2 – 17.1	0.158
volume <8.9 cc	9.6	8.8 – 10.3		17.8	13.7 – 21.8	
Solitary	8.42	5.3 – 11.5	0.101	15.7	10.3 – 21.0	0.673
2 lesions	14.1	10.7- 17.6		11.3	0.85 – 21.8	
>2 lesions	6.1	5.1 – 12.2		not reached		

Table 3.5: Which factors were associated with survival and progression?

3.2.4.2 ADC readings from the metastases & tumour cellularity

The median ADCmean for cerebral metastases in this series was 1148.1 x $10^{-6}mm^2/s$ and the median ADCmin was 919.4 x $10^{-6}mm^2/s$. There were significant differences in ADC between cerebral metastases from different primary cancers by one-way ANOVA (F=2.797, p=0.025). On post hoc comparison, this was seen to be because metastases from the so-called "poorly differentiated" cancers such as melanoma (n=5) and small cell lung carcinoma (n=6) had a lower ADC compared to the metastases from carcinomas such as breast (n=10), ovarian (n=4) and colorectal (n=4), as shown in **Figure 3.5**.

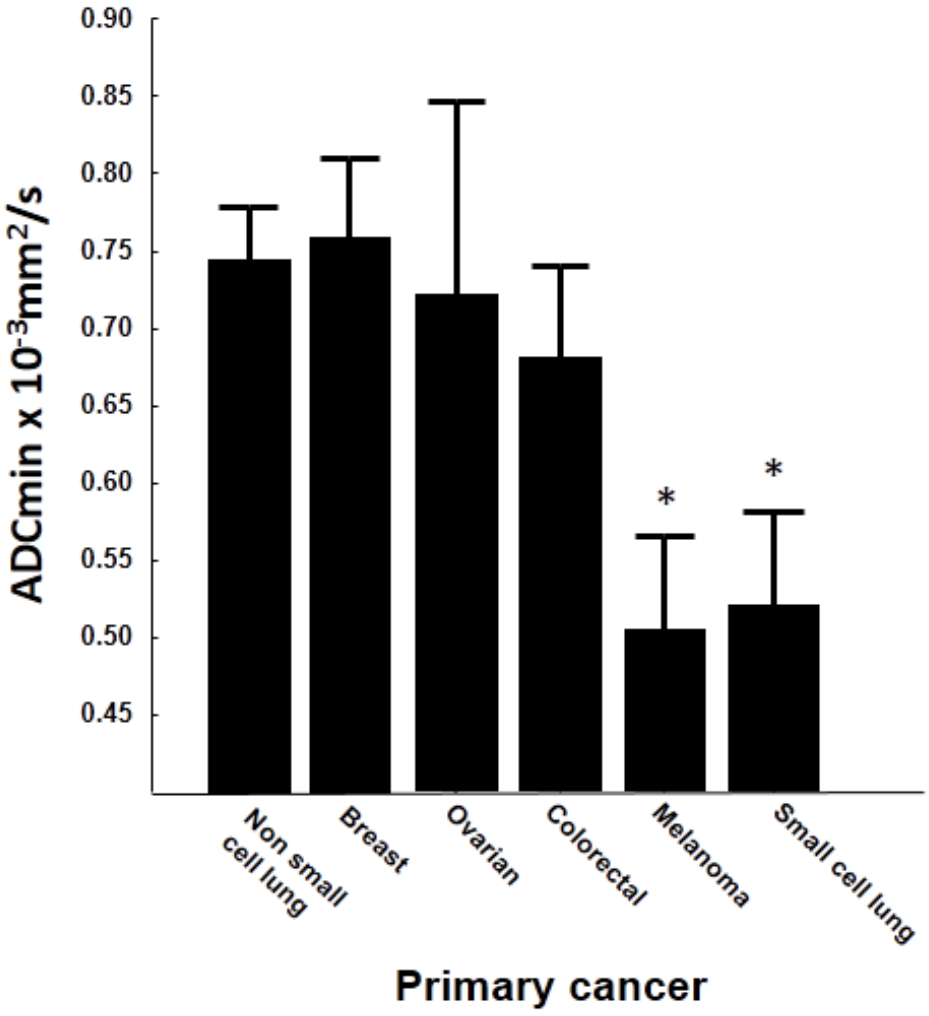

Figure 3.5: ADC values of 76 brain metastases by primary cancer of origin. The mean ADCmin value for each primary cancer type is shown +/- standard error and * indicates significant difference from the group at p<0.05 by independent student t-test. All histological diagnoses were confirmed by neuropathology assessment after biopsy or resection and correlation with clinical data.

Tissue was only available for 16 of 76 cases. Cellularity assessment by ImageJ software as compared to pathologist assessment appeared to be valid with consistency between the two observers (intraclass correlation coefficient= 0.61, $p<0.05$). The mean cellularity was negatively correlated with both the ADCmin and the ADCmean and could be fitted to either of these with a simple linear regression model which was highly significant (for ADCmin, F = 7.99, p=0.013 and for ADCmean F=5.56, p=0.033). ATC was strongly correlated with cellularity as shown in **Figure 3.6** and was predicted by it using a simple linear regression model (F=9.84, p=0.007).

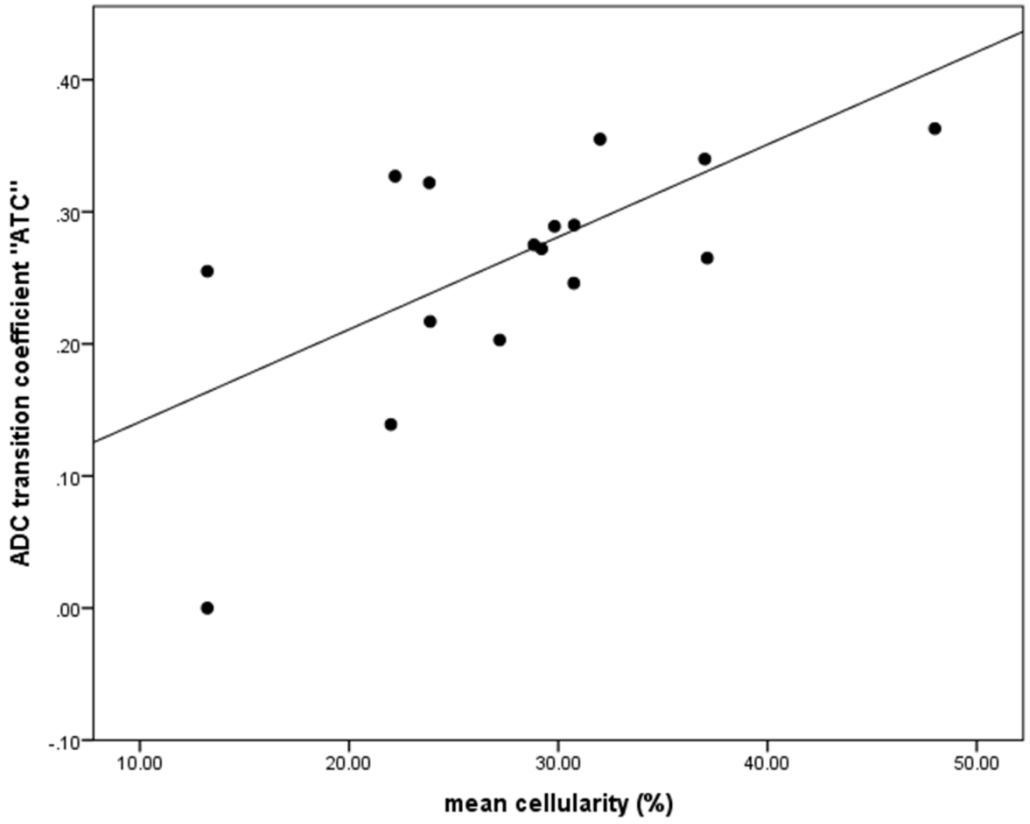

Figure 3.6: The gradient in change of ADC across the tumour border on preoperative DWI for brain metastases, called the ATC (see *Methods*) was strongly predictive of the cellularity, as shown in the scatterplot above. Cellularity was assessed in a semi-automated fashion using ImageJ software from five different high power fields and ATC measured as shown in **Figure 3.6**. The line shows a simple linear regression model which was highly significant (ATC = 0.007* mean cellularity + 0.07, ANOVA F=9.84, $p<0.001$).

3.2.4.3 Relation of tumour ADC to patient outcomes

For survival analysis, the patients were grouped based on each of the diffusion characteristics of their cerebral metastases and the two groups compared. The cases having a higher than median ADCmin (>919.4 x $10^{-6}mm^2/s$) showed a longer overall survival, median 9.7 months (95% CI: 8.5 – 11.0) versus those with a lower ADCmin (median survival 6.2 months, 95% CI: 3.7 – 8.8, Breslow Chi square 3.87, p=0.049). There was no difference in the proportion of patients receiving WBRT in the high versus the low ADCmin groups that would confound the effect on survival (Chi square = 3.49, p =0.062). The effect was also seen if the median ADCmean was used as the cut-off to define the two groups but was not statistically significant: OS 9.7 months, 95% CI 7.9 – 11.5 for patients with metastases having a higher ADCmean (>1148.1 x $10^{-6}mm^2/s$) versus 6.7months for lower ADCmean, 95% CI 4.9 – 8.5, Breslow Chi square = 2.83, p = 0.093.

Regarding local control, the median progression free survival was 11.3 months (95% 5.8 – 16.8) in those cases with a low ADCmean reading versus 18.4 months (95% CI 11.6 – 25.1) in those with a high ADCmean (Log rank test, Chi Square 4.263, p=0.039). This is illustrated in **Figure 3.7.** This effect was also seen when the median ADCmin was used as the cut-off to define the two groups but did not reach statistical significance (high ADCmin, progression free survival 18.4 months, 95% CI 13.2 – 23.6 versus low ADCmin, progression free survival 11.3 months, 95% CI 8.4 – 14.3, Log rank = 2.93, p = 0.087).

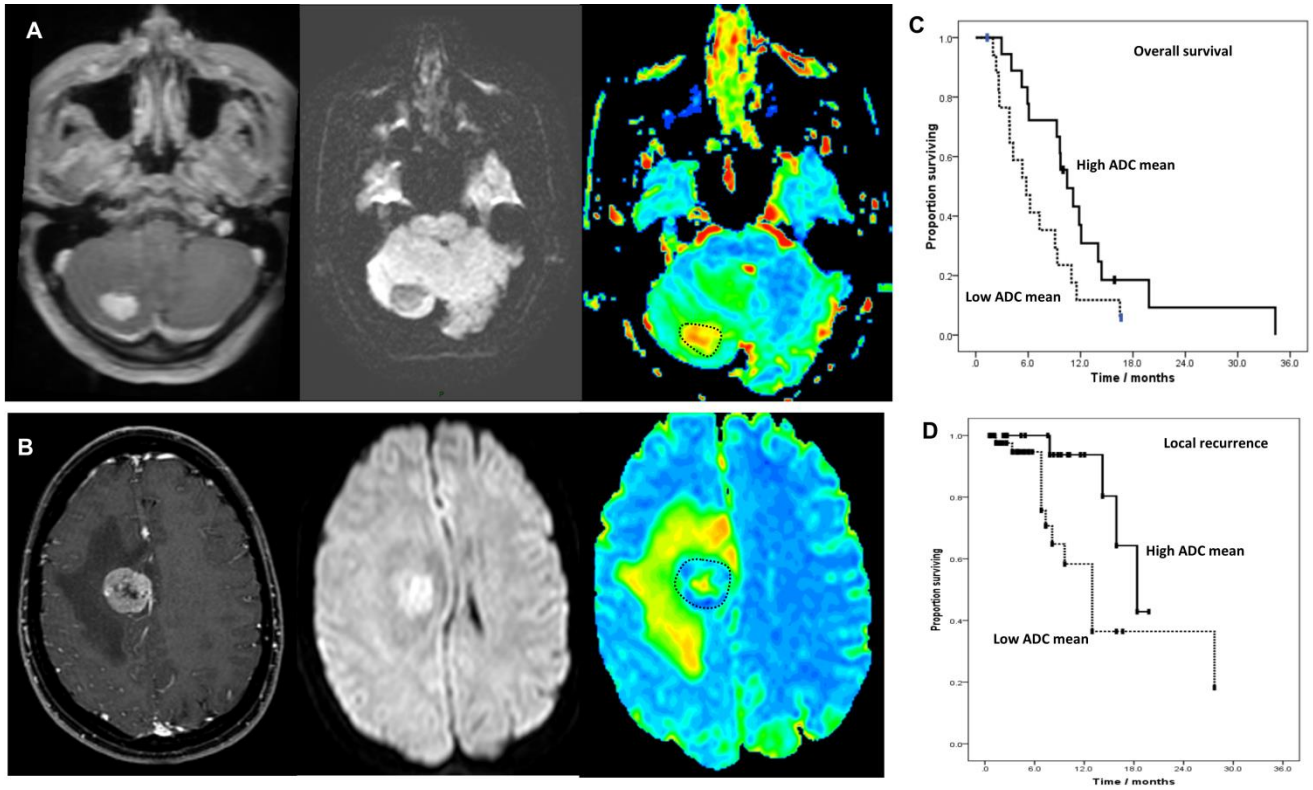

Figure 3.7: ADC of the metastasis predicts subsequent patient outcomes. Cases such as that in A. an enhancing lesion with hypo-intense DWI signal and higher than median ADC were compared to those such as B. an enhancing lesion but with hyper-intense DWI signal and corresponding low readings on ADC map. C. The largest group of metastases (n=36) from a single primary - lung non-small cell carcinoma – were stratified into two groups by these readings of tumour ADC. Overall survival was significantly longer for cases with a high tumour ADCmean (10.5months, CI 7.7 – 13.2) versus a low tumour ADCmean (5.8 months, CI 3.2 – 8.4, Log rank=4.135, p = 0.042). D. For the 66 cases where gross total resection was performed, local recurrence in the brain occurred in 16. Metastases with a higher ADC showed significantly longer progression free survival, 18.4 months (95% CI 11.6 – 25.1) versus 11.3 months (95% 5.8 – 16.8) in those with a low ADCmean (Log rank test, Chi Square 4.263, p=0.039).

Non-small cell lung cancer metastases represented the largest group of cases from a single primary cancer (although this group also has subdivisions, predominantly these were adenocarcinoma cases and they are at least more uniform than any previous analysis which includes multiple different primary sites) and this subgroup of 36 cases was therefore analysed separately in order to confirm that the ADC has value in and of itself as a prognostic marker not simply as a surrogate of the primary tumour type. Overall survival was significantly longer for non-small cell lung cancer cases with a high tumour ADCmin at 9.7 months (CI 6.7 – 12.6) versus 5.3 months (CI 2.2 – 8.5) for those with low ADCmin, Log rank Chi square = 4.008, p=0.045. The same effect was observed and was significant using median ADCmean as the cut-off because higher ADC group had median OS 10.5months (CI 7.7 – 13.2) versus 5.8 months, (CI 3.2 – 8.4) for low ADC group, Log rank=4.135, p = 0.042.

3.2.4.4 ADC changes at the brain-metastasis interface

The change in diffusion across the brain-metastasis interface might be expected to reflect to changes at the cellular level and hence even reflect tumour-stroma interactions. We devised and applied a measure of the changing ADC at the metastasis-brain boundary, called the ADC transition coefficient or ATC. This could be calculated for 70 cases (as described in the methods there needs to be a boundary to surrounding tissue to measure and calculate a reading) and found the ATC to have a median value of 0.279 (range 0.063 - 0.453). The ATC showed no relationship to the primary cancer type on one-way ANOVA (df=11, F=0.348, p=0.9) and weak negative correlation with ADCmean and ADCmin (Pearson correlation coefficient -0.39 and -0.33 respectively, p>0.05) suggesting it was measuring some novel feature rather than just acting as a surrogate of the other ADC characteristics or the primary cancer.

The group was divided into two based on the ATC, and those patients with a metastasis showing high ATC (> median) and therefore a sharp boundary on the ADC map had a shorter overall survival 6.8 months (95% CI 5.3 – 8.4) as compared to those with a low ATC and hence diffuse boundary on ADC map (11.2 months,

95% CI 8.3 – 14.0, Log rank Chi-Square = 4.19, p=0.041). This is illustrated more clearly in the conventional MRI scans and accompanying ADC maps in **Figure 3.8**. There was also a tendency to earlier local recurrence in high ATC cases versus low ATC but this was not statistically significant (shown in **Table 3.5**).

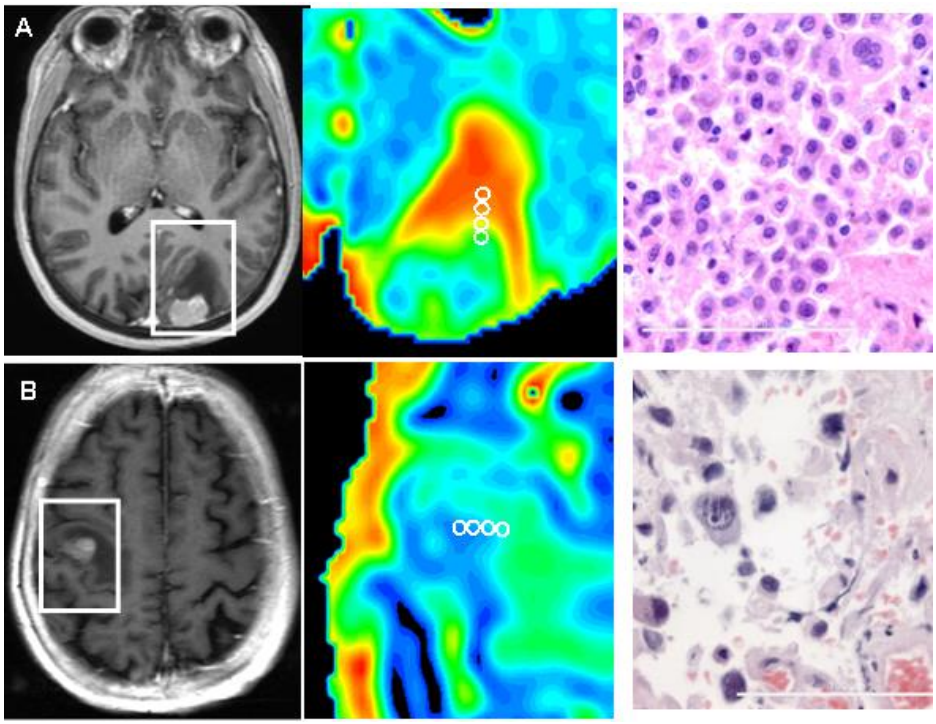

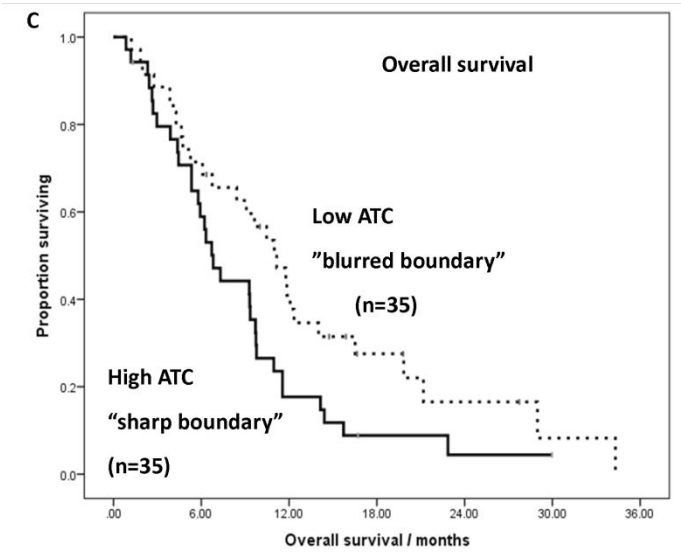

Figure 3.8: Panel A. demonstrates a lesion with a high ATC or "ADC transition coefficient" implying a sharp border. This type of metastasis tended to have a high cellularity (H&E section x200). Panel B. demonstrates a case which looks superficially similar on T1 weighted sequence with gadolinium but actually has a much more diffuse border on the ADC map and hence a low ATC, Panel C. These metastases differ in their outcomes and the cases with a high ATC (> median) and therefore a sharp boundary had a shorter overall survival 6.8 months (95% CI 5.3 – 8.4) as compared to those with a low ATC and hence diffuse boundary (11.2 months, 95% CI 8.3 – 14.0, Log rank Chi-Square = 4.19, p=0.041). This effect was significant even in multivariate analysis.

3.2.4.5 ADC readings in the peritumoural region

Initially we did not find a large variability in the ADC around a given metastasis and for the 76 cases together, the mean "near" peritumoural ADC was 2028.4 x $10^{-6}mm^2/s$ which did not differ significantly from the mean "far" peritumoural ADC of 1994.9 x $10^{-6}mm^2/s$. There was no significant variation of either variable by primary cancer type on one-way ANOVA. There was also no significant differences in patient outcomes (overall survival, local recurrence) when the cohort was divided into two "high" and "low" groups by either near peritumoural ADC, far peritumoural ADC or near:far ADC ratio and actuarial survival analysis performed.

When visually inspecting the ADC maps for the 76 cases, however, it appeared that for a minority of metastases, in particular those from melanoma primaries, diffusion *did* vary greatly between the near and far peritumoural regions. The values of ADC at each point going out from the tumour towards normal white matter were plotted to give the "ADC signature" for that type of metastasis and an example of this is illustrated in **Figure 3.9**. It was relevant to directly compare such patterns of ADC change in two types of cancer known to show differing mechanisms of brain invasion, as discussed. The ratio of the near and far ADC values were therefore calculated for metastases of melanoma and non-small cell lung cancer and it was seen that for melanoma metastases this ratio was significantly higher (independent 2-tailed t test = 2.259, df 36, p = 0.03).

3.2.4.6 Multivariate analysis

A Cox regression model was generated using the radiological and non-radiological factors found to be significant discriminators of overall survival in univariate analysis. Only post-operative WBRT (hazard ratio 3.1, 95% CI 1.5 – 6.8, p =0.004) and low ATC (hazard ratio 0.54, 95% CI 0.3 – 0.97, p=0.04) were found to be significantly associated with prolonged overall survival in this series. Multivariate analysis was attempted for progression free survival however modelling was inaccurate with large errors due to the high proportion of censored data (only 24% of the group or 16 cases developed local recurrence, as stated).

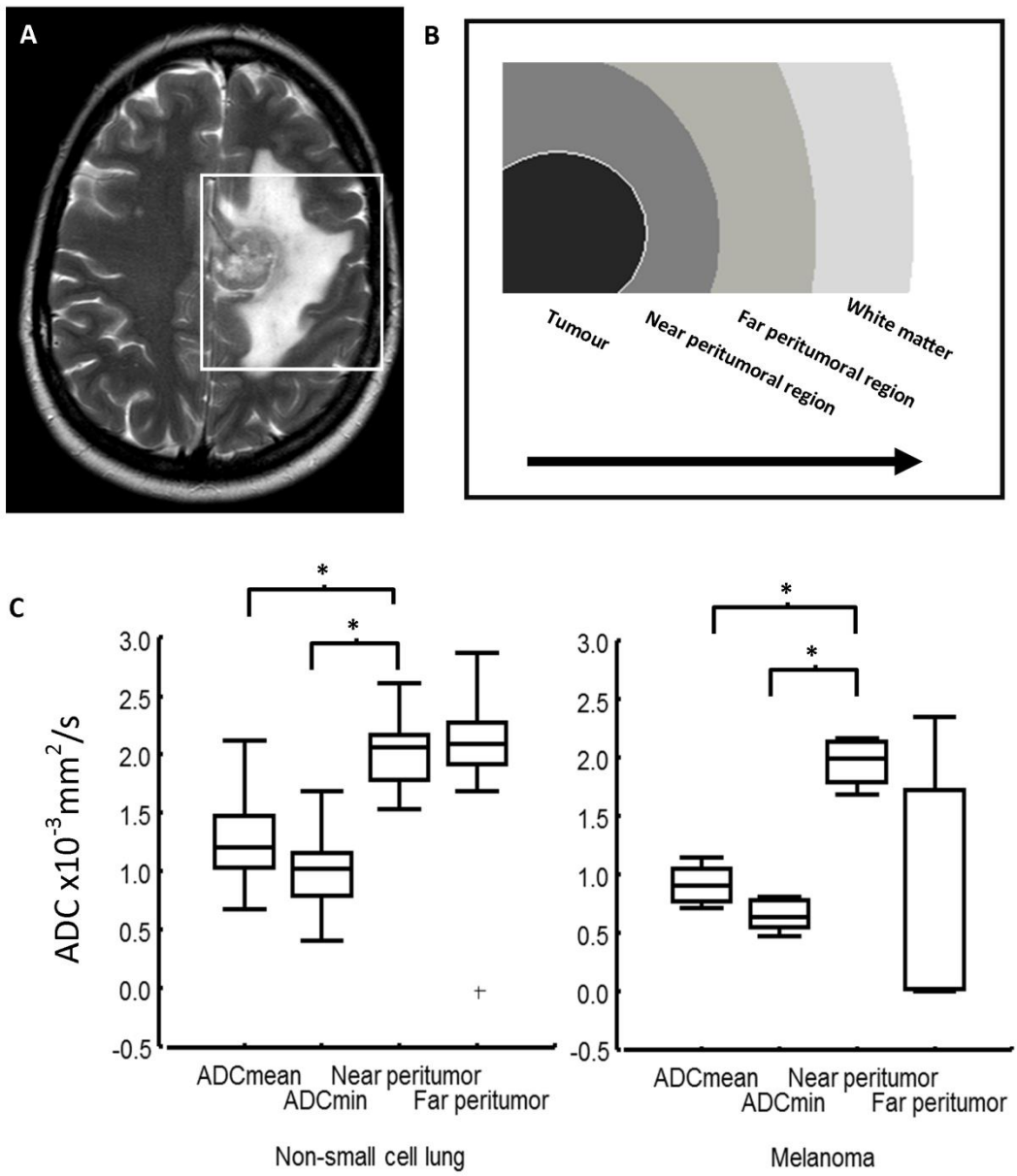

Figure 3.9: Changes in diffusion around a brain metastasis. A typical metastasis is shown in (A) with a clear boundary, necrotic centre and surrounding oedema, visible on the T2 sequence. What is happening in the region around the metastasis? There is substantial evidence that this region consists of vasogenic oedema, higher diffusion and lower perfusion when compared to high grade glioma for example, but what about comparing *within* a group of metastases. (B). One can place serial regions of interest and measure and plot the ADC changes from the necrotic centre of the tumour through the leading edge and into the peritumoural regions. (C) Box and whisker plots showing the median, interquartile range and outliers for ADC readings in and around melanoma (n=5) and non-small cell lung cancer (n=36) metastases demonstrates differences in this ADC signature between the two groups and within them but the biological correlate of these differences needs to be investigated.

3.2.5 Conclusions

3.2.5.1 The value of tumor ADC in cerebral metastases

This is the largest examination of diffusion weighted MRI and cerebral metastases to date. The numerical values for tumor ADC are in line with previous investigations of cerebral metastases which would be expected given the standard methods and protocols used for imaging and analysis (Berghoff et al., 2013c, Byrnes et al., 2011, Calli et al., 2006, Chen et al., 2012b, Chiang et al., 2004, Stadnik et al., 2001, Wang et al., 2009). We used a variety of methods of taking measurements from the ADC maps so as not to miss an effect due to our measurement technique. We have confirmed that ADC varies between cerebral metastases from different primary cancers but like others not sufficiently to distinguish the individual primary cancer type (Duygulu et al., 2010, Hayashida et al., 2006). This may be because the ADC reflects more general characteristics like cellularity. In support of this, ADC values were lower for the group of poorly differentiated metastases of melanoma and small cell lung cancer compared to the group of metastases from carcinomas (including breast and colorectal). We also corroborate the suggestion that tumor cellularity is inversely related to tumor ADC for a sample of our cases where tissue was available, whether measured by the minimum or the mean ADC. This is logical as more densely packed cells would broadly be expected to restrict diffusion, with the caveat that this coarse method of calculating ADC maps does not reflect the more subtle distinctions between intra and extracellular diffusion that others have derived using more advanced models in animals (Iima et al., 2014, Panagiotaki et al., 2014). However it has also been shown in cerebral metastases *post mortem* that a dense extracellular matrix correlates with low ADC, similarly suggesting a role for the tumor-stroma interaction we discuss later (Berghoff et al., 2013c).

Our survival analyses generally support the finding of this smaller study (Berghoff et al., 2013c) that the pre-operative mean ADC of a cerebral metastasis is correlated with subsequent overall patient survival and we have now demonstrated this for a single tissue type; non-small cell lung carcinoma. We did not find that this effect persists in multivariate analysis. This may be due to including oligometastatic disease but it seemed reasonable to include such cases as they all had a single larger,

dominant lesion and we included the number of lesions as a confounding factor as it is included in the GPA score. These findings that ADC predicts prognosis are in keeping with a number of reports from other brain tumors where DWI has been applied to predict stage and prognosis (Porto et al., 2013, Mahmoud et al., 2011, Barajas et al., 2010) as well as other organ systems such as renal, rectal head and neck or cervical tumors (Somoye et al., 2012, Frankel et al., 2012, Squillaci et al., 2004, Lambregts et al., 2011a, Matoba et al., 2013). In our series, in addition to whole brain radiotherapy - which is a treatment – it was only the *change* in diffusion across the tumour boundary which we call the ADC transition coefficient (ATC) that independently predicted the overall survival in multivariate analysis despite all other clinical factors. Why should this be?

3.2.5.2 The brain-metastasis interface

We have shown that changes in ADC across the brain-metastasis interface can be used to define the "sharpness" of this boundary, yielding additional information compared to assessing the boundary on T1 weighted contrast enhanced sequences alone. Rather than a low ATC and diffuse boundary on ADC map being associated with poor survival, as one might expect if this simply represented a more infiltrative pattern of growth, the reverse was true. A high ATC may in fact reflect high cellularity at the leading edge of the metastasis and hence greater tendency to recur. In support of this, the ATC was strongly linearly related to tumor cellularity in a sample of cases where tissue was available. One might predict that these cases may benefit from more aggressive local adjuvant treatments, such as wider surgical margins or radiosurgery "boost" to the cavity. Previous work on the interface between cerebral metastases and the surrounding brain has been conducted using histological methods on surgically resected or *post mortem* specimens (Raore et al., 2011, Baumert et al., 2006, Neves et al., 2001) and this has certainly suggested that there are different patterns and depths of invasion, even if this has not been related to clinical outcomes. Furthermore, it has been shown that wider resection margins may improve clinical survival (Patel et al., 2010) and that ADC changes across the border of another brain tumor - oligodendroglioma - may predict growth pattern and aggressiveness.(Jenkinson et al., 2007) Novel therapies acting at the brain-metastasis

interface are being developed (Goodman and Picard, 2012), therefore more accurate non-invasive, radiological methods may be needed to assess the degree of invasion of cerebral metastases and characterise the tumor boundary changes seen at diffusion MRI.

3.2.5.3 The peritumoural region

The MRI characteristics of the peritumoural region of cerebral metastases have previously been examined only in order to distinguish these tumors from glioma and abscess.(Sternberg et al., 2013, Mills et al., 2012, Price and Gillard, 2011) In this context the contrast enhancing margin has been taken as the reference and the near peritumoural region has been taken as being within 1cm of this edge. We have shown that for some metastases the ADC varies considerably from the core of the tumor, toward the leading edge and out into both the near and far peritumoural regions. It is known that the degree of T2 oedema may be a prognostic factor (Spanberger et al., 2013a) and the different peritumoural ADC values in different metastases may be due to differences in the intensity of peritumoural oedema and/or underlying vascular permeability due to different patterns of infiltration. Melanoma metastases, for example, showed a significantly higher near:far peritumoural ADC ratio than non-small cell lung cancer metastases in this study. These tumors are known to show different patterns of growth (Kienast et al., 2010), melanoma metastases co-opt existing vessels whereas lung adenocarcinoma stimulates neoangiogenesis and the pattern of peritumoural ADC changes might reflect this. In animal models suggest peritumoural ADC changes appear *before* T1 weighted gadolinium enhancement as micrometastasis formation and multiplication occurs (Serres et al., 2014). Tissue samples with paired radiological data would be needed to confirm what the correlate of these ADC changes are in humans, however it is unlikely that one would be practically able to gather tissue from deep within the region of peritumoural oedema around a metastasis as has been done for glioma (Kelly et al., 1987). The brain-metastasis boundary is therefore a more fruitful area to investigate in the first instance. What are the biological differences in pattern of infiltration, vascularity, protein expression, inflammatory response in and around metastases with a sharp

versus a diffuse ADC border and therefore could the ATC or similar measures of diffusion change be used as a surrogate of such biological activity.

3.2.5.4 Directions & limitations

Image guided tissue specimens with matched radiological regions of interest are needed within and around cerebral metastases (as has been done with glioma) in order to confirm the underlying biological changes which account for the ADC patterns seen. This was a retrospective study, tissue was not universally available and was in paraffin embedded blocks from non-specific areas of the tumor, hence such an analysis was not possible. This study only examined ADC maps as more gradient directions were not available (again due to the MRI data having already been acquired and the analysis being retrospective) but ideally, more MRI sequences would be analysed pre-operatively including tractography and perfusion to allow a number of radiological metrics to be examined in and around metastases. These findings are also cautioned by the need for validated, reproducible methods of measuring DWI metrics. In particular, we found differences in "tumor ADC" between measuring whole tumor values, minimum values and taking the mean of multiple ROIs. A logical step would be to validate these metrics – in particular the ATC - on a separate dataset or series of cases with data gathered independently by another group and compare to conventional predictive models such as RPA and GPA. Different MR protocols have had to be combined in this series due to a need for large enough numbers for survival analysis. Again, data gathered in a prospective fashion on a single scanner with uniform protocols would be preferable. However the variations in T1 weighted contrast enhanced sequences (used as the reference for the tumor border) ought to be offset by the relatively hard boundary seen in these sequences and we have previously described good inter and intra-observer agreement measuring ADC metrics in brain metastases on different platforms. The prevalence of intratumoral haemorrhage in many brain metastasis types is a problem and reduces the number of cases which are suitable for analysis (cases with overwhelming haemorrhage were excluded as stated in the **Methods**) as well as potentially making these findings less relevant to cases which tend to bleed such as melanoma and renal. Nonetheless a reasonable spread of common histological types was used here. Newer

systemic therapies for treating cerebral metastases may lead to significant differences in survival between different tumor types and comprehensive clinical data with large numbers would be needed to stratify cases in future, for example by HER2 responsiveness in breast carcinoma metastases. This makes large scale biomarker studies practically difficult and the need for collaboration between centres paramount.

Chapter 4: Combined *in vivo* analysis of the brain-brain metastasis boundary using advanced MRI and image guided sampling

4.1 Introduction

There are strong reasons for investigating the interface between the brain and the brain metastasis (B-BM interface) as a potential source of therapeutic opportunities and biomarkers. First, it has recently been shown that, far from being discrete, encapsulated tumours, brain metastases show a variety of growth patterns at the leading edge, with implications for prognosis (Siam et al., 2015) and treatment (Winkler, 2015, Berghoff et al., 2013b, Kienast et al., 2010). Second, the B-BM interface is the region in which the tumour interacts with the host immune system (Berghoff et al., 2013a, Puhalla et al., 2015, Hamilton and Sibson, 2013). Third, there are new therapies in each modality which act at the B-BM interface: cavity boost radiosurgery (Roberge et al., 2012), immune modulating drugs (Kluger et al., 2015, Sugihara et al., 2009, Jones et al., 2015), and supra-marginal or *en bloc* surgical resection (Yoo et al., 2009, Patel et al., 2010).

MRI provides a modality to assess the B-BM interface non-invasively, and could deliver biomarkers that apply to both resected and non-resected tumours. Advanced MRI and, in particular, diffusion MRI appears to be more sensitive at detecting changes in this region, on both the tumour and the brain side, earlier than other modalities (Serres et al., 2014, O'Connor et al., 2015, Mills et al., 2012). In addition to isotropic diffusion, it will be important to examine changes in anisotropic diffusion, as disruption of white matter tracts may be a sensitive marker of local tumour invasion (as it is in glioma) or other peritumoural changes, such as inflammation or neoangiogenesis.

The final experiment in this thesis was therefore to perform image-guided neurosurgical sampling of the B-BM interface to assess MRI features (conventional, DWI and DTI), cellularity, growth pattern, cell division and host inflammatory responses for metastases from different primary cancers.

4.2 Methods

4.2.1 Patients & follow up

Overall 26 patients were studied prospectively and the clinical details are summarised in **Table 4.1**. All patients were undergoing complete resection of a supratentorial metastasis in the course of routine clinical care at a single institution. All patients had received dexamethasone 16mg per day in divided doses for at least 72 hours prior to surgery. Performance status was assessed by clinicians at presentation.

Characteristic		Count	% of total
Age at surgery / years (range)		62.9	(23.8 – 76.0)
Gender	Female	14	53.8%
	Male	12	46.2%
Karnofsky performance score	80	5	19.2%
	90	18	69.2%
	100	3	11.5%
Primary cancer	Non-small cell lung	13	50%
	Breast	4	15.4%
	Melanoma	4	15.4%
	Colorectal	2	7.7%
	Renal	1	3.8%
	Other	2	7.7%
Extra-cranial metastases	Absent	18	69.2%
	Present	8	30.8%
Control of primary disease	Synchronous	9	34.6%
	Controlled	17	65.4%
Adjuvant WBRT (30Gy in 15#)	No	5	19.2%
	Yes	21	80.8%
Adjuvant chemotherapy	None	13	50.0%
	Yes	9	34.6%
	Targeted agent	4	15.4%
Overall Survival /months (range)		5.8	(1.6 – 15.5)
Intracranial progression	None	16	61.5%
	Local	7	26.9%
	Distant	3	11.5%
Progression free survival /months (range)		3.8	(0.2 – 12.9)

Table 4.1: Clinical details of brain metastases patients studied prospectively

Post-operative clinical course and oncology care, especially administration of whole brain radiotherapy (WBRT) or the use of adjuvant systemic chemotherapy (including targeted agents such as Herceptin©) were recorded from tumour board and patient notes prospectively, since these were potential confounding factors. Intracranial progression was determined by a neuro-radiologist as per the RANO criteria (Lin et al., 2015) in combination with the clinical findings, and all patients were discussed at the weekly tumour board / multidisciplinary team meeting.

4.2.2 Image-guided sampling

ADC maps and structural sequences were fused on the StealthStation S7 planning software (Medtronic Inc., MN, USA) and exported to an intraoperative workstation (**Figure 4.1**). The fused ADC sequence displayed as a colour map was used to avoid areas of cyst, necrosis which would not have been visible on the standard post-contrast T1 weighted sequence alone, and the change in ADC was an indicator of cellular tumour "leading edge" transition to surrounding vasogenic oedema, with the latter having a very high ADC (Zakaria and Jenkinson, 2014d).

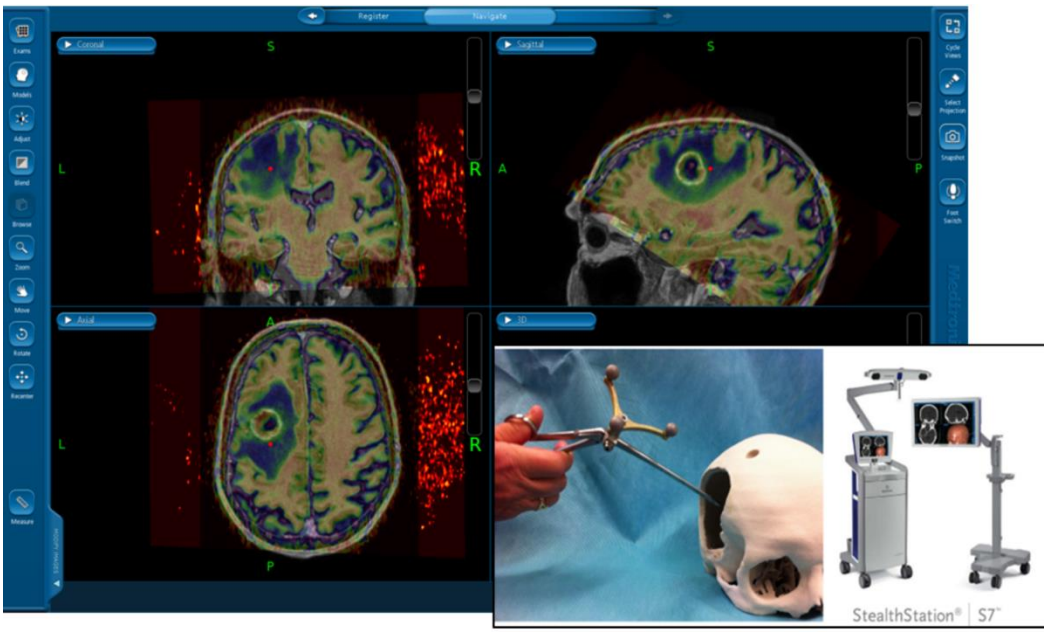

Figure 4.1: Intraoperative screenshot of the fused ADC map (displayed as a colour image with high ADC in blue and low ADC in yellow) and inset, the Suretrak© probe attached to a biopsy forceps for use with the StealthStation S7©.

Using these fused sequences, samples were taken using the Suretrak© probe mounted on biopsy forceps. This technique allowed excellent specimens to be taken, demonstrating the transition from tumour to surrounding brain. For each case, an edge location was chosen which showed a radiological and histological interface with brain. The vector specifying the location of this sample ("edge"), along with one from the tumour interior ("core") were extracted from the image-guidance software post-operatively (StealthStation S7, Medtronic Inc., MN, USA) and transferred to the offline image analysis software described below. Each location was double checked visually with screenshots taken in three orthogonal planes at each biopsy location during surgery. Regions of interest placed at this location, which was therefore co-localised to the tissue sample taken intra-operatively, could then be applied to any parametric maps generated. This is illustrated in **Figure 4.2.**

4.2.3 MRI studies

At a median of 5 days prior to surgery, patients underwent an MRI brain scan. Sequences were requested by the managing clinician and protocoled by a clinical neuro-radiologist; for diagnosis T2 and unenhanced T1 sequences were acquired using standard parameters. For diagnosis and neuro-navigation, a volumetric fast spoiled gradient echo sequence was taken after gadolinium injection at a standard dose of 0.1mmol/kg (repetition time/echo time 9/1.4ms, flip angle 15 degrees, acquisition matrix 256×256, volume 180 × 1 mm slices at zero angle gantry); this is referred to as the planning scan. In 11/26 cases DWI with single-shot echo planar imaging at b values of 0 and 1000 second/mm^2 was obtained and in 15/26 patients a DTI sequence (General Electric, 5 cases and Philips medical systems, 10 cases) enabling FA and MD maps to be generated. Philips scanner parameters were: Achieva 3.0T scanner with proprietary head coil, spin echo "DwiSE" sequence, total acquisition time 44.7 min, repetition time/echo time 2828/73 ms, field of view 230x230mm, acquired matrix 128x128, slice thickness 4mm, 27 slice per volume, one volume without diffusion weighting (b=0 s/mm^2) followed by 32 diffusion sensitised images with gradients applied in non-collinear directions (b=1000 s/mm^2). GE scanner parameters were: Discovery MR750 3.0T scanner with proprietary head coil. Total acquisition time 40.3 min, repetition time/echo time 8000/87.8ms, field of

view 240x240mm, acquired matrix 128x128, slice thickness 4mm, 37 slices per volume, one volume without diffusion weighting (b=0 s/mm^2) followed by 25 diffusion sensitised images with gradients applied in non-collinear directions (b=1000 s/mm^2). There was no difference in any ADC, MD, FA metrics from tumour, peritumoural regions or white matter by scanner vendor (independent median samples test $p>0.05$ for all comparisons), and it has been recently confirmed that the parameters being measured have good inter-scanner reproducibility (Grech-Sollars et al., 2015).

4.2.4 Image analysis

The planning scan was reviewed by a neuro-radiologist blind to the clinical or histological data to assess the number and size of metastases as per recognised clinical criteria (Quant and Wen, 2011, Lin et al., 2015) as well as the degree of oedema on T2 weighted MRI using a previously defined scale (Spanberger et al., 2013a). Additionally, contour segmentation software (ITK-SNAP version 3.0 (Yushkevich et al., 2006)) was used to delineate the contrast-enhancing tumour and measure its volume.

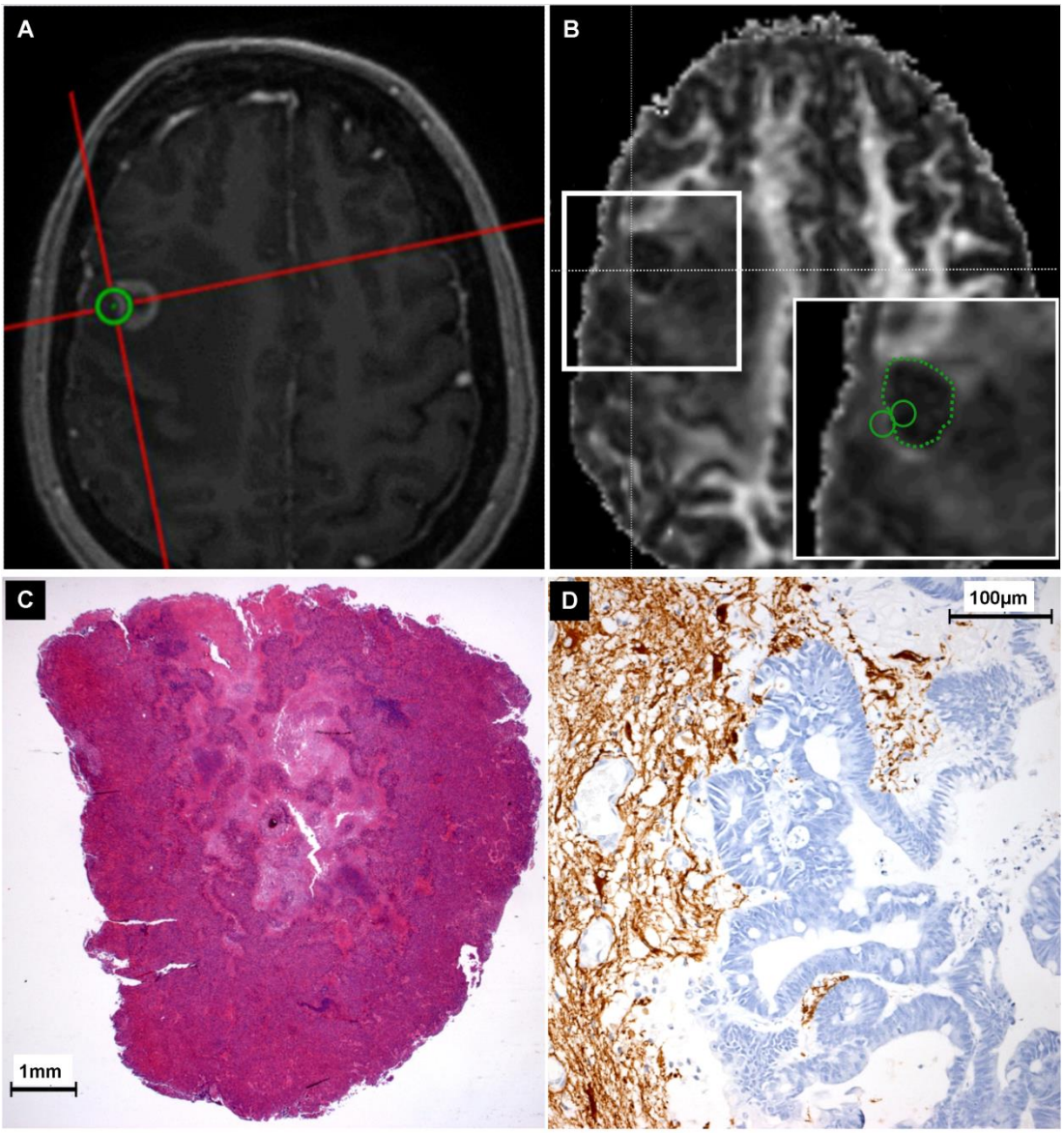

Figure 4.2: A colorectal cancer brain metastasis removed for histological diagnosis and to relieve mass effect. An image-guided sample is taken intra-operatively and marked on the neuronavigation software (A). These coordinates are extracted and applied to the processed images after co-registration with the planning scan used in theatre, here the FA map is shown (B). Regions of interest are placed at the tissue sample location on both the tumour (edge) side and peritumoural side of the B-BM interface. The whole tumour is also demarcated using the contrast-enhancing margin and segmentation software. Whereas normally the whole, heterogeneous tumour (C, H&E stain) is analysed by MRI, now one can examine samples from the specific MRI location in (A) and see both the peritumoural and tumour characteristics that correlated with the MRI changes in these regions, here (D) on a section stained for GFAP (brown), the focal glial reaction to the tumour (blue) is shown.

For diffusion sequences, raw DICOM data was imported into DTIstudio, version 3.0.3 (Jiang et al., 2006) with additional use of the ROIeditor module, version 1.7 and MRIcron, version 6.6 (Rorden and Brett, 2000) as needed. Using the default settings (affine linear transformation, tri-linear interpolation, standard deriation of the ratio image) realignment and co-registration to b0 images was performed to remove eddy current distortions and quality control of baseline images was also checked visually. Tensors were calculated using standard linear regression and brain masking applied, inspecting the mask and correcting manually if required. An ADC trace map from DWI and, if more directions were available, the equivalent (Prah et al., 2014) mean diffusivity (MD) map from DTI were then generated. 2D fractional anisotropy (FA) maps were generated from tensors. Readings of average and minimum FA, MD/ADC were taken on the tumour and the peritumoural side of the location at the B-BM interface where the tissue sample was from as shown in **Figure 4.2**. The change in ADC/MD *across* the B-BM interface at the same location (the ADC transition coefficient or ATC) was calculated as previously described (Zakaria et al., 2014c). Control readings were taken from the contralateral white matter by flipping the ROIs across the anatomical midline within the software, having double checked visually that this avoided any confounding structures such as ventricles or bone. Reduced FA indicates white matter tract disruption (anisotropic diffusion), whereas reduced ADC or MD represents restriction of diffusion in any direction (isotropic diffusion).

4.2.5 Tissue analysis

Histological assessment by a neuropathologist blind to MRI and clinical outcome was performed in the course of routine care to determine the primary cancer of origin and confirm the diagnosis. There were no misdiagnoses (e.g. pre-operative lesion operated as metastasis then found to be high grade glioma or lymphoma) and no lesions were excluded from analysis due to excessive haemorrhage (previously (Zakaria et al., 2014a) defined as >50% of the lesion being haemorrhagic at MRI or if haemorrhage precluded tissue analysis when IHC was performed). Primary cancer types are listed in **Table 4.1.**

4.2.5.1 Assessment of growth pattern at B-BM interface

In the course of resection, the operating neurosurgeon gave a subjective assessment from microsurgical dissection of whether the tumour was well demarcated from the surrounding brain or not (henceforth termed the macroscopic assessment). A single neuropathologist was asked following completion of clinical care to categorise the growth pattern of all cases blind to the other MRI and immunological stains. They undertook this categorisation using a previously described system as either encapsulated, perivascular invasion or diffuse invasion (Berghoff et al., 2013b). All cases were then re-assessed by an independent observer for evidence of local invasion and any disagreements resolved (henceforth termed the microscopic assessment).

4.2.5.2 Immunohistochemistry at B-BM interface

Samples were taken using biopsy forceps (**Figure 4.3**) yielding specimens approximately 4x 3x 2mm. Samples were marked with a dot of black medical ink in theatre to show the deep pole, then stored in formalin for up to 24 hours before being placed into paraffin blocks with their orientation preserved, such that serial sections would not bisect tumour and adjacent brain (illustrated in **Figure 4.4).** Sections of 5 micron thickness were cut and staining with haematoxylin & eosin (H&E) performed.

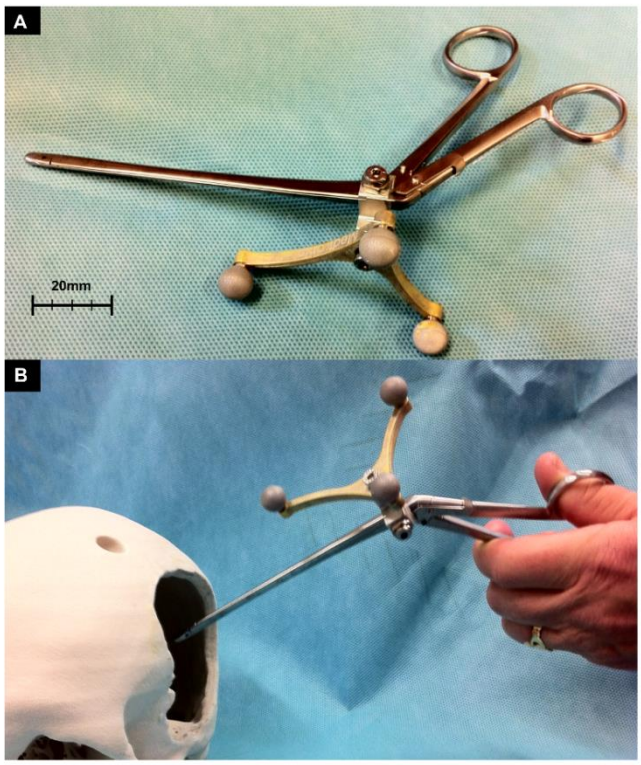

Figure 4.3: Biopsy forceps A. and in use on a model skull B. showing the size and planes available in 3 dimensions when taking intraoperative specimens.

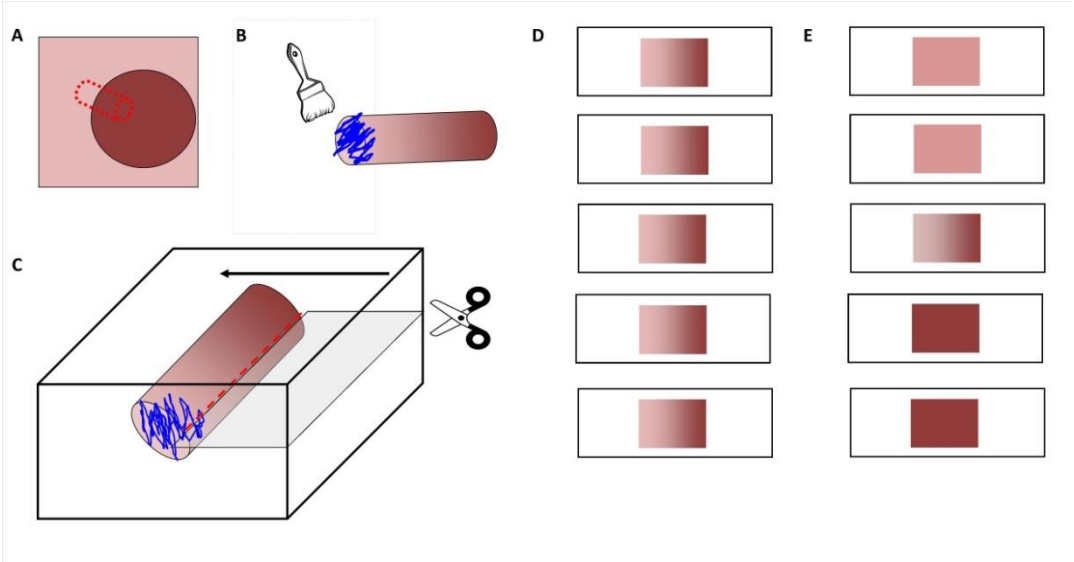

Figure 4.4: Illustration of specimen handling. A. The sausage shaped biopsy specimen taken from the leading edge of the brain metastasis (dark brown circle) was marked with medical ink (B) in theatre to denote the “brain” as opposed to the tumour pole. C. This mark was used in the laboratory to orient the specimen in the cassette to embed in paraffin, so that subsequent sections, taken along the plane marked with the scissors, gave an even distribution of tumour and peritumoural regions in each slide, seen in D. Other orientations produce serial sections at varying points across and even through the brain-brain metastasis interface, such as in E. where most slides contain only tumour and others only peritumoural white matter.

Table 4.2: Stains used to assess image-guided samples from tumour edge and core.

Marker	Function	Antibody / stain	Dilution	Antigen retrieval
CD34	Endothelial antibody used to assess vascularity (Ramani et al., 1990)	Mouse monoclonal #M7165 Dako	1:25 EnVmse	Proteinase K
GFAP	Filament protein found in astrocytes and used to assess reactive gliosis (Frank et al., 1986)	Rabbit polyclonal #Z0334 Dako	1:1500 EnVrbt	Proteinase K
CD20	B cell differentiation antigen (Reinherz et al., 1986b)	Mouse monoclonal #M0755 Dako	1:300 EnVmse	Citrate buffer (pH6)
CD68	Receptor involved in phagocytosis and expressed on macrophages (Micklem et al., 1989)	Mouse monoclonal #M0814 Dako	1:100 EnVmse	Citrate buffer (pH6)
CD3	Non-specific T cell marker (Reinherz et al., 1986a)	Rabbit polyclonal #A0452 Dako	1:50 EnVrbt	Tris-EDTA buffer (pH9)
Reticulin	Component of extra-cellular matrix (Bolonyi, 1958)	(Gordon and Sweets, 1936)		
S100A4	Calcium binding protein shown to promote metastasis in several animal models (Gross et al., 2014); over-expression associated with intracranial progression in brain metastases	Rabbit polyclonal #A5114 Dako	1:400 EnVrbt	none
OPN	Varied role in cell-matrix interaction, binds the cell surface integrins $\alpha_V\beta_3/\alpha_V\beta_5$ and promotes metastases (Anborgh et al., 2010, Hahnel et al., 2010, Guttler et al., 2013). May be involved in radiation response in human brain metastases.	Mouse monoclonal #MP111B10(1) Developmental Studies Hybridoma Bank(DSHB)	1:300 EnVmse	none
S100P	Calcium binding protein inducing metastasis in breast cancer animal models (Wang et al., 2006).	Mouse monoclonal #610307 BD Biosciences	1:75 EnVmse	none
AGR2	Normal component of ER highly overexpressed in range of human cancers. (Barraclough et al., 2009).	Rabbit polyclonal #ARP42290 Aviva Systems Biology	1:750 EnVrbt	none
MMP2	Matrix metalloproteinases are zinc-dependent, secreted endopeptidases essential for degradation and remodelling of the extracellular matrix. They are highly implicated in metastasis to and survival of cancer cells in the brain.(Vandenbroucke and Libert, 2014, Cathcart et al., 2015)	Mouse monoclonal #MAB13431 Chemicon	1:40 EnVmse	none
MMP9		Rabbit monoclonal #ab137867 Abcam	1:100 EnVrbt	none
MMP13		Mouse monoclonal #MA5-14238 Thermo Scientific	1:60 EnVmse	none
Ki67	Marker of proliferation (Plate et al., 1990)	Mouse monoclonal #M7240 Dako	1:75 EnVmse	Tris-EDTA buffer (pH9)

NB: EnVrbt /EnVmse refers to the method used following primary antibody incubation: Dako Envision+ System-HRP (#K4011 for rabbit or #K4007 for mouse primaries).

Additionally, a number of other proteins acting as markers of proliferation, glial cells, inflammatory cells, connective tissue, ECM adhesion/remodelling and metastasis were examined and these are listed with details in **Table 4.2**. Stained slides were scored using a well described (Rudland et al., 2000) semi-quantitative method for the percentage and intensity of staining by two separate observers and the results compared to resolve any discrepancy. Lymphocytes and macrophages were manually counted (Rasheed Zakaria & Angela Platt-Higgins) up to a maximum of 100 per high powered field (HPF, = 400x magnification) in as many fields as possible in the core and the edge samples (tumour infiltrating cells were defined as those in contact with cancer cells) as well as in the peritumoural region (defined as <1 high powered field of the tumour boundary on the edge sample) and distant white matter (>2 high powered fields from tumour edge). Cell counts were highly consistent between observers at intra-class correlation coefficient testing (Cronbach's alpha=0.762, $p<0.001$). For Ki67, GFAP and connective tissue density, automated analysis with NIH ImageJ software was performed; version 1.49t (Schneider et al., 2012) running in a 64-bit Windows environment using previously validated plugins e.g. (Tuominen et al., 2010). Slide photographs were taken using a Leica DFC310FX camera attached to a DM2000 microscope with the LAS V3 software suite (Leica microsystems, 2014) with no additional filtering. Images were stored using an uncompressed image file format (bitmap). For every imaging session, an image from an empty area of slide background was acquired (the blankfield image), which was used to correct for image colour balance and uneven illumination.

4.2.6 Statistical methods

Overall survival (OS) was taken as time from surgery to death and non-cancer deaths or those lost to follow up censored at last recorded follow up. Patients who died before progression were censored at the last date of follow up imaging. Proportions were assessed using Fisher's two-sided exact test. Time-to-event comparisons were made using the Kaplan-Meier method with Log Rank tests and multivariate analyses conducted using Cox's method. Correlations were assessed using Spearman's rank test and pairwise comparisons using Wilcoxon's signed rank test. Significance levels are generally stated, but were taken as $p<0.01$ if not given. Data processing was

performed using SPSS version 22.0 (IBM, Chicago, IL) and R version 3.10 (R Core Team, 2013).

4.3 Results

4.3.1 Clinical features

Post-operative CT brain within 24 hours confirmed complete contrast enhancing lesion resection in all cases and there were no post-operative complications such as infection or haematoma in this series. Patients were generally of good performance status with controlled disease, as expected in a surgical cohort. Median overall survival (OS) was 5.5 months (95% CI 4.2 – 6.8) with 4 censored cases. Adjuvant WBRT was the only feature associated with increased OS, of 6.53 months (95% CI: 5.4-7.7) versus 2.73 months (95% CI: 1.8 -3.6) untreated (log rank 16.26, $p<0.001$). 10 of 26 patients experienced intracranial progression after surgery (3 distant, 7 local – i.e. in or around the surgical cavity) and the median progression-free survival (PFS) was 7.2 months (95% CI 4.6 – 9.8). There were no associations of any clinical factor with PFS time or site of progression (distant brain versus cavity).

4.3.2 Conventional MRI measures

There were 22 truly solitary metastases and 4 with a dominant lesion with additional unmeasurable lesions, effectively considered solitary. RANO "longest measurable diameter" ranged from 10mm – 57mm (median 28mm). Median volume was 8.5 cm^3 (range 0.4 – 65cm^3). All metastases showed peritumoural oedema on T2 weighted sequences and in most cases (22/26) this was moderate (>1cm from but not crossing the midline), but in one case was mild (<1cm), and in three more severe (crossing midline or causing midline shift). The number of metastases, volume of disease and degree of peritumoural oedema were not associated with outcomes, however, tumours > 30mm in their longest axis showed a significantly shorter OS (HR for death if smaller than 30mm = 0.28, CI 0.11-0.70, p=0.006) even when controlling for WBRT.

4.3.3 DWI measurements reflect intra-tumoural heterogeneity

The mean ADC of the 26 metastases was $1128x10^{-6}mm^2/s$ when considering the whole tumour, but this varied considerably by region (analysis of variance, Kruskal-Wallis test highly significant, $p < 0.001$) with higher values of $1505x10^{-6}mm^2/s$ for the core locations but $1059x10^{-6}mm^2/s$ at the leading edge locations and $1.414x10^{-6}mm^2/s$ in the peritumoural region. Core and edge MD readings for each metastasis were analysed in pairwise fashion and showed significant differences in distribution, illustrated in **Figure 4.5** (related samples Wilcoxon-signed rank test = -4.286, $p<0.001$). There was no relationship of the ADC or MD readings - either of the whole tumours or in any of the specific regions - to primary tumour histology, clinical factors or clinical outcomes.

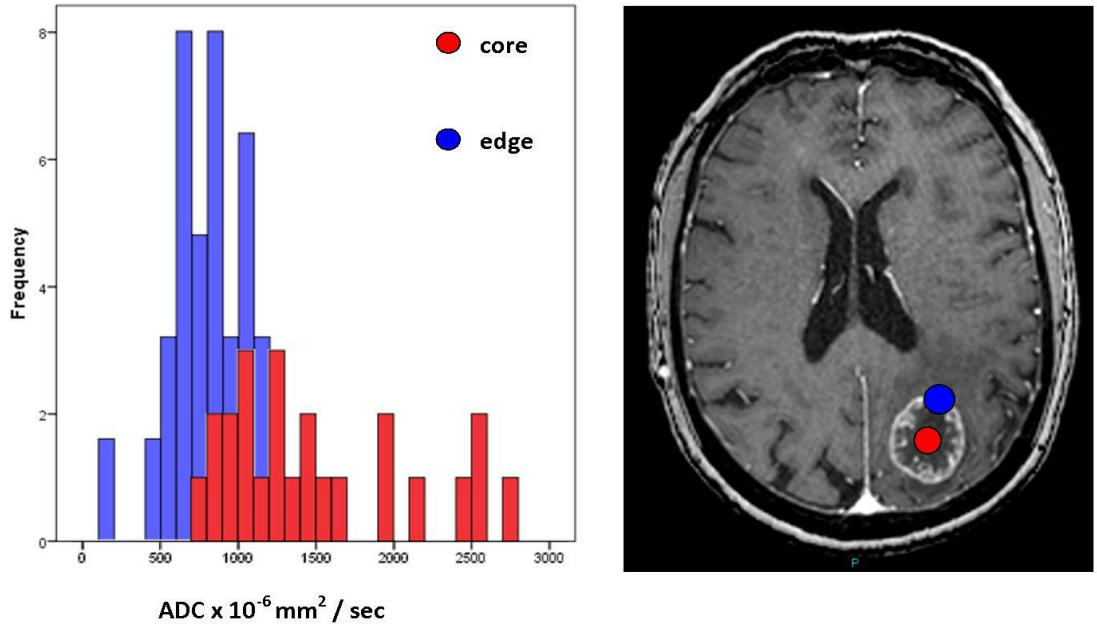

Figure 4.5: MRI showing the location of core and edge regions of interest for measuring ADC. The ADC varies depending on the region of the tumour assessed and the histogram of values coded by location shows this intra-tumoural heterogeneity. Metrics which group the whole tumour together as a single region would effectively miss this heterogeneity.

4.3.4 Lower peritumoural FA is associated with longer overall survival

To assess the B-BM interface, the change in ADC from tumour edge out into peritumoural tissue (the ATC) was derived and found to be comparable to the previous, larger series (median = 0.2314); nonetheless there were no differences in

microscopic invasion, peritumoural inflammation or any other biological measure between those metastases with a lower versus a higher ATC and accordingly no association with overall survival (log rank statistic = 0.065, p=0.799) or with time/site of intracranial progression was found.

The peritumoural region alone was therefore considered separately from the tumour readings. The average FA measured in both the metastases (median 0.1090, range 0.073 - 0.263) and the peritumoural region (median 0.1400, range 0.050 - 0.220) were significantly lower than in unaffected, contralateral white matter (median 0.1980, range 0.103 – 0.341) indicating disruption of white matter tracts in both regions (related samples Wilcoxon-signed rank test for both comparisons, $p<0.001$). The peritumoural FA, but *not* the tumour FA, was strongly associated with overall survival in this surgical cohort. **Figure 4.6** demonstrates that cases with a lower peritumoural FA, indicating more disruption of white matter tracts, showed longer survival times (median 9.9 months, 95% CI: 7.4-12.4 versus 5.3 months, 95% CI: 3.4 – 7.13), even if tumour size and adjuvant WBRT were taken into consideration (in proportional hazards multivariate model, HR for death in lower peritumoural FA cases was 0.07, p=0.036). This result is counterintuitive, because in glioma studies variation in anisotropic diffusion is said to indicate tumour infiltrating and disrupting white matter tracts (White et al., 2011, Lu et al., 2004), whereas this would not be expected of BMs. Thus matched samples from the tumour and brain side at the same locations were examined to determine what the biological cause for increased survival and reduced anisotropic diffusion in these cases might be.

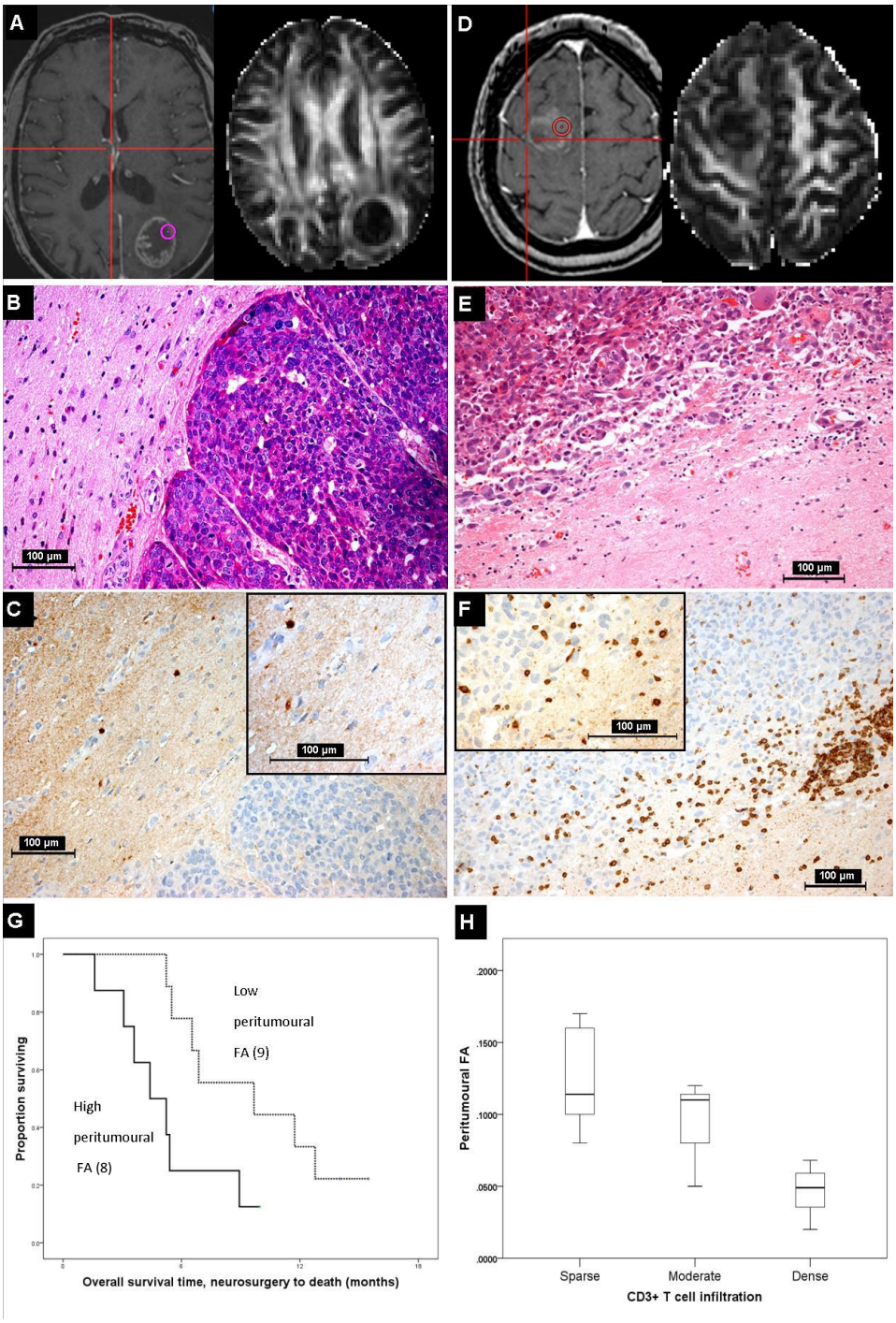

Figure 4.6: A. A lung adenocarcinoma brain metastasis which shows little peritumoural white matter disruption and has a high peritumoural fractional anisotropy (FA) value at the biopsy location shown. B. H&E, C. CD3 stained serial section showing sparse T cell infiltration in this same region (inset, magnified). This contrasts with the breast cancer brain metastasis in D, where there is more change in the peritumoural white matter and the FA value in the peritumoural region shown is lower. Here, there is dense peritumoural T cell infiltration (E, F and inset, magnified). G. The cases with a peritumoural FA >median (n=8, thick line) died sooner after neurosurgical resection of their metastasis than those with a lower peritumoural FA (n=9, dashed line) (log rank statistic = 4.566, $p<0.05$). H. The FA values differentiated categories of peritumoural CD3+ T cell density (<5, 5-25 and >25 per high power field) in the co-localised image-guided biopsy regions (Kruskal-Wallis, $p<0.05$), although such a relation is not seen with other immune cells such as CD68+ macrophages or CD20+ B cells nor is it seen with other MRI measures, such as the mean diffusivity (MD).

4.3.5 The leading edge is a distinct biological region but this does not explain the variation in peritumoural FA

The intra-tumoural heterogeneity seen at DWI was mirrored when examining tissue samples. The paired samples from edge and core locations indicated lower necrosis (Wilcoxon paired samples test -2.921, p=0.03) and higher vascularity (CD34+ vessels, 1.98, p=0.048) in the leading edge over the core. However, there was no significant difference in connective tissue density, proliferation (Ki67 index) or the expression of metastasis inducing proteins & matrix-metallo-proteinases between the regions. These results are summarised in **Table 4.3**.

Parameter assessed:	Core (units given)	Leading edge (units given)	Comparison of core vs. edge (test & significance given)	
Connective tissue (reticulin) density	High = 22 cases Low = 4 cases	High = 18 cases Low = 7 cases	Fishers' Exact test, p=0.3	
Proliferation (Ki67 index)	28% (6 – 64)	21% (5 – 99)	Wilcoxon matched pairs, p=0.637	
Necrosis	30% of field (range 0 – 90)	5% of field (range 0 – 50)	Wilcoxon matched pairs, p=0.003*	
Vascularity	1.9 CD34 + vessels per $0.5mm^2$ (range 0 – 11)	4.9 CD34 + vessels per $0.5mm^2$ (range 0 – 33)	Wilcoxon matched pairs, p=0.032*	
Protein:	**Core (% positive cells/sample)**	**Core, proportion positive (1% cut-off)**	**Leading edge (% positive cells/sample)**	**Edge, proportion positive (1% cut-off)**
S100A4	70	19/24 (79%)	55	23/26 (88%)
S100P	60	20/24 (83%)	60	20/26 (77%)
AGR2	5	15/24 (63%)	5	18/26 (69%)
OPN	45	21/24 (88%)	70	22/26 (85%)
MMP2	43	17/24 (71%)	60	19/26 (73%)
MMP9	55	22/24 (92%)	45	23/26 (88%)
MMP13	20	15/24 (63%)	20	15/25 (60%)

Table 4.3: Table comparing edge and core biologically for a number of different parameters.

There was a trend to increased positive staining for the protein S100A4 - which is associated with intracranial progression - at the leading edge versus the core. There were no differences in cellularity, proliferative index, vascularity, necrosis or connective tissue density in the tumour edges adjacent to peritumoural regions that had lower versus higher FA readings.

4.3.6 Invasive growth patterns are poorly predicted macroscopically, but not associated with altered peritumoural FA or reduced survival

Overall 118 samples were obtained from the 26 metastases with a median of 5 samples per case. Microscopically 71/118 samples showed evidence of tumour cells beyond the apparent B-BM margin, whereas 20/26 cases were reported macroscopically by the operating neurosurgeon to have a clearly defined border to white matter; the kappa statistic (0.02) indicated the significant discordance of micro and macroscopic assessments, illustrated in **Figure 4.7.** There was no infiltration of tumour cells beyond one high powered field width or 0.5mm, from the apparent B-BM margin.

All the breast cancer metastases studied (4/4) showed diffusely infiltrating growth patterns microscopically, whereas lung cancers were less likely to have a surgical plane at operation (only 2/13 were encapsulated), however, overall there was no significant association of invasive growth with primary cancer histology (Fisher's test = 2.166, p=0.939). Importantly, there was no relation of growth pattern to the subsequent survival (HR for death of an encapsulated metastasis = 0.73, 95% CI 0.42 – 1.28, p=0.28). There was no association of growth pattern with the FA in the peritumoural region, whether classified by a pathologist microscopically (Kruskal-Wallis test p=0.539) or a neurosurgeon macroscopically (Mann-Whitney U, p=1.0).

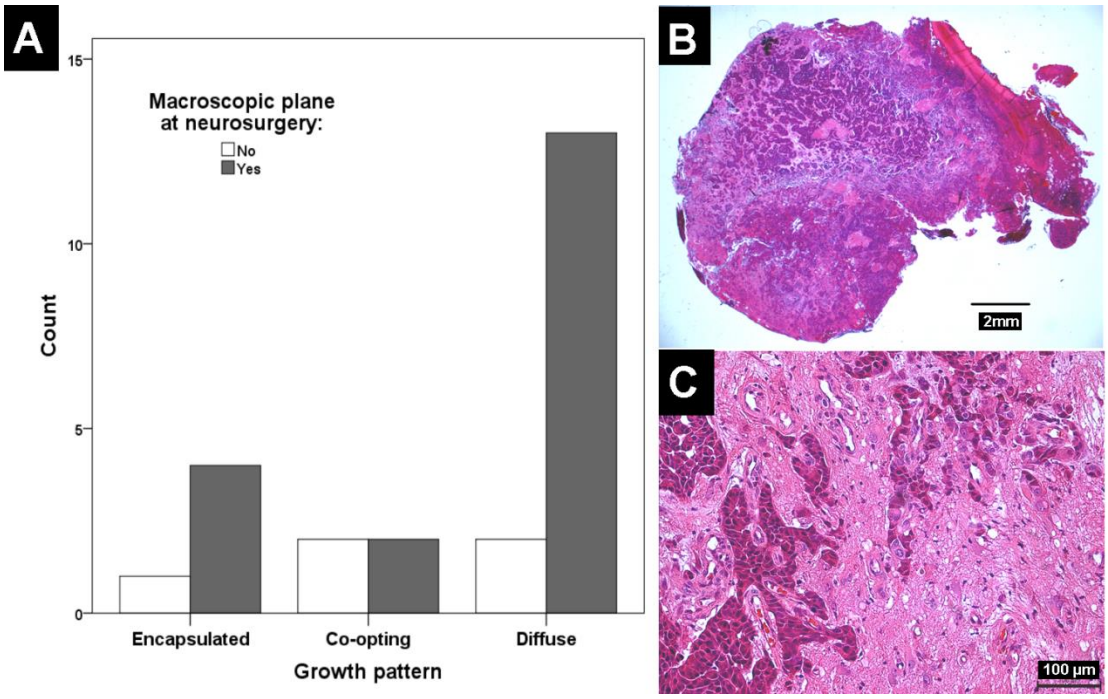

Figure 4.7: A. Macroscopic assessment by the operating neurosurgeon – defined as a clear plane found at microsurgical dissection – was discordant with the microscopic growth pattern observed in the laboratory using samples from the leading edge of the tumour. B. For example, in this breast cancer brain metastasis, the operating neurosurgeon recorded a complete macroscopic resection with a clear plane to surrounding brain in the operative notes (H&E stained specimen, 12.5x magnification). C. Microscopically, however, there was a diffusely invasive leading edge (H&E, 200x magnification). Neither the macroscopic nor the microscopic growth patterns seen at surgery were predictive of overall survival or time to intracranial progression.

Peritumoural FA was not a surrogate of biological differences in the metastasis' leading edge, such as cellularity or the expression of metastasis inducing proteins, and it was not a surrogate of a particular phenotype, such as diffusely invasive growth. We therefore hypothesised that the peritumoural FA might be related to host response to the brain metastasis.

4.3.7 T-cell infiltration at the B-BM interface is variable, associated with survival and reflected by peritumoural FA

We consistently observed dense macrophage infiltration at the B-BM interface across tumours from different primaries **(**median 62 CD68-positive cells per HPF in peritumoural regions versus 21 per HPF in control regions, shown by primary cancer type in **Figure 4.8)**. This peritumoural infiltration was also significantly greater than

in the core or the edge of the metastases **(**related samples Wilcoxon tests p<0.001 for all comparisons, cell counts shown in **Table 4.4)** and qualitatively we observed a wall of macrophages surrounding the tumour rather than islands or a diffuse infiltrate extending away from the tumour edge. Metastases were accompanied by a diffuse glial reaction in the adjacent brain (peritumoural GFAP-positive cell density was significantly greater than control white matter, related samples Wilcoxon test, p=0.003, see **Stable 4.4)**, however only 5/26 tumours were noted to have the pseudocapsule of compressed glial material around them as reflected in the growth pattern assessment described earlier. There was some evidence of increased peritumoural vascularity (median 2 CD34-positive vessels per HPF, compared to <1 in control regions, p=0.001) but this was not significantly different to the core or edge of the metastases (paired Wilcoxon tests p=0.57 and p=0.17 respectively, cell counts in **Table 4.4**). No difference was seen even when those tumours with a co-opting growth pattern (4/26) - which would not be expected to rely on neo-angiogenesis - were excluded. CD20-positive B cell infiltration was sparse (median <1 cells per HPF in the edge and peritumoural regions, no significant difference from control white matter, **Table 4.4).**

Parameter/ region	Core	Leading edge	Peri-tumoural	Control WM	Edge vs. Core	Peri-tumoural vs. Edge	Peri-tumoural vs. Control
Macrophage infiltration (CD68)	19.0 (5 – 108)	20.3 (0 – 110)	62.3 (9 – 320)	20.5 (3 - 72)	0.67*	0.04	0.17
B cell infiltration (CD20)	0 (0 - 10)	0.2 (0 - 37)	0.1 (0 - 5)	0 (0)	0.73*	0.60*	0.58*
T cell infiltration (CD3)	4.1 (0 – 95)	10.1 (0 - 195)	16.3 (0 - 113)	1.4 (0 - 15)	0.73*	0.63*	0.39
Glial reaction (GFAP+ cell density)			41% (26 - 68)	34% (16 - 45)			0.21
Vascularity (CD34+ vessels per HPF)	1.9 (0 -11)	3.1 (0 - 33)	2.2 (0 – 9)	0.4 (0 – 5)	0.30	-0.09	-0.03

Table 4.4: Inflammatory cell infiltration in different regions around brain metastases, expressed as median number of immunoreactive cells per high powered field (=0.5mm^2) for each given stain, range in brackets. Spearman rank correlation test statistics are shown and asterisk highlights significant correlations.
WM = white matter, HPF = high powered field.

CD3-positive lymphocytes, assumed to be T-cells, were seen in the peritumoural region in all except 1 case (median 16 cells per HPF, significantly greater than control white matter, $p<0.001$). A single patient with malignant melanoma was taking ipilimumab (an immune checkpoint inhibitor) prior to surgery and their brain metastasis demonstrated significantly higher peritumoural T-cell infiltration (Mann-Whitney U statistic = 3.583, $p<0.001$) than the other three malignant melanoma metastases and a trend to higher macrophage infiltration (Mann-Whitney U statistic = 2.049, $p=0.056$), both highlighted in **Figure 4.8.**

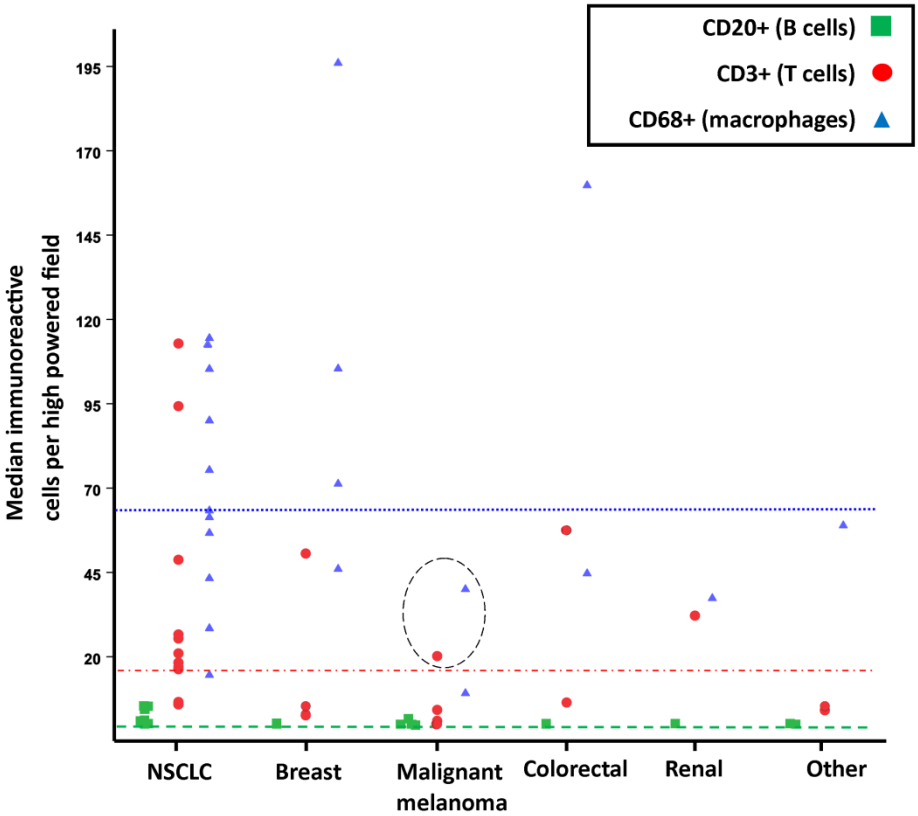

Figure 4.8: The distribution of inflammatory cells in the peritumoural region expressed as number of immunoreactive cells per high powered field ($0.5mm^2$) and categorised by primary cancer. Dashed lines show the group median number of each cell type. The dashed circle highlights a patient with malignant melanoma who had been receiving immune stimulating therapy (ipilimumab, a CTLA-4 blocking antibody).

Even when excluding this case, there was no significant variation in numbers of any type of immunoreactive cells in any region (core, edge or peritumoural) by primary cancer of origin for these brain metastases (Kruskal-Wallis tests $p>0.05$ for each comparison). Cancers with extracranial metastases had a significantly lower tumoural and peritumoural T-cell infiltration in the brain whereas synchronous cases showed significantly elevated numbers of immunoreactive cells compared to control white matter (Mann-Whitney U, $p<0.05$). No other clinical factors, such as the control of the primary disease, number or location of cranial metastases, patient age or gender had any significant association with immunoreactive cell counts.

The different immune response in different metastases appears clinically relevant since peritumoural T cell infiltration, but **not** edge or core T cell infiltration and **not** peritumoural macrophage or B cell infiltration, was associated with prolonged OS, even when controlling for the confounders WBRT and tumour size by multivariate Cox regression analysis (illustrated in **Figure 4.9A** and **Table 4.5).** When the response was further categorised into 3 groups (<5, 5-25 and >25 median immunoreactive cells per high powered field), those with moderate peritumoural T cell infiltration appeared to be at no advantage compared to those with low infiltration, whereas those with the highest T cell infiltrates still maintained a survival advantage (**Figure 4.9B**).

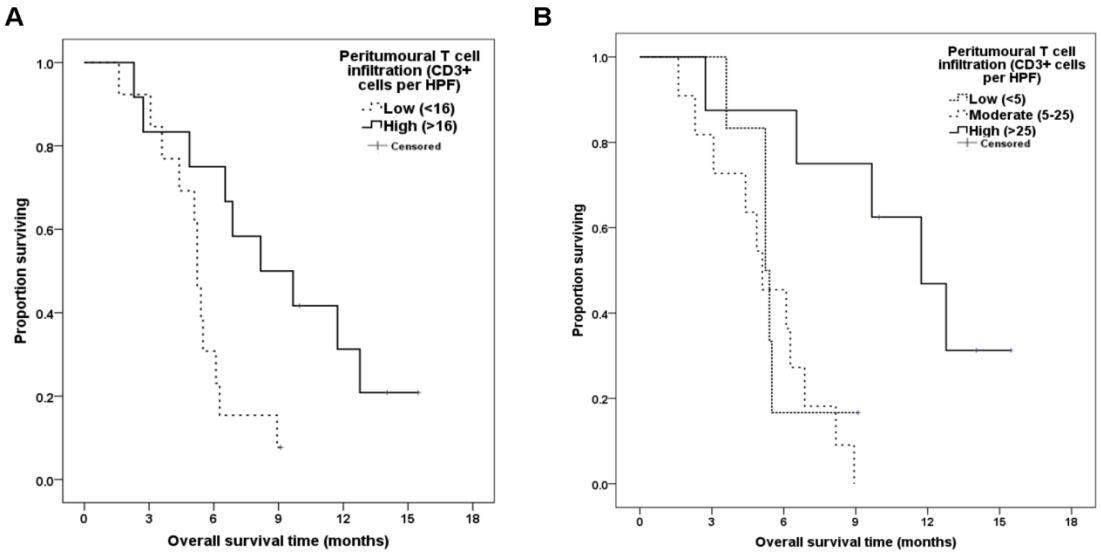

Figure 4.9: A. Higher than median peritumoural T cell count is associated with improved overall survival for resected brain metastases, compared to lower than median (log rank test

= 5.77, p = 0.016) and the highest counts are associated with longer overall survival compared to moderate and low counts (log rank = 10.06, p=0.007).

	HR for death	95% CI for HR	Sig.
Adjuvant WBRT	0.117	0.031 – 0.435	.001
Longest axis > 30mm	3.226	1.190 – 8.748	.021
Density of CD3+ cells in peritumoural region	0.962	0.931 - 0.994	.021

Table 4.5: Multivariate Cox proportional hazards model for overall survival.

Since peritumoural FA was also associated with survival, and biologically white matter may be expected to be disrupted by lymphocyte infiltration, the co-localised MRI and tissue data were compared for these features. Only the peritumoural density of CD3+ T-cells differed between the high and low peritumoural FA regions (Mann Whitney U, p=0.037), as seen in **Figure 4.6H**. The continuous values for peritumoural CD3+ T-cell density and peritumoural FA were compared for co-localised samples and were strongly correlated (Spearman's rho, p=0.004), whereas MR features such as ADC, MD in that region, or FA in the tumour at that location, showed no such association.

4.4 Discussion

In this first-in-man examination of the relationship between advanced MRI measurements and inflammation at the B-BM interface, we have shown that the FA in the peritumoural region is significantly associated with the density of T cell infiltration there and that increased CD3+ T cell infiltration is associated with prolonged overall survival after macroscopic resection. This effect is independent of giving adjuvant WBRT or smaller tumour size, the only other factors significantly extending overall survival in this cohort. These novel findings highlight the role of the tumour microenvironment in mediating BM behaviour and suggests inflammatory responses in this region can be measured non-invasively in patients with different primary cancers in a clinically relevant context.

4.4.1 Advanced MRI findings at the B-BM interface

The MRI characteristics of brain metastases have been extensively studied using DWI for isotropic and DTI for anisotropic diffusion (Zakaria et al., 2014b, Mills et al., 2012, Price et al., 2004). Numerical findings in this series are entirely in keeping with those previously recorded by ourselves and other groups (Zakaria et al., 2014a). Even those studies which focused on the B-BM interface by measuring changes in the peritumoural region, rather than just in the tumour, have exclusively examined tumour invasion (Price et al., 2004, Lu et al., 2004, Lemercier et al., 2014). The finding that brain metastases are only locally invasive to a small depth compared to glioma - also extensively characterised by advanced MRI – has led to a number of studies seeking to distinguish these two tumour types. In such schemes, the peritumoural FA is shown to be significantly less in glioma (i.e. white matter more disrupted), in keeping with the biological nature of this cancer, invading through and along white matter tracts e.g. (Price and Gillard, 2011, Byrnes et al., 2011, Kelly et al., 1987). There has been little or no attempt to look at the intra- and inter-tumoural heterogeneity for brain metastases (Duygulu et al., 2010, Hayashida et al., 2006). It may be that a focus on measuring the degree of tumour infiltration or invasion is missing an important biological effect. The brain is uniquely sensitive to inflammatory changes which disrupt white matter and this can be assessed by changes in anisotropic diffusion, as has been shown for large series of patients with a variety of pathologies including multiple sclerosis (Commowick et al., 2008), stroke (Jiang et al., 2010), dementia and head injury (Fakhran et al., 2013). Brain metastases offer a unique opportunity for investigation, since there is no diffuse invasion of tumour cells to disrupt the white matter signal being measured. MRI changes may appear with very little inflammatory response as the brain is a privileged environment and DTI is often obtained in the routine course of clinical assessment and surgical planning.

Taken in concert with our previous work (Zakaria et al., 2014c), we suggest that ours and other previous studies assessing the B-BM interface may have been imaging immune response rather than tumour differences across the leading edge, and this has only become clear when MRI data in both regions along with matched tissue are analysed together. This analysis has been undertaken here for the first time in

patients with active disease as opposed to post mortem tissue (Berghoff et al., 2013a) or in animal models (Serres et al., 2014).

4.4.2 The immune cell response at the B-BM interface varies between patients and is associated with prolonged survival

Immune response and in particular quantifying tumour-associated CD3+ T cells is currently of great interest as a means of improving prognostication and developing therapies in cancer medicine (Gooden et al., 2011). A small number of reports have disagreed on the degree of T cell infiltration in brain metastases from solid organ cancers (Kluger et al., 2015, Berghoff et al., 2015). From our findings, this is not surprising, since there is a considerable variation in numbers of immune and inflammatory cells with location. Random tumour "cores" of the type obtained and used in high throughput studies may be missing the effects seen here, where larger samples have been taken *in vivo* from the B-BM interface. There is already post-mortem data suggesting the presence of immune cells may be more pronounced at this location (Berghoff et al., 2015) and we have now shown measurable intra-tumoural heterogeneity in brain metastases. We have also shown that in patients with brain metastases taking oral steroids at clinically meaningful doses, who have been treated with systemic chemotherapy, CD3+ T cells can be reliably detected in their brain metastases and their presence is associated with increased survival. In one case, a patient had been treated with immune stimulating therapy in the form of anti-CTLA4 antibody (ipilimumab), which has been shown to improve metastatic brain disease in melanoma patients (Margolin et al., 2012). Demonstrating increased peritumoural T cell infiltration in such a patient compared to others with a similar tumour is important because it confirms that in a neurosurgical patient on chemotherapy and oral steroids, the cellular immune response around the tumour is still measurably increased.

4.4.3 Intra-tumoural and inter-tumoural heterogeneity did not predict survival in this series, but can be detected at MRI

Recent studies have divided brain metastases of various primary cancers into more and less invasive phenotypes both *in vivo* (Neves et al., 2001, Siam et al., 2015) and post mortem (Berghoff et al., 2013b) and attempted to relate this invasive phenotype to primary cancer type and prognosis. These studies all recognise that whilst there may be varying degrees of invasion locally, metastases do not show the degree of deep, widespread tumour infiltration seen in glioma (Kelly et al., 1987) and, indeed, some surgical studies have found the B-BM interface to be strongly demarcated (Baumert et al., 2006). We have confirmed that there is intra-tumoural heterogeneity in brain metastases with necrotic, fluid cores and more cellular leading edges. Further, we found inter-tumoural heterogeneity at these edges with varying patterns and degrees of local invasion which were not predicted by the operating surgeon's assessment of the B-BM interface. Nonetheless, there were no significant differences found in the potential drivers of invasion, such as MMP, MIP expression nor in the downstream hallmarks of more aggressive tumours, such as high nuclear:cytoplasmic ratio, higher Ki67 index or increased vascularity. Purely descriptive studies are useful in increasing biological understanding, but the overriding clinical evidence on treatment of brain metastasis from many diverse trials suggests a more complex interaction between local (SRS, surgery) and whole brain treatments (WBRT) than could be explained simply by a binary classification of the B-BM interface as invasive or circumscribed. Genetic analysis of the tumour core and the edge, using RNA sequencing for example, or from edges of rapidly locally recurring cases versus the opposite, may deepen understanding about what underlies the observed differences on the tumour side, even if some changes on the brain side have already been described (Siam et al., 2015).

4.4.4 Limitations and future directions

It is important to note that the samples obtained in the course of this study are not routinely available, unless one is intentionally undertaking a supra marginal excision, as has been proposed by some neurosurgeons (Patel et al., 2010, Yoo et al., 2009). Normally one would obtain a core biopsy or piecemeal tumour specimens which are

sufficient for diagnosis and, increasingly, genetic analysis (Brastianos et al., 2015) but not for any peritumoural changes. This is why it is so important to have demonstrated a potential non-invasive surrogate marker of peritumoural T cell infiltration, since it offers the possibility of assaying the immune response even for inaccessible or non-surgical cases.

The IHC techniques are intentionally simple so as to make clinical applicability as broad as possible. We need to apply more specific stains to serial sections from the leading edge locations in order to determine the type and activation of the T cells seen. It would also be of note to determine if potential modifiable drug targets such as PD-1 and PD-L1 are present in the adjacent tumour tissue, as this would offer further evidence for using existing drugs to modify the immune response.

The image guidance system used here is of the sort routinely available in clinical neurosurgical practice in Europe and North America. The system is not designed or licensed for obtaining co-localised MRI and tissue data specifically, and the accuracy of this localisation is dependent on a number of factors ranging from the fidelity of the "planning" preoperative MRI scan to the type of image registration algorithms applied (Widmann et al., 2012). One could have improved this accuracy, feasibly, by using an instrument- or robot-mounted tool to take samples, as opposed to hand held forceps. Such tools would limit the freedom of movement and angle of sampling, reducing the surgeon's ability to manoeuvre the probe to the true B-BM interface under direct visual and computer-aided navigation, as compared to taking needle biopsies from a closed cavity through a burr hole for example. To reflect this uncertainty we have used a 5mm diameter "region" of biopsy rather than a voxel-sized point and have taken average readings across this region to mirror the median cell counts used to assay immune cell infiltration in a given area. Finally, in neuronavigation there is an issue of brain shift (Kuhnt et al., 2012) where the pre-registered navigation is rendered inaccurate once CSF is released and, although one can try to correct for this shift using intraoperative ultrasound, this is not our routine clinical practice, since it requires intense computational power and incurs a time delay. This is of little practical benefit in navigation when dealing with mostly

superficial tumours (metastases are mostly seen at the grey-white matter zone), where the brain oedema balances the loss of CSF on opening the dura.

Further study could be directed at using DTI to measure the response to immune therapy over time, e.g. during ipilimumab therapy in melanoma patients, or by matching T cell infiltration to further advanced imaging techniques such as perfusion and spectroscopy. These imaging techniques may be equally good surrogates for T cell infiltration in the peritumoural region. It would also be pertinent to use differing MR analysis tools, e.g. generating tracts and measuring the FA change along these where they overlap with a biopsy region.

4.5 Conclusion

We have tested the hypothesis that the immune reaction to brain metastases is variable and shown that the CD3+ T cell density in the peritumoural region is independently associated with overall survival for patients with an operated brain metastasis from solid organ cancer. Higher T cell infiltration in this region is associated with white matter disruption and a decrease in anisotropic diffusion as measured non-invasively by diffusion weighted MRI.

Chapter 5: Conclusions and future directions

5.1 Summary of the clinical problem

Brain metastases are an important clinical problem and there are a number of unmet needs that have been discussed in the course of this thesis. Despite a variety of scoring systems to predict patient survival, there are no individualised markers of overall survival or intracranial progression in brain metastases. Such markers would be useful because there is deep uncertainty about the best combination of local therapies (surgery, SRS) and whole brain radiotherapy in treating these tumours. Furthermore, there is limited understanding of the brain-brain metastasis (B-BM) interface, but early investigations have suggested a more complicated interaction between the tumour and host than had been assumed previously and certainly more complex than the macroscopic appearance suggests. This has implications for clinical management, since there is currently no diagnostic means to determine those tumours that are more invasive and would potentially benefit from more aggressive local treatments such as cavity boost radiation or wider surgical resection margins. The B-BM interface is also the focus of the host-tumour interaction, including the immune response and therefore a source of potential therapeutic targets.

5.2 Summary of experimental findings in relation to original hypotheses

The aim of this thesis was to derive biological and radiological markers of local brain metastasis invasion, intracranial progression and survival which may be used in clinical practice, whilst deepening scientific understanding of the brain-brain metastasis interface.

The first hypothesis was that proteins which induce a metastatic phenotype in solid organ cancers are also involved in local invasion in brain metastases and that levels of expression of such proteins may be associated with clinical outcomes such as survival and progression for patients with brain metastases. I have shown that proteins known to be associated with metastasis in other cancers are also widely expressed in brain metastases, regardless of the primary cancer of origin. In

particular, the metastasis-inducing protein S100A4 was overexpressed in brain metastases that progressed after surgical removal, although there was insufficient detail in this retrospective series to determine if this was local or distant brain recurrence. Overexpression of the metastasis inducing protein osteopontin was associated with a survival benefit after WBRT. These are potentially useful clinical markers because there is a trend to try and omit whole brain irradiation after surgery for these metastases. If used in combination, for example, patients with a resected metastasis expressing S100A4 and osteopontin might be stratified for treatment with adjuvant WBRT, rather than active surveillance, as they have a higher risk of progression and better radiation response.

The second hypothesis was that measurements may be taken from diffusion weighted MRI brain scans of patients with brain metastases with high reliability on clinical grade hardware and software. This was well demonstrated and subsequent larger studies have repeatedly confirmed such findings across different pathologies and different MRI scanning facilities. Next we hypothesised that these MRI measures may be associated with clinical outcomes such as survival and progression in patients with brain metastases. Analysis of pre-operative MRI scans showed that the diffusion change across the B-BM boundary, rather than any diffusion characteristic of the metastasis itself, was independently associated with overall survival. A sharp change in ADC from tumour edge into peritumoural brain predicted worse survival. This was initially felt to be counterintuitive, as one would expect such cases to be more completely resected and show less local invasion at the leading edge. However, using unmatched tissue, we demonstrated that a sharp change in ADC reflected high leading edge cellularity and intense vasogenic oedema.

The final hypothesis was that differences between tumours in diffusion weighted MRI characteristics at the B-BM boundary reflected underlying differences in invasive growth pattern, metastasis inducing protein expression and markers of aggressive behaviour such as vascularity, cellularity and proliferation. In fact, analysis of image-guided samples from the B-BM interface revealed that ADC changes at the leading edge were not indicative of local invasion or invasive growth patterns in this region, but instead found that there was variable infiltration of T cells in the peritumoural region. Those cases with a higher peritumoural T cell density

showed longer overall survival, even when controlling for other confounding variables and radiation treatment. Instead of detecting this change by isotropic diffusion on the ADC maps, we observed only changes in anisotropic diffusion, measured by the FA values and reflecting peritumoural white matter infiltration by these immune cells. In hindsight this is actually a very logical result, since we know that white matter is uniquely sensitive to changes in inflammation and immune infiltration from other more widely studied pathologies such as head injury and multiple sclerosis.

5.3 Areas for further investigation

The T cell findings provide a biological rationale for the recent emergence of immune therapy as a possible treatment in cancer and brain metastases. There are licensed drugs (such as ipilimumab) that enhance and deregulate the cellular immune response. Disease monitoring of brain metastasis response currently relies on contrast-enhanced margins on MRI. Our data suggest that diffusion MRI could be used to measure the immune cellular response (i.e. the host response) by determining the degree of peritumoural inflammation. Serial DTI data in a series of patients undergoing immune-modifying therapy is essential to investigate this further. One patient with melanoma in this series receiving ipilimumab showed an enhanced response and appropriate FA changes demonstrating proof of concept for disease monitoring. A future study in brain metastases, therefore, might be based on using DTI to stratify patients for immune modifying therapy. A number of clinical trial concepts also arise from this thesis. A randomised trial of cavity SRS versus observation versus WBRT has never been performed and one possibility is to stratify solitary metastases after resection using the markers OPN or S100A4 to observation if there is a low risk of intracranial progression as opposed to radiotherapy if there is a high risk. A surgical trial would be to randomise solitary metastases to either standard of care surgical resection or intentional “super marginal” resection where a cuff of normal appearing brain around the metastasis is also resected to include microscopic infiltrates with or without a local SRS boost to the cavity. This thesis has highlighted new approaches and possibilities that will inform the field and stimulate collaboration and hopefully progress for the unfortunate and increasing number of patients suffering with brain metastases.

Bibliography

ABEL, T. J., RYKEN, T., LESNIAK, M. S. & GABIKIAN, P. 2013. Gliadel for brain metastasis. *Surg Neurol Int,* 4**,** S289-93.

ANBORGH, P. H., MUTRIE, J. C., TUCK, A. B. & CHAMBERS, A. F. 2010. Role of the metastasis-promoting protein osteopontin in the tumour microenvironment. *J Cell Mol Med,* 14**,** 2037-44.

ANZALONE, N., ESSIG, M., LEE, S. K., DÖRFLER, A., GANSLANDT, O., COMBS, S. E. & PICOZZI, P. 2013. Optimizing contrast-enhanced magnetic resonance imaging characterization of brain metastases: relevance to stereotactic radiosurgery. *Neurosurgery,* 72, 691-701.

BARAJAS JR, R. F., RUBENSTEIN, J. L., CHANG, J. S., HWANG, J. & CHA, S. 2010. Diffusion-weighted MR imaging derived apparent diffusion coefficient is predictive of clinical outcome in primary central nervous system lymphoma. *American Journal of Neuroradiology,* 31**,** 60-66.

BARAJAS, R. F., CHANG, J. S., SNEED, P. K., SEGAL, M. R., MCDERMOTT, M. W. & CHA, S. 2009. Distinguishing recurrent intra-axial metastatic tumor from radiation necrosis following gamma knife radiosurgery using dynamic susceptibility-weighted contrast-enhanced perfusion MR imaging. *AJNR Am J Neuroradiol,* 30, 367-72.

BARAJAS, R. F., JR., RUBENSTEIN, J. L., CHANG, J. S., HWANG, J. & CHA, S. 2010. Diffusion-weighted MR imaging derived apparent diffusion coefficient is predictive of clinical outcome in primary central nervous system lymphoma. *AJNR Am J Neuroradiol,* 31**,** 60-6.

BARNHOLTZ-SLOAN, J. S., SLOAN, A. E., DAVIS, F. G., VIGNEAU, F. D., LAI, P. & SAWAYA, R. E. 2004. Incidence proportions of brain metastases in patients diagnosed (1973 to 2001) in the Metropolitan Detroit Cancer Surveillance System. *J Clin Oncol,* 22**,** 2865-72.

BARRACLOUGH, D. L., PLATT-HIGGINS, A., DE SILVA RUDLAND, S., BARRACLOUGH, R., WINSTANLEY, J., WEST, C. R. & RUDLAND, P. S. 2009. The metastasis-associated anterior gradient 2 protein is correlated with poor survival of breast cancer patients. *Am J Pathol,* 175**,** 1848-57.

BAUMERT, B. G., RUTTEN, I., DEHING-OBERIJE, C., TWIJNSTRA, A., DIRX, M. J., DEBOUGNOUX-HUPPERTZ, R. M., LAMBIN, P. & KUBAT, B. 2006. A pathology-based substrate for target definition in radiosurgery of brain metastases. *Int J Radiat Oncol Biol Phys,* 66**,** 187-94.

BEASLEY, K. D. & TOMS, S. A. 2011. The molecular pathobiology of metastasis to the brain: a review. *Neurosurg Clin N Am,* 22**,** 7-14, v.

BERGHOFF, A. S., KOVANDA, A. K., MELCHARDT, T., BARTSCH, R., HAINFELLNER, J. A., SIPOS, B., SCHITTENHELM, J., ZIELINSKI, C. C., WIDHALM, G., DIECKMANN, K., WELLER, M., GOODMAN, S. L., BIRNER, P. & PREUSSER, M. 2014. alphavbeta3, alphavbeta5 and alphavbeta6 integrins in brain metastases of lung cancer. *Clin Exp Metastasis,* 31**,** 841-51.

BERGHOFF, A. S., LASSMANN, H., PREUSSER, M. & HOFTBERGER, R. 2013a. Characterization of the inflammatory response to solid cancer metastases in the human brain. *Clin Exp Metastasis,* 30**,** 69-81.

BERGHOFF, A. S., RAJKY, O., WINKLER, F., BARTSCH, R., FURTNER, J., HAINFELLNER, J. A., GOODMAN, S. L., WELLER, M., SCHITTENHELM, J. & PREUSSER, M. 2013b. Invasion patterns in brain metastases of solid cancers. *Neuro Oncol,* 15**,** 1664-72.

BERGHOFF, A. S., RICKEN, G., WIDHALM, G., RAJKY, O., DIECKMANN, K., BIRNER, P., BARTSCH, R., HOLLER, C. & PREUSSER, M. 2015. Tumour-infiltrating lymphocytes

and expression of programmed death ligand 1 (PD-L1) in melanoma brain metastases. *Histopathology,* 66**,** 289-99.

BERGHOFF, A. S., SPANBERGER, T., ILHAN-MUTLU, A., MAGERLE, M., HUTTERER, M., WOEHRER, A., HACKL, M., WIDHALM, G., DIECKMANN, K., MAROSI, C., BIRNER, P., PRAYER, D. & PREUSSER, M. 2013c. Preoperative diffusion-weighted imaging of single brain metastases correlates with patient survival times. *PLoS One,* 8**,** e55464.

BILGILI, Y. & UNAL, B. 2004. Effect of Region of Interest on Interobserver Variance in Apparent Diffusion Coefficient Measures. *American Journal of Neuroradiology,* 25**,** 108-111.

BLASEL, S., JURCOANE, A., FRANZ, K., MORAWE, G., PELLIKAN, S. & HATTINGEN, E. 2010. Elevated peritumoural rCBV values as a mean to differentiate metastases from high-grade gliomas. *Acta Neurochir,* 152, 1893-99.

BOLONYI, F. 1958. Study of the reticulin fibers of brain tumors. *J Neuropathol Exp Neurol,* 17**,** 240-6.

BRASTIANOS, P. K., CARTER, S. L., SANTAGATA, S., CAHILL, D. P., TAYLOR-WEINER, A., JONES, R. T., VAN ALLEN, E. M., LAWRENCE, M. S., HOROWITZ, P. M., CIBULSKIS, K., LIGON, K. L., TABERNERO, J., SEOANE, J., MARTINEZ-SAEZ, E., CURRY, W. T., DUNN, I. F., PAEK, S. H., PARK, S. H., MCKENNA, A., CHEVALIER, A., ROSENBERG, M., BARKER, F. G., 2ND, GILL, C. M., VAN HUMMELEN, P., THORNER, A. R., JOHNSON, B. E., HOANG, M. P., CHOUEIRI, T. K., SIGNORETTI, S., SOUGNEZ, C., RABIN, M. S., LIN, N. U., WINER, E. P., STEMMER-RACHAMIMOV, A., MEYERSON, M., GARRAWAY, L., GABRIEL, S., LANDER, E. S., BEROUKHIM, R., BATCHELOR, T. T., BASELGA, J., LOUIS, D. N., GETZ, G. & HAHN, W. C. 2015. Genomic characterization of brain metastases reveals branched evolution and potential therapeutic targets. *Cancer Discov,* 5**,** 1164-77.

BRESNICK, A. R., WEBER, D. J. & ZIMMER, D. B. 2015. S100 proteins in cancer. *Nat Rev Cancer,* 15**,** 96-109.

BRODBELT, A. 2012. Delaying emergency treatment for patients with cerebral abscesses and brain tumours: a consequence of the neuroscience MDT? *Br J Neurosurg,* 26, 325.

BRODBELT, A., GREENBERG, D., WINTERS, T., WILLIAMS, M., VERNON, S. & COLLINS, V. P. 2015. Glioblastoma in England: 2007-2011. *Eur J Cancer,* 51**,** 533-42.

BULAKBASI, N., KOCAOGLU, M., FARZALIYEV, A., TAYFUN, C., UCOZ, T. & SOMUNCU, I. 2005. Assessment of diagnostic accuracy of perfusion MR imaging in primary and metastatic solitary malignant brain tumors. *AJNR Am J Neuroradiol,* 26, 2187-99.

BULAKBASI, N., KOCAOGLU, M., ORS, F., TAYFUN, C. & UÇÖZ, T. 2003. Combination of single-voxel proton MR spectroscopy and apparent diffusion coefficient calculation in the evaluation of common brain tumors. *AJNR Am J Neuroradiol,* 24, 225-33.

BYRNES, T. J., BARRICK, T. R., BELL, B. A. & CLARK, C. A. 2011. Diffusion tensor imaging discriminates between glioblastoma and cerebral metastases in vivo. *NMR Biomed,* 24**,** 54-60.

CALLI, C., KITIS, O., YUNTEN, N., YURTSEVEN, T., ISLEKEL, S. & AKALIN, T. 2006. Perfusion and diffusion MR imaging in enhancing malignant cerebral tumors. *Eur J Radiol,* 58**,** 394-403.

CARBONELL, W. S., ANSORGE, O., SIBSON, N. & MUSCHEL, R. 2009. The vascular basement membrane as "soil" in brain metastasis. *PLoS One,* 4**,** e5857.

CATHCART, J., PULKOSKI-GROSS, A. & CAO, J. 2015. Targeting matrix metalloproteinases in cancer: Bringing new life to old ideas. *Genes Dis,* 2**,** 26-34.

CHANG, E. L., WEFEL, J. S., HESS, K. R., ALLEN, P. K., LANG, F. F., KORNGUTH, D. G., ARBUCKLE, R. B., SWINT, J. M., SHIU, A. S., MAOR, M. H. & MEYERS, C. A. 2009. Neurocognition in patients with brain metastases treated with radiosurgery or

radiosurgery plus whole-brain irradiation: a randomised controlled trial. *The Lancet Oncology,* 10**,** 1037-44.

CHEN, W., WANG, L., ZHU, W., XIA, L., QI, J., FENG, D. & LUO, X. 2012a. Multicontrast single-slab 3D MRI to detect cerebral metastasis. *AJR Am J Roentgenol,* 198, 27-32.

CHEN, X. Z., YIN, X. M., AI, L., CHEN, Q., LI, S. W. & DAI, J. P. 2012b. Differentiation between brain glioblastoma multiforme and solitary metastasis: qualitative and quantitative analysis based on routine MR imaging. *AJNR Am J Neuroradiol,* 33**,** 1907-12.

CHERNOV, M. F., ONO, Y., KUBO, O. & HORI, T. 2006. Comparison of 1H-MRS-detected metabolic characteristics in single metastatic brain tumors of different origin. *Brain Tumor Pathol,* 23, 35-40.

CHIANG, I. C., KUO, Y. T., LU, C. Y., YEUNG, K. W., LIN, W. C., SHEU, F. O. & LIU, G. C. 2004. Distinction between high-grade gliomas and solitary metastases using peritumoral 3-T magnetic resonance spectroscopy, diffusion, and perfusion imagings. *Neuroradiology,* 46**,** 619-27.

COMMOWICK, O., FILLARD, P., CLATZ, O. & WARFIELD, S. K. 2008. Detection of DTI white matter abnormalities in multiple sclerosis patients. *Medical image computing and computer-assisted intervention : MICCAI ... International Conference on Medical Image Computing and Computer-Assisted Intervention,* 11**,** 975-82.

CONNELL, J. J., CHATAIN, G., CORNELISSEN, B., VALLIS, K. A., HAMILTON, A., SEYMOUR, L., ANTHONY, D. C. & SIBSON, N. R. 2013. Selective permeabilization of the blood-brain barrier at sites of metastasis. *J Natl Cancer Inst,* 105**,** 1634-43.

CRISI, G., ORSINGHER, L. & FILICE, S. 2013. Lipid and macromolecules quantitation in differentiating glioblastoma from solitary metastasis: A short-echo time single-voxel magnetic resonance spectroscopy study at 3 T. *J Comput Assist Tomogr,* 37, 265-71.

DANCEY, J. E., DOBBIN, K. K., GROSHEN, S., JESSUP, J. M., HRUSZKEWYCZ, A. H., KOEHLER, M., PARCHMENT, R., RATAIN, M. J., SHANKAR, L. K., STADLER, W. M., TRUE, L. D., GRAVELL, A. & GREVER, M. R. 2010. Guidelines for the development and incorporation of biomarker studies in early clinical trials of novel agents. *Clin Cancer Res,* 16**,** 1745-55.

DAVIS, F. G., DOLECEK, T. A., MCCARTHY, B. J. & VILLANO, J. L. 2012. Toward determining the lifetime occurrence of metastatic brain tumors estimated from 2007 United States cancer incidence data. *Neuro Oncol,* 14**,** 1171-7.

DAVIS, P. C., HUDGINS, P. A., PETERMAN, S. B. & HOFFMAN, J. C. 1991. Diagnosis of cerebral metastases: double-dose delayed CT vs contrast-enhanced MR imaging. *Am J Neuroradiol,* 12, 293-300.

DE SILVA RUDLAND, S., MARTIN, L., ROSHANLALL, C., WINSTANLEY, J., LEINSTER, S., PLATT-HIGGINS, A., CARROLL, J., WEST, C., BARRACLOUGH, R. & RUDLAND, P. 2006. Association of S100A4 and osteopontin with specific prognostic factors and survival of patients with minimally invasive breast cancer. *Clin Cancer Res,* 12**,** 1192-200.

DE SILVA RUDLAND, S., PLATT-HIGGINS, A., WINSTANLEY, J. H., JONES, N. J., BARRACLOUGH, R., WEST, C., CARROLL, J. & RUDLAND, P. S. 2011. Statistical association of basal cell keratins with metastasis-inducing proteins in a prognostically unfavorable group of sporadic breast cancers. *Am J Pathol,* 179**,** 1061-72.

DELATTRE, J. Y., KROL, G., THALER, H. T. & POSNER, J. B. 1988. Distribution of brain metastases. *Arch Neurol,* 45**,** 741-4.

DEQUESADA, I. M., QUISLING, R. G., YACHNIS, A. & FRIEDMAN, W. A. 2008. Can standard magnetic resonance imaging reliably distinguish recurrent tumor from radiation necrosis after radiosurgery for brain metastases? A radiographic-pathological study. *Neurosurgery,* 63, 898-903.

DESPRECHINS, B., STADNIK, T., KOERTS, G., SHABANA, W., BREUCQ, C. & OSTEAUX, M. 1999. Use of diffusion-weighted MR imaging in differential diagnosis between

intracerebral necrotic tumors and cerebral abscesses. *AJNR Am J Neuroradiol,* 20, 1252-57.

DMYTRIYEVA, O., PANKRATOVA, S., OWCZAREK, S., SONN, K., SOROKA, V., RIDLEY, C. M., MARSOLAIS, A., LOPEZ-HOYOS, M., AMBARTSUMIAN, N., LUKANIDIN, E., BOCK, E., BEREZIN, V. & KIRYUSHKO, D. 2012. The metastasis-promoting S100A4 protein confers neuroprotection in brain injury. *Nat Commun,* 3**,** 1197.

DUYGULU, G., OVALI, G. Y., CALLI, C., KITIS, O., YUNTEN, N., AKALIN, T. & ISLEKEL, S. 2010. Intracerebral metastasis showing restricted diffusion: correlation with histopathologic findings. *Eur J Radiol,* 74**,** 117-20.

EBISU, T., TANAKA, C., UMEDA, M., KITAMURA, M., NARUSE, S., HIGUCHI, T., UEDA, S. & SATO, H. 1996. Discrimination of brain abscess from necrotic or cystic tumors by diffusion-weighted echo planar imaging. *Magn Reson Imaging,* 14**,** 1113-16.

EL KADY, R. M., CHOUDHARY, A. K. & TAPPOUNI, R. 2011. Accuracy of apparent diffusion coefficient value measurement on PACS workstation: A comparative analysis. *American Journal of Roentgenology,* 196**,** W280-W284.

FAKHRAN, S., YAEGER, K. & ALHILALI, L. 2013. Symptomatic white matter changes in mild traumatic brain injury resemble pathologic features of early Alzheimer dementia. *Radiology,* 269**,** 249-57.

FARQUHARSON, S., TOURNIER, J. D., CALAMANTE, F., FABINYI, G., SCHNEIDER-KOLSKY, M., JACKSON, G. D. & CONNELLY, A. 2013. White matter fiber tractography: why we need to move beyond DTI. *J Neurosurg,* 118, 1367-77.

FERTIKH, D., KREJZA, J., CUNQUEIRO, A., DANISH, S., ALOKAILI, R. & MELHEM, E. R. 2007. Discrimination of capsular stage brain abscesses from necrotic or cystic neoplasms using diffusion-weighted magnetic resonance imaging. *J Neurosurg,* 106, 76-81.

FINK, K. R. & FINK, J. R. 2013. Imaging of brain metastases. *Surg Neurol Int,* 4**,** S209-19.

FOX, B. D., CHEUNG, V. J., PATEL, A. J., SUKI, D. & RAO, G. 2011. Epidemiology of metastatic brain tumors. *Neurosurg Clin N Am,* 22**,** 1-6, v.

FRANK, E., PULVER, M. & DE TRIBOLET, N. 1986. Expression of class II major histocompatibility antigens on reactive astrocytes and endothelial cells within the gliosis surrounding metastases and abscesses. *J Neuroimmunol,* 12**,** 29-36.

FRANKEL, T. L., GIAN, R. K. & JARNAGIN, W. R. 2012. Preoperative imaging for hepatic resection of colorectal cancer metastasis. *J Gastrointest Oncol,* 3**,** 11-8.

FRIEDMAN, D. P., MORALES, R. E. & GOLDMAN, H. W. 2001. MR imaging findings after stereotactic radiosurgery using the gamma knife. *AJR Am J Roentgenol,* 176, 1589-95.

GASPAR, L., SCOTT, C., ROTMAN, M., ASBELL, S., PHILLIPS, T., WASSERMAN, T., MCKENNA, W. G. & BYHARDT, R. 1997. Recursive partitioning analysis (RPA) of prognostic factors in three Radiation Therapy Oncology Group (RTOG) brain metastases trials. *Int J Radiat Oncol Biol Phys,* 37**,** 745-51.

GINSBERG, L. E. & LANG, F. F. 1998. Neuroradiologic screening for brain metastases–can quadruple dose gadolinium be far behind? *AJNR Am J Neuroradiol,* 19, 829-30.

GOH, V., SCHAEFFTER, T. & LEACH, M. 2013. Reproducibility of dynamic contrast-enhanced MR imaging: Why we should care. *Radiology,* 266**,** 698-700.

GOLDMAN, M., BOXERMAN, J. L., ROGG, J. M. & NORÉN, G. 2006. Utility of apparent diffusion coefficient in predicting the outcome of Gamma Knife-treated brain metastases prior to changes in tumor volume: a preliminary study. *J Neurosurg,* 105, S175-82.

GOODEN, M. J., DE BOCK, G. H., LEFFERS, N., DAEMEN, T. & NIJMAN, H. W. 2011. The prognostic influence of tumour-infiltrating lymphocytes in cancer: a systematic review with meta-analysis. *Br J Cancer,* 105**,** 93-103.

GOODMAN, S. L. & PICARD, M. 2012. Integrins as therapeutic targets. *Trends Pharmacol Sci,* 33**,** 405-12.

GORDON, H. & SWEETS, H. H. 1936. A simple method for the silver impregnation of reticulum. *Am J Pathol,* 12**,** 545-552.1.

GRECH-SOLLARS, M., HALES, P. W., MIYAZAKI, K., RASCHKE, F., RODRIGUEZ, D., WILSON, M., GILL, S. K., BANKS, T., SAUNDERS, D. E., CLAYDEN, J. D., GWILLIAM, M. N., BARRICK, T. R., MORGAN, P. S., DAVIES, N. P., ROSSITER, J., AUER, D. P., GRUNDY, R., LEACH, M. O., HOWE, F. A., PEET, A. C. & CLARK, C. A. 2015. Multi-centre reproducibility of diffusion MRI parameters for clinical sequences in the brain. *NMR Biomed,* 28**,** 468-85.

GROSS, S. R., SIN, C. G., BARRACLOUGH, R. & RUDLAND, P. S. 2014. Joining S100 proteins and migration: for better or for worse, in sickness and in health. *Cell Mol Life Sci,* 71**,** 1551-79.

GROSSMAN, R. & RAM, Z. 2014. The utility of modified recursive partitioning analysis class 2 in predicting survival among surgical candidates with intracranial metastases. *World Neurosurg,* 82**,** e111-3.

GUTTLER, A., GIEBLER, M., CUNO, P., WICHMANN, H., KESSLER, J., OSTHEIMER, C., SOLING, A., STRAUSS, C., ILLERT, J., KAPPLER, M., VORDERMARK, D. & BACHE, M. 2013. Osteopontin and splice variant expression level in human malignant glioma: radiobiologic effects and prognosis after radiotherapy. *Radiother Oncol,* 108**,** 535-40.

HA, D. H., CHOI, S., OH, J. Y., YOON, S. K., KANG, M. J. & KIM, K. U. 2013. Application of 31P MR spectroscopy to the brain tumors. *Korean J Radiol,* 14, 477-86.

HABA, D., PASCO PAPON, A., TANGUY, J. Y., BURTIN, P., AUBE, C. & CARON-POITREAU, C. 2001. Use of half-dose gadolinium-enhanced MRI and magnetization transfer saturation in brain tumors. *Eur Radiol,* 11, 117-22.

HAHNEL, A., WICHMANN, H., KAPPLER, M., KOTZSCH, M., VORDERMARK, D., TAUBERT, H. & BACHE, M. 2010. Effects of osteopontin inhibition on radiosensitivity of MDA-MB-231 breast cancer cells. *Radiat Oncol,* 5**,** 82.

HAMILTON, A. & SIBSON, N. R. 2013. Role of the systemic immune system in brain metastasis. *Mol Cell Neurosci,* 53**,** 42-51.

HART, M. G., GRANT, R., WALKER, M. & DICKINSON, H. 2005. Surgical resection and whole brain radiation therapy versus whole brain radiation therapy alone for single brain metastases. *Cochrane Database Syst Rev***,** Cd003292.

HAYASHIDA, Y., HIRAI, T., MORISHITA, S., KITAJIMA, M., MURAKAMI, R., KOROGI, Y., MAKINO, K., NAKAMURA, H., IKUSHIMA, I., YAMURA, M., KOCHI, M., KURATSU, J. I. & YAMASHITA, Y. 2006. Diffusion-weighted imaging of metastatic brain tumors: comparison with histologic type and tumor cellularity. *AJNR Am J Neuroradiol,* 27**,** 1419-25.

HERAS A, E. A. 1995. Enhanced labelled-polymer system for immunohistochemistry. *XVth Eur Cong Pathol.* Copenhagen, Denmark.

HERNANDEZ, J. L., PADILLA, L., DAKHEL, S., COLL, T., HERVAS, R., ADAN, J., MASA, M., MITJANS, F., MARTINEZ, J. M., COMA, S., RODRIGUEZ, L., NOE, V., CIUDAD, C. J., BLASCO, F. & MESSEGUER, R. 2013. Therapeutic targeting of tumor growth and angiogenesis with a novel anti-S100A4 monoclonal antibody. *PLoS One,* 8**,** e72480.

HEYE, T., MERKLE, E. M., REINER, C. S., DAVENPORT, M. S., HORVATH, J. J., FEUERLEIN, S., BREAULT, S. R., GALL, P., BASHIR, M. R., DALE, B. M., KIRALY, A. P. & BOLL, D. T. 2013. Reproducibility of dynamic contrast-enhanced MR imaging part II. Comparison of intra- and interobserver variability with manual region of interest placement versus semiautomatic lesion segmentation and histogram analysis. *Radiology,* 266**,** 812-21.

HOEFNAGELS, F. W., LAGERWAARD, F. J., SANCHEZ, E., HAASBEEK, C. J., KNOL, D. L., SLOTMAN, B. J. & VANDERTOP, W. P. 2009. Radiological progression of cerebral

metastases after radiosurgery: assessment of perfusion MRI for differentiating between necrosis and recurrence. *J Neurol,* 256, 878-87.

HOLTAS, S., GEIJER, B., STRÖMBLAD, L. G., MALY-SUNDGREN, P. & BURTSCHER, I. M. 2000. A ring-enhancing metastasis with central high signal on diffusion-weighted imaging and low apparent diffusion coefficients. *Neuroradiology,* 42, 824-27.

HONG, X. Y., WANG, J. & LI, Z. 2013. AGR2 expression is regulated by HIF-1 and contributes to growth and angiogenesis of glioblastoma. *Cell Biochem Biophys,* 67**,** 1487-95.

HUANG, B. Y., KWOCK, L., CASTILLO, M. & SMITH, J. K. 2010. Association of choline levels and tumor perfusion in brain metastases assessed with proton MR spectroscopy and dynamic susceptibility contrast-enhanced perfusion weighted MRI. *Technol Cancer Res T,* 9, 327-37.

IIMA, M., REYNAUD, O., TSURUGIZAWA, T., CIOBANU, L., LI, J. R., GEFFROY, F., DJEMAI, B., UMEHANA, M. & LE BIHAN, D. 2014. Characterization of Glioma Microcirculation and Tissue Features Using Intravoxel Incoherent Motion Magnetic Resonance Imaging in a Rat Brain Model. *Invest Radiol*, 49, 485-90

JAKOLA, A. S., GULATI, S., NERLAND, U. S. & SOLHEIM, O. 2012. Patient selection and clinical outcomes in patients operated for brain metastases--is specialty of the referring physicians a prognostic factor? *Br J Neurosurg,* 26**,** 679-83.

JENKINSON, M. D., HAYLOCK, B., SHENOY, A., HUSBAND, D. & JAVADPOUR, M. 2011. Management of cerebral metastasis: evidence-based approach for surgery, stereotactic radiosurgery and radiotherapy. *Eur J Cancer,* 47**,** 649-55.

JENKINSON, M. D., SMITH, T. S., BRODBELT, A. R., JOYCE, K. A., WARNKE, P. C. & WALKER, C. 2007. Apparent diffusion coefficients in oligodendroglial tumors characterized by genotype. *J Magn Reson Imaging,* 26**,** 1405-12.

JETHWA, P. R., BARRESE, J. C., GOWDA, A., SHETTY, A. & DANISH, S. F. 2012. Magnetic resonance thermometry-guided laser-induced thermal therapy for intracranial neoplasms: initial experience. *Neurosurgery,* 71, S133-44.

JIANG, H., VAN ZIJL, P. C., KIM, J., PEARLSON, G. D. & MORI, S. 2006. DtiStudio: resource program for diffusion tensor computation and fiber bundle tracking. *Comput Methods Programs Biomed,* 81**,** 106-16.

JIANG, Q., ZHANG, Z. G. & CHOPP, M. 2010. MRI evaluation of white matter recovery after brain injury. *Stroke,* 41**,** S112-3.

JONES, P. S., CAHILL, D. P., BRASTIANOS, P. K., FLAHERTY, K. T. & CURRY, W. T. 2015. Ipilimumab and craniotomy in patients with melanoma and brain metastases: a case series. *Neurosurg Focus,* 38**,** E5.

KAKEDA, S., KOROGI, Y., HIAI, Y., OHNARI, N., MORIYA, J., KAMADA, K., HANAMIYA, M., SATO, T. & KITAJIMA, M. 2007. Detection of brain metastasis at 3T: comparison among SE, IR-FSE and 3D-GRE sequences. *Eur Radiol,* 17, 2345-51.

KANG, T. W., KIM, S. T., BYUN, H. S., JEON, P., KIM, K., KIM, H. & LEE, J. I. 2009. Morphological and functional MRI, MRS, perfusion and diffusion changes after radiosurgery of brain metastasis. *Eur J Radiol,* 72, 370-80.

KARNOFSKY DA, B. J. 1949. The clinical evaluation of chemotherapeutic agents in cancer. *In:* CM, M. (ed.) *Evaluation of Chemotherapeutic Agents.* New York: Columbia University Press.

KELLY, P. J., DAUMAS-DUPORT, C., SCHEITHAUER, B. W., KALL, B. A. & KISPERT, D. B. 1987. Stereotactic histologic correlations of computed tomography- and magnetic resonance imaging-defined abnormalities in patients with glial neoplasms. *Mayo Clin Proc,* 62**,** 450-9.

KIENAST, Y., VON BAUMGARTEN, L., FUHRMANN, M., KLINKERT, W. E., GOLDBRUNNER, R., HERMS, J. & WINKLER, F. 2010. Real-time imaging reveals the single steps of brain metastasis formation. *Nat Med,* 16**,** 116-22.

KIM, Y. J., CHANG, K. H., SONG, I. C., KIM, H. D., SEONG, S. O., KIM, Y. H. & HAN, M. H. 1998. Brain abscess and necrotic or cystic brain tumor: discrimination with signal intensity on diffusion-weighted MR imaging. *AJR Am J Roentgenol,* 171**,** 1487-90.

KLUGER, H. M., ZITO, C. R., BARR, M. L., BAINE, M. K., CHIANG, V. L., SZNOL, M., RIMM, D. L., CHEN, L. & JILAVEANU, L. B. 2015. Characterization of PD-L1 expression and associated T-cell infiltrates in metastatic melanoma samples from variable anatomic sites. *Clin Cancer Res,* 21**,** 3052-60.

KOCHER, M., SOFFIETTI, R., ABACIOGLU, U., VILLA, S., FAUCHON, F., BAUMERT, B. G., FARISELLI, L., TZUK-SHINA, T., KORTMANN, R. D., CARRIE, C., BEN HASSEL, M., KOURI, M., VALEINIS, E., VAN DEN BERGE, D., COLLETTE, S., COLLETTE, L. & MUELLER, R. P. 2011. Adjuvant whole-brain radiotherapy versus observation after radiosurgery or surgical resection of one to three cerebral metastases: results of the EORTC 22952-26001 study. *J Clin Oncol,* 29**,** 134-41.

KONDZIOLKA, D., KALKANIS, S. N., MEHTA, M. P., AHLUWALIA, M. & LOEFFLER, J. S. 2014. It is time to reevaluate the management of patients with brain metastases. *Neurosurgery,* 75**,** 1-9.

KRABBE, K., GIDEON, P., WAGN, P., HANSEN, U., THOMSEN, C. & MADSEN, F. 1997. MR diffusion imaging of human intracranial tumours. *Neuroradiology,* 39, 483-89.

KRUGER, S., MOTTAGHY, F. M., BUCK, A. K., MASCHKE, S., KLEY, H., FRECHEN, D., WIBMER, T., RESKE, S. N. & PAULS, S. 2011. Brain metastasis in lung cancer. Comparison of cerebral MRI and 18F-FDG-PET/CT for diagnosis in the initial staging. *Nuklearmedizin,* 50, 101-06.

KUHNT, D., BAUER, M. H. & NIMSKY, C. 2012. Brain shift compensation and neurosurgical image fusion using intraoperative MRI: current status and future challenges. *Crit Rev Biomed Eng,* 40**,** 175-85.

LACERDA, S. & LAW, M. 2009. Magnetic resonance perfusion and permeability imaging in brain tumors. *Neuroimaging Clin N Am,* 19, 527-57.

LAMBREGTS, D. M., BEETS, G. L., MAAS, M., CURVO-SEMEDO, L., KESSELS, A. G., THYWISSEN, T. & BEETS-TAN, R. G. 2011a. Tumour ADC measurements in rectal cancer: effect of ROI methods on ADC values and interobserver variability. *Eur Radiol,* 21**,** 2567-74.

LAMBREGTS, D. M. J., BEETS, G. L., MAAS, M., CURVO-SEMEDO, L., KESSELS, A. G. H., THYWISSEN, T. & BEETS-TAN, R. G. H. 2011b. Tumour ADC measurements in rectal cancer: Effect of ROI methods on ADC values and interobserver variability. *European Radiology,* 21**,** 2567-74.

LANGLEY, R. E., STEPHENS, R. J., NANKIVELL, M., PUGH, C., MOORE, B., NAVANI, N., WILSON, P., FAIVRE-FINN, C., BARTON, R., PARMAR, M. K. & MULVENNA, P. M. 2013. Interim data from the Medical Research Council QUARTZ Trial: does whole brain radiotherapy affect the survival and quality of life of patients with brain metastases from non-small cell lung cancer? *Clin Oncol (R Coll Radiol),* 25**,** e23-30.

LAUTENSCHLAEGER, T., PERRY, J., PEEREBOOM, D., LI, B., IBRAHIM, A., HUEBNER, A., MENG, W., WHITE, J. & CHAKRAVARTI, A. 2013. In vitro study of combined cilengitide and radiation treatment in breast cancer cell lines. *Radiat Oncol,* 8**,** 246.

LAW, M., CHA, S., KNOPP, E. A., JOHNSON, G., ARNETT, J. & LITT, A. W. 2002. High-grade gliomas and solitary metastases: differentiation by using perfusion and proton spectroscopic MR imaging. *Radiology,* 222, 715-21.

LEE, E. J., TERBRUGGE, K., MIKULIS, D., CHOI, D. S., BAE, J. M., LEE, S. K. & MOON, S. Y. 2011. Diagnostic value of peritumoral minimum apparent diffusion coefficient for differentiation of glioblastoma multiforme from solitary metastatic lesions. *AJR Am J Roentgenol,* 196**,** 71-6.

LEENDERS, W. P., KUSTERS, B., VERRIJP, K., MAASS, C., WESSELING, P., HEERSCHAP, A., RUITER, D., RYAN, A. & DE WAAL, R. 2004. Antiangiogenic therapy of cerebral

melanoma metastases results in sustained tumor progression via vessel co-option. *Clin Cancer Res,* 10**,** 6222-30.

LEMERCIER, P., PAZ MAYA, S., PATRIE, J. T., FLORS, L. & LEIVA-SALINAS, C. 2014. Gradient of apparent diffusion coefficient values in peritumoral edema helps in differentiation of glioblastoma from solitary metastatic lesions. *AJR Am J Roentgenol,* 203**,** 163-9.

LIN, N. U., LEE, E. Q., AOYAMA, H., BARANI, I. J., BARBORIAK, D. P., BAUMERT, B. G., BENDSZUS, M., BROWN, P. D., CAMIDGE, D. R., CHANG, S. M., DANCEY, J., DE VRIES, E. G., GASPAR, L. E., HARRIS, G. J., HODI, F. S., KALKANIS, S. N., LINSKEY, M. E., MACDONALD, D. R., MARGOLIN, K., MEHTA, M. P., SCHIFF, D., SOFFIETTI, R., SUH, J. H., VAN DEN BENT, M. J., VOGELBAUM, M. A. & WEN, P. Y. 2015. Response assessment criteria for brain metastases: proposal from the RANO group. *Lancet Oncol,* 16**,** e270-8.

LIU, D., RUDLAND, P. S., SIBSON, D. R., PLATT-HIGGINS, A. & BARRACLOUGH, R. 2005. Human homologue of cement gland protein, a novel metastasis inducer associated with breast carcinomas. *Cancer Res,* 65**,** 3796-805.

LU, S., AHN, D., JOHNSON, G., LAW, M., ZAGZAG, D. & GROSSMAN, R. I. 2004. Diffusion-tensor MR imaging of intracranial neoplasia and associated peritumoral edema: introduction of the tumor infiltration index. *Radiology,* 232**,** 221-8.

LUNSFORD, L. D., KONDZIOLKA, D., MAITZ, A. & FLICKINGER, J. C. 1998. Black holes, white dwarfs and supernovas: imaging after radiosurgery. *Stereotact Funct Neurosurg,* 70, S2-10.

MAHMOUD, O. M., TOMINAGA, A., AMATYA, V. J., OHTAKI, M., SUGIYAMA, K., SAKOGUCHI, T., KINOSHITA, Y., TAKESHIMA, Y., ABE, N., AKIYAMA, Y., EL-GHORIANY, A. I., ABD ALLA, A. K., EL-SHARKAWY, M. A., ARITA, K., KURISU, K. & YAMASAKI, F. 2011. Role of PROPELLER diffusion-weighted imaging and apparent diffusion coefficient in the evaluation of pituitary adenomas. *Eur J Radiol,* 80**,** 412-7.

MARGOLIN, K., ERNSTOFF, M. S., HAMID, O., LAWRENCE, D., MCDERMOTT, D., PUZANOV, I., WOLCHOK, J. D., CLARK, J. I., SZNOL, M., LOGAN, T. F., RICHARDS, J., MICHENER, T., BALOGH, A., HELLER, K. N. & HODI, F. S. 2012. Ipilimumab in patients with melanoma and brain metastases: an open-label, phase 2 trial. *Lancet Oncol,* 13**,** 459-65.

MATOBA, M., TUJI, H., SHIMODE, Y., TOYODA, I., KUGINUKI, Y., MIWA, K. & TONAMI, H. 2013. Fractional Change in Apparent Diffusion Coefficient as an Imaging Biomarker for Predicting Treatment Response in Head and Neck Cancer Treated with Chemoradiotherapy. *AJNR Am J Neuroradiol*, 35, 379-85.

MEHTA, M., NOYES, W., CRAIG, B., LAMOND, J., AUCHTER, R., FRENCH, M., JOHNSON, M., LEVIN, A., BADIE, B., ROBBINS, I. & KINSELLA, T. 1997. A cost-effectiveness and cost-utility analysis of radiosurgery vs. resection for single-brain metastases. *Int J Radiat Oncol Biol Phys,* 39**,** 445-54.

MICKLEM, K., RIGNEY, E., CORDELL, J., SIMMONS, D., STROSS, P., TURLEY, H., SEED, B. & MASON, D. 1989. A human macrophage-associated antigen (CD68) detected by six different monoclonal antibodies. *Br J Haematol,* 73**,** 6-11.

MILLER, K. D., WEATHERS, T., HANEY, L. G., TIMMERMAN, R., DICKLER, M., SHEN, J. & SLEDGE, G. W., JR. 2003. Occult central nervous system involvement in patients with metastatic breast cancer: prevalence, predictive factors and impact on overall survival. *Ann Oncol,* 14**,** 1072-77.

MILLS, S. J., THOMPSON, G. & JACKSON, A. 2012. Advanced magnetic resonance imaging biomarkers of cerebral metastases. *Cancer Imaging,* 12**,** 245-52.

MONTEITH, S., SHEEHAN, J., MEDEL, R., WINTERMARK, M., EAMES, M., SNELL, J., KASSELL, N. F. & ELIAS, W. J. 2013. Potential intracranial applications of magnetic resonance-guided focused ultrasound surgery. *J Neurosurg,* 118, 215-21.

MOYE, V. E., BARRACLOUGH, R., WEST, C. & RUDLAND, P. S. 2004. Osteopontin expression correlates with adhesive and metastatic potential in metastasis-inducing DNA-transfected rat mammary cell lines. *Br J Cancer,* 90**,** 1796-802.

NAGAI, A., SHIBAMOTO, Y., MORI, Y., HASHIZUME, C., HAGIWARA, M. & KOBAYASHI, T. 2010. Increases in the number of brain metastases detected at frame-fixed, thin-slice MRI for gamma knife surgery planning. *Neuro Oncol,* 12, 1187-92.

NEVES, S., MAZAL, P. R., WANSCHITZ, J., RUDNAY, A. C., DRLICEK, M., CZECH, T., WUSTINGER, C. & BUDKA, H. 2001. Pseudogliomatous growth pattern of anaplastic small cell carcinomas metastatic to the brain. *Clin Neuropathol,* 20**,** 38-42.

NIEDER, C., MARIENHAGEN, K., ASTNER, S. T. & MOLLS, M. 2009. Prognostic scores in brain metastases from breast cancer. *BMC Cancer,* 9, 105.

NORDEN, A. D., WEN, P. Y. & KESARI, S. 2005. Brain metastases. *Curr Opin Neurol,* 18**,** 654-61.

NUSSBAUM, E. S., DJALILIAN, H. R., CHO, K. H. & HALL, W. A. 1996. Brain metastases. Histology, multiplicity, surgery, and survival. *Cancer,* 78**,** 1781-8.

O'CONNOR, J. P., ROSE, C. J., WATERTON, J. C., CARANO, R. A., PARKER, G. J. & JACKSON, A. 2015. Imaging intratumor heterogeneity: role in therapy response, resistance, and clinical outcome. *Clin Cancer Res,* 21**,** 249-57.

OBERMUELLER, T., SCHAEFFNER, M., SHIBAN, E., DROESE, D., NEGWER, C., MEYER, B., RINGEL, F. & KRIEG, S. M. 2015. Intraoperative neuromonitoring for function-guided resection differs for supratentorial motor eloquent gliomas and metastases. *BMC Neurol,* 15**,** 211.

OHANA, M., JEUNG, M. Y., BAZILLE, G. & ROY, C. 2014. Cerebral staging of lung cancer: is one single contrast-enhanced T1-weighted three-dimensional gradient-echo sequence sufficient? *Neuroradiology,* 56**,** 621-27.

OJERHOLM, E., LEE, J. Y., THAWANI, J. P., MILLER, D., O'ROURKE, D. M., DORSEY, J. F., GEIGER, G. A., NAGDA, S., KOLKER, J. D., LUSTIG, R. A. & ALONSO-BASANTA, M. 2014. Stereotactic radiosurgery to the resection bed for intracranial metastases and risk of leptomeningeal carcinomatosis. *J Neurosurg,* 121 S75-83.

OOUCHI, H., YAMADA, K., SAKAI, K., KIZU, O., KUBOTA, T., ITO, H. & NISHIMURA, T. 2007. Diffusion anisotropy measurement of brain white matter is affected by voxel size: Underestimation occurs in areas with crossing fibers. *American Journal of Neuroradiology,* 28**,** 1102-06.

OSTROM, Q. T., GITTLEMAN, H., LIAO, P., ROUSE, C., CHEN, Y., DOWLING, J., WOLINSKY, Y., KRUCHKO, C. & BARNHOLTZ-SLOAN, J. 2014. CBTRUS statistical report: primary brain and central nervous system tumors diagnosed in the United States in 2007-2011. *Neuro Oncol,* 16 S4**,** iv1-63.

OWONIKOKO, T. K., ARBISER, J., ZELNAK, A., SHU, H.-K. G., SHIM, H., ROBIN, A. M., KALKANIS, S. N., WHITSETT, T. G., SALHIA, B., TRAN, N. L., RYKEN, T., MOORE, M. K., EGAN, K. M. & OLSON, J. J. 2014. Current approaches to the treatment of metastatic brain tumours. *Nat Rev Clin Oncol,* 11**,** 203-22.

OZTURK, A., SASSON, A. D., FARRELL, J. A. D., LANDMAN, B. A., DA MOTTA, A. C. B. S., ARALASMAK, A. & YOUSEM, D. M. 2008. Regional differences in diffusion tensor imaging measurements: Assessment of intrarater and interrater variability. *American Journal of Neuroradiology,* 29**,** 1124-27.

PAEK, S. H., AUDU, P. B., SPERLING, M. R., CHO, J. & ANDREWS, D. W. 2005. Reevaluation of surgery for the treatment of brain metastases: review of 208 patients with single or multiple brain metastases treated at one institution with modern neurosurgical techniques. *Neurosurgery,* 56**,** 1021-34; discussion 1021-34.

PAGET, S. 1889. The distribution of secondary growths in cancer of the breast. 1889. *Cancer Metastasis Rev,* 8**,** 98-101.

PANAGIOTAKI, E., WALKER-SAMUEL, S., SIOW, B., JOHNSON, S. P., RAJKUMAR, V., PEDLEY, R. B., LYTHGOE, M. F. & ALEXANDER, D. C. 2014. Noninvasive Quantification of Solid Tumor Microstructure Using VERDICT MRI. *Cancer Res,* 74**,** 1902-12.

PATCHELL, R. A., TIBBS, P. A., REGINE, W. F., DEMPSEY, R. J., MOHIUDDIN, M., KRYSCIO, R. J., MARKESBERY, W. R., FOON, K. A. & YOUNG, B. 1998. Postoperative radiotherapy in the treatment of single metastases to the brain: a randomized trial. *Jama,* 280**,** 1485-9.

PATCHELL, R. A., TIBBS, P. A., WALSH, J. W., DEMPSEY, R. J., MARUYAMA, Y., KRYSCIO, R. J., MARKESBERY, W. R., MACDONALD, J. S. & YOUNG, B. 1990. A randomized trial of surgery in the treatment of single metastases to the brain. *N Engl J Med,* 322**,** 494-500.

PATEL, A. J., SUKI, D., HATIBOGLU, M. A., ABOUASSI, H., SHI, W., WILDRICK, D. M., LANG, F. F. & SAWAYA, R. 2010. Factors influencing the risk of local recurrence after resection of a single brain metastasis. *J Neurosurg,* 113**,** 181-9.

PEKMEZCI, M. & PERRY, A. 2013. Neuropathology of brain metastases. *Surg Neurol Int,* 4**,** S245-55.

PETERSON, A. M., MELTZER, C. C., EVANSON, E. J., FLICKINGER, J. C. & KONDZIOLKA, D. 1999. MR imaging response of brain metastases after gamma knife stereotactic radiosurgery. *Radiology,* 211.

PIERGA, J. Y., BIDARD, F. C., CROPET, C., TRESCA, P., DALENC, F., ROMIEU, G., CAMPONE, M., MAHIER AIT-OUKHATAR, C., LE RHUN, E., GONCALVES, A., LEHEURTEUR, M., DOMONT, J., GUTIERREZ, M., CURE, H., FERRERO, J. M., LABBE-DEVILLIERS, C. & BACHELOT, T. 2013. Circulating tumor cells and brain metastasis outcome in patients with HER2-positive breast cancer: the LANDSCAPE trial. *Ann Oncol,* 24**,** 2999-3004.

PINKER, K., STADLBAUER, A., BOGNER, W., GRUBER, S. & HELBICH, T. H. 2012. Molecular imaging of cancer: MR spectroscopy and beyond. *Eur J Radiol,* 81.

PLATE, K. H., RUSCHOFF, J., BEHNKE, J. & MENNEL, H. D. 1990. Proliferative potential of human brain tumours as assessed by nucleolar organizer regions (AgNORs) and Ki67-immunoreactivity. *Acta Neurochir (Wien),* 104**,** 103-9.

PORTO, L., JURCOANE, A., SCHWABE, D., KIESLICH, M. & HATTINGEN, E. 2013. Differentiation between high and low grade tumours in paediatric patients by using apparent diffusion coefficients. *European Journal of Paediatric Neurology,* 17**,** 302-07.

POSNER, J. B. & CHERNIK, N. L. 1978. Intracranial metastases from systemic cancer. *Adv Neurol,* 19**,** 579-92.

PRAH, M., MUFTULER, L. T. & SCHMAINDA, K. M. 2014. Can ADC and Mean Diffusivity derived from DWI and DTI be used interchangeably in patients with glioblastoma? (Conference Paper). *The International Society for Magnetic Resonance in Medicine.* Milan.

PREUSSER, M., CAPPER, D., ILHAN-MUTLU, A., BERGHOFF, A. S., BIRNER, P., BARTSCH, R., MAROSI, C., ZIELINSKI, C., MEHTA, M. P., WINKLER, F., WICK, W. & VON DEIMLING, A. 2012. Brain metastases: pathobiology and emerging targeted therapies. *Acta Neuropathol,* 123**,** 205-22.

PRICE, S. J. & GILLARD, J. H. 2011. Imaging biomarkers of brain tumour margin and tumour invasion. *Br J Radiol,* 84 Spec No 2**,** S159-67.

PRICE, S. J., PENA, A., BURNET, N. G., JENA, R., GREEN, H. A., CARPENTER, T. A., PICKARD, J. D. & GILLARD, J. H. 2004. Tissue signature characterisation of diffusion tensor abnormalities in cerebral gliomas. *Eur Radiol,* 14**,** 1909-17.

PUHALLA, S., ELMQUIST, W., FREYER, D., KLEINBERG, L., ADKINS, C., LOCKMAN, P., MCGREGOR, J., MULDOON, L., NESBIT, G., PEEREBOOM, D., SMITH, Q., WALKER, S.

& NEUWELT, E. 2015. Unsanctifying the sanctuary: challenges and opportunities with brain metastases. *Neuro Oncol,* 17**,** 639-51.
QUANT, E. C. & WEN, P. Y. 2011. Response assessment in neuro-oncology. *Curr Oncol Rep,* 13**,** 50-6.
RAHMATHULLA, G., TOMS, S. A. & WEIL, R. J. 2012. The molecular biology of brain metastasis. *J Oncol,* 2012, 1-16
RAM, Z., COHEN, Z. R., HARNOF, S., TAL, S., FAIBEL, M., NASS, D., MAIER, S. E., HADANI, M. & MARDOR, Y. 2006. Magnetic resonance imaging-guided, high-intensity focused ultrasound for brain tumor therapy. *Neurosurgery,* 59.
RAMANI, P., BRADLEY, N. J. & FLETCHER, C. D. 1990. QBEND/10, a new monoclonal antibody to endothelium: assessment of its diagnostic utility in paraffin sections. *Histopathology,* 17**,** 237-42.
RAORE, B., SCHNIEDERJAN, M., PRABHU, R., BRAT, D. J., SHU, H. K. & OLSON, J. J. 2011. Metastasis infiltration: an investigation of the postoperative brain-tumor interface. *Int J Radiat Oncol Biol Phys,* 81**,** 1075-80.
REINHERZ, E. L., HAYNES, B. F., NADLER, L. M., BERNSTEIN, I. D. & SPRINGERLINK (ONLINE SERVICE) 1986a. Leukocyte Typing II Volume 1: Human T Lymphocytes. New York, NY: Springer New York,.
REINHERZ, E. L., HAYNES, B. F., NADLER, L. M., BERNSTIEN, I. D. & SPRINGERLINK (ONLINE SERVICE) 1986b. Leukocyte Typing II Volume 2 Human B Lymphocytes. New York, NY: Springer New York,.
ROBERGE, D., PARNEY, I. & BROWN, P. D. 2012. Radiosurgery to the postoperative surgical cavity: who needs evidence? *Int J Radiat Oncol Biol Phys,* 83**,** 486-93.
RORDEN, C. & BRETT, M. 2000. Stereotaxic display of brain lesions. *Behav Neurol,* 12**,** 191-200.
RUDLAND, P. S., PLATT-HIGGINS, A., EL-TANANI, M., DE SILVA RUDLAND, S., BARRACLOUGH, R., WINSTANLEY, J. H., HOWITT, R. & WEST, C. R. 2002. Prognostic significance of the metastasis-associated protein osteopontin in human breast cancer. *Cancer Res,* 62**,** 3417-27.
RUDLAND, P. S., PLATT-HIGGINS, A., RENSHAW, C., WEST, C. R., WINSTANLEY, J. H., ROBERTSON, L. & BARRACLOUGH, R. 2000. Prognostic significance of the metastasis-inducing protein S100A4 (p9Ka) in human breast cancer. *Cancer Res,* 60**,** 1595-603.
RUDLAND, P. S., PLATT-HIGGINS, A. M., DAVIES, L. M., DE SILVA RUDLAND, S., WILSON, J. B., ALADWANI, A., WINSTANLEY, J. H., BARRACLOUGH, D. L., BARRACLOUGH, R., WEST, C. R. & JONES, N. J. 2010. Significance of the Fanconi anemia FANCD2 protein in sporadic and metastatic human breast cancer. *Am J Pathol,* 176**,** 2935-47.
SCHAG, C. C., HEINRICH, R. L. & GANZ, P. A. 1984. Karnofsky performance status revisited: reliability, validity, and guidelines. *J Clin Oncol,* 2**,** 187-93.
SCHELLINGER, P. D., MEINCK, H. M. & THRON, A. 1999. Diagnostic accuracy of MRI compared to CCT in patients with brain metastases. *J Neurooncol,* 44, 275-81.
SCHITTENHELM, J., KLEIN, A., TATAGIBA, M. S., MEYERMANN, R., FEND, F., GOODMAN, S. L. & SIPOS, B. 2013. Comparing the expression of integrins alphavbeta3, alphavbeta5, alphavbeta6, alphavbeta8, fibronectin and fibrinogen in human brain metastases and their corresponding primary tumors. *Int J Clin Exp Pathol,* 6**,** 2719-32.
SCHNEIDER, C. A., RASBAND, W. S. & ELICEIRI, K. W. 2012. NIH Image to ImageJ: 25 years of image analysis. *Nat Methods,* 9**,** 671-75.
SCHNEIDER, G., KIRCHIN, M. A., PIROVANO, G., COLOSIMO, C., RUSCALLEDA, J., KORVES, M., SALERIO, I., LA NOCE, A. & SPINAZZI, A. 2001. Gadobenate dimeglumine-enhanced magnetic resonance imaging of intracranial metastases: Effect of dose on lesion detection and delineation. *J Magn Reson Imaging,* 14, 525-39.

SCHÖGGL, A., KITZ, K., REDDY, M., WOLFSBERGER, S., SCHNEIDER, B., DIECKMANN, K. & UNGERSBÖCK, K. 2000. Defining the Role of Stereotactic Radiosurgery Versus Microsurgery in the Treatment of Single Brain Metastases. *Acta Neurochirurgica,* 142**,** 621-26.

SERRES, S., MARTIN, C. J., SARMIENTO SOTO, M., BRISTOW, C., O'BRIEN, E. R., CONNELL, J. J., KHRAPITCHEV, A. A. & SIBSON, N. R. 2014. Structural and functional effects of metastases in rat brain determined by multimodal MRI. *Int J Cancer,* 134**,** 885-96.

SERRES, S., SOTO, M. S., HAMILTON, A., MCATEER, M. A., CARBONELL, W. S., ROBSON, M. D., ANSORGE, O., KHRAPITCHEV, A., BRISTOW, C., BALATHASAN, L., WEISSENSTEINER, T., ANTHONY, D. C., CHOUDHURY, R. P., MUSCHEL, R. J. & SIBSON, N. R. 2012. Molecular MRI enables early and sensitive detection of brain metastases. *Proc Natl Acad Sci U S A,* 109, 6674-79.

SERVER, A., GRAFF, B. A., DØLI ORHEIM, T. E., SCHELLHORN, T., JOSEFSEN, R., GADMAR, O. B. & NAKSTAD, P. H. 2011. Diagnostic examination performance by using microvascular leakage, cerebral blood volume, and blood flow derived from 3-T dynamic susceptibility-weighted contrast-enhanced perfusion MR imaging in the differentiation of glioblastoma multiforme and brain metastasis. *Neuroradiology,* 53, 319-30.

SERVER, A., JOSEFSEN, R., KULLE, B., MAEHLEN, J., SCHELLHORN, T., GADMAR, Ø., KUMAR, T., HAAKONSEN, M., LANGBERG, C. W. & NAKSTAD, P. H. 2010. Proton magnetic resonance spectroscopy in the distinction of high-grade cerebral gliomas from single metastatic brain tumors. *Acta Radiol,* 51, 326-28.

SIAM, L., BLECKMANN, A., CHAUNG, H. N., MOHR, A., KLEMM, F., BARRANTES-FREER, A., BLAZQUEZ, R., WOLFF, H. A., LUKE, F., ROHDE, V., STADELMANN, C. & PUKROP, T. 2015. The metastatic infiltration at the metastasis/brain parenchyma-interface is very heterogeneous and has a significant impact on survival in a prospective study. *Oncotarget,* 6**,** 29254-67.

SIU, T. L., JEFFREE, R. L. & FULLER, J. W. 2011. Current strategies in the surgical management of cerebral metastases: an evidence-based review. *J Clin Neurosci,* 18.

SOFFIETTI, R., CORNU, P., DELATTRE, J. Y., GRANT, R., GRAUS, F., GRISOLD, W., HEIMANS, J., HILDEBRAND, J., HOSKIN, P., KALLJO, M., KRAUSENECK, P., MAROSI, C., SIEGAL, T. & VECHT, C. 2006. EFNS Guidelines on diagnosis and treatment of brain metastases: report of an EFNS Task Force. *Eur J Neurol,* 13**,** 674-81.

SOMOYE, G., HARRY, V., SEMPLE, S., PLATANIOTIS, G., SCOTT, N., GILBERT, F. J. & PARKIN, D. 2012. Early diffusion weighted magnetic resonance imaging can predict survival in women with locally advanced cancer of the cervix treated with combined chemo-radiation. *Eur Radiol,* 22**,** 2319-27.

SOTO, M. S., SERRES, S., ANTHONY, D. C. & SIBSON, N. R. 2014. Functional role of endothelial adhesion molecules in the early stages of brain metastasis. *Neuro Oncol,* 16**,** 540-51.

SPANBERGER, T., BERGHOFF, A. S., DINHOF, C., ILHAN-MUTLU, A., MAGERLE, M., HUTTERER, M., PICHLER, J., WOHRER, A., HACKL, M., WIDHALM, G., HAINFELLNER, J. A., DIECKMANN, K., MAROSI, C., BIRNER, P., PRAYER, D. & PREUSSER, M. 2013a. Extent of peritumoral brain edema correlates with prognosis, tumoral growth pattern, HIF1a expression and angiogenic activity in patients with single brain metastases. *Clin Exp Metastasis,* 30**,** 357-68.

SPANBERGER, T., BERGHOFF, A. S., DINHOF, C., ILHAN-MUTLU, A., MAGERLE, M., HUTTERER, M., PICHLER, J., WÖHRER, A., HACKL, M., WIDHALM, G., HAINFELLNER, J. A., DIECKMANN, K., MAROSI, C., BIRNER, P., PRAYER, D. & PREUSSER, M. 2013b. Extent of peritumoral brain edema correlates with prognosis, tumoral growth pattern, HIF1a expression and angiogenic activity in patients with single brain metastases. *Clin Exp Metastasis,* 30, 357-68.

SPERDUTO, P. W., BERKEY, B., GASPAR, L. E., MEHTA, M. & CURRAN, W. 2008. A new prognostic index and comparison to three other indices for patients with brain metastases: an analysis of 1,960 patients in the RTOG database. *Int J Radiat Oncol Biol Phys,* 70**,** 510-14.

SPERDUTO, P. W., CHAO, S. T., SNEED, P. K., LUO, X., SUH, J., ROBERGE, D., BHATT, A., JENSEN, A. W., BROWN, P. D., SHIH, H., KIRKPATRICK, J., SCHWER, A., GASPAR, L. E., FIVEASH, J. B., CHIANG, V., KNISELY, J., SPERDUTO, C. M. & MEHTA, M. 2010. Diagnosis-specific prognostic factors, indexes, and treatment outcomes for patients with newly diagnosed brain metastases: a multi-institutional analysis of 4,259 patients. *Int J Radiat Oncol Biol Phys,* 77**,** 655-61.

SPERDUTO, P. W., KASED, N., ROBERGE, D., XU, Z., SHANLEY, R., LUO, X., SNEED, P. K., CHAO, S. T., WEIL, R. J., SUH, J., BHATT, A., JENSEN, A. W., BROWN, P. D., SHIH, H. A., KIRKPATRICK, J., GASPAR, L. E., FIVEASH, J. B., CHIANG, V., KNISELY, J. P., SPERDUTO, C. M., LIN, N. & MEHTA, M. 2012. Summary report on the graded prognostic assessment: an accurate and facile diagnosis-specific tool to estimate survival for patients with brain metastases. *J Clin Oncol,* 30, 419-25.

SQUILLACI, E., MANENTI, G., DI STEFANO, F., MIANO, R., STRIGARI, L. & SIMONETTI, G. 2004. Diffusion-weighted MR imaging in the evaluation of renal tumours. *Journal of experimental & clinical cancer research : CR,* 23**,** 39-45.

STADNIK, T. W., CHASKIS, C., MICHOTTE, A., SHABANA, W. M., VAN ROMPAEY, K., LUYPAERT, R., BUDINSKY, L., JELLUS, V. & OSTEAUX, M. 2001. Diffusion-weighted MR imaging of intracerebral masses: comparison with conventional MR imaging and histologic findings. *AJNR Am J Neuroradiol,* 22**,** 969-76.

STERNBERG, E. J., LIPTON, M. L. & BURNS, J. 2013. Utility of diffusion tensor imaging in evaluation of the peritumoral region in patients with primary and metastatic brain tumors. *AJNR Am J Neuroradiol*, 35, 439-44

STOCKHAM, A. L., TIEVSKY, A. L., KOYFMAN, S. A., REDDY, C. A., SUH, J. H., VOGELBAUM, M. A., BARNETT, G. H. & CHAO, S. T. 2012. Conventional MRI does not reliably distinguish radiation necrosis from tumor recurrence after stereotactic radiosurgery. *J Neurooncol,* 109, 149-58.

SUGIHARA, A. Q., ROLLE, C. E. & LESNIAK, M. S. 2009. Regulatory T cells actively infiltrate metastatic brain tumors. *Int J Oncol,* 34**,** 1533-40.

SVOKOS, K. A., SALHIA, B. & TOMS, S. A. 2014. Molecular biology of brain metastasis. *Int J Mol Sci,* 15**,** 9519-30.

SZE, G., JOHNSON, C., KAWAMURA, Y., GOLDBERG, S. N., LANGE, R., FRIEDLAND, R. J. & WOLF, R. J. 1998. Comparison of single- and triple-dose contrast material in the MR screening of brain metastases. *AJNR Am J Neuroradiol,* 19, 821-28.

TAILLIBERT, S. & DELATTRE, J. Y. 2005. Palliative care in patients with brain metastases. *Curr Opin Oncol,* 17**,** 588-92.

TAN, T. C. & BLACK, P. M. 2007. Image-guided craniotomy for cerebral metastases: techniques and outcomes. *Neurosurgery,* 61**,** 349-56; discussion 356-7.

TEAM, R. C. 2013. R: A Language and Environment for Statistical Computing. Vienna, Austria: R Foundation for Statistical Computing.

THOMPSON, G., MILLS, S. J., STIVAROS, S. M. & JACKSON, A. 2010. Imaging of brain tumors: perfusion/permeability. *Neuroimaging Clin N Am,* 20, 337-53.

TOH, C. H., WEI, K. C., NG, S. H., WAN, Y. L., LIN, C. P. & CASTILLO, M. 2011. Differentiation of brain abscesses from necrotic glioblastomas and cystic metastatic brain tumors with diffusion tensor imaging. *AJNR Am J Neuroradiol,* 32**,** 1646-51.

TOMAR, V., YADAV, A., RATHORE, R. K., VERMA, S., AWASTHI, R., BHARADWAJ, V., OJHA, B. K., PRASAD, K. N. & GUPTA, R. K. 2011. Apparent diffusion coefficient with higher b-value correlates better with viable cell count quantified from the cavity of brain abscess. *AJNR Am J Neuroradiol,* 32, 2120-25.

TORIGIAN, D. A., ZAIDI, H., KWEE, T. C., SABOURY, B., UDUPA, J. K., CHO, Z. H. & ALAVI, A. 2013. PET/MR imaging: technical aspects and potential clinical applications. *Radiology,* 267, 26-44.

TSAO, M., XU, W., SAHGAL, A., TSAO, M., XU, W., SAHGAL, A., TSAO, M., XU, W., SAHGAL, A., TSAO, M., XU, W. & SAHGAL, A. 2012. A meta-analysis evaluating stereotactic radiosurgery, whole-brain radiotherapy, or both for patients presenting with a limited number of brain metastases : Meta-Analysis for Brain Metastases. *Cancer,* 118**,** 2486.

TSUCHIYA, K., FUJIKAWA, A., NAKAJIMA, M. & HONYA, K. 2005. Differentiation between solitary brain metastasis and high-grade glioma by diffusion tensor imaging. *British Journal of Radiology,* 78**,** 533-537.

TUOMINEN, V. J., RUOTOISTENMÄKI, S., VIITANEN, A., JUMPPANEN, M. & ISOLA, J. 2010. ImmunoRatio: a publicly available web application for quantitative image analysis of estrogen receptor (ER), progesterone receptor (PR), and Ki-67. *Breast Cancer Research : BCR,* 12**,** R56-R56.

URGER, E., DEBELLIS, M. D., HOOPER, S. R., WOOLLEY, D. P., CHEN, S. & PROVENZALE, J. M. 2013. Influence of analysis technique on measurement of diffusion tensor imaging parameters. *American Journal of Roentgenology,* 200**,** W510-W517.

VAN DER GRAAF, M. 2010. In vivo magnetic resonance spectroscopy: basic methodology and clinical applications. *Eur Biophys J,* 39, 527-40.

VANDENBROUCKE, R. E. & LIBERT, C. 2014. Is there new hope for therapeutic matrix metalloproteinase inhibition? *Nat Rev Drug Discov,* 13**,** 904-27.

WALTER, J., KUHN, S. A., WASCHKE, A., KALFF, R. & EWALD, C. 2011. Operative treatment of subcortical metastatic tumours in the central region. *J Neurooncol,* 103, 567-73.

WANG, G., PLATT-HIGGINS, A., CARROLL, J., DE SILVA RUDLAND, S., WINSTANLEY, J., BARRACLOUGH, R. & RUDLAND, P. S. 2006. Induction of metastasis by S100P in a rat mammary model and its association with poor survival of breast cancer patients. *Cancer Res,* 66**,** 1199-207.

WANG, S., KIM, S., CHAWLA, S., WOLF, R. L., ZHANG, W. G., O'ROURKE, D. M., JUDY, K. D., MELHEM, E. R. & POPTANI, H. 2009. Differentiation between glioblastomas and solitary brain metastases using diffusion tensor imaging. *Neuroimage,* 44**,** 653-60.

WEIDE, B., RICHTER, S., BUTTNER, P., LEITER, U., FORSCHNER, A., BAUER, J., HELD, L., EIGENTLER, T. K., MEIER, F. & GARBE, C. 2013. Serum S100B, lactate dehydrogenase and brain metastasis are prognostic factors in patients with distant melanoma metastasis and systemic therapy. *PLoS One,* 8**,** e81624.

WHITE, M. L., ZHANG, Y., YU, F. & JAFFAR KAZMI, S. A. 2011. Diffusion tensor MR imaging of cerebral gliomas: evaluating fractional anisotropy characteristics. *AJNR Am J Neuroradiol,* 32**,** 374-81.

WIDMANN, G., SCHULLIAN, P., ORTLER, M. & BALE, R. 2012. Frameless stereotactic targeting devices: technical features, targeting errors and clinical results. *Int J Med Robot,* 8**,** 1-16.

WILSON, J. B., YAMAMOTO, K., MARRIOTT, A. S., HUSSAIN, S., SUNG, P., HOATLIN, M. E., MATHEW, C. G., TAKATA, M., THOMPSON, L. H., KUPFER, G. M. & JONES, N. J. 2008. FANCG promotes formation of a newly identified protein complex containing BRCA2, FANCD2 and XRCC3. *Oncogene,* 27**,** 3641-52.

WINKLER, F. 2015. The brain metastatic niche. *J Mol Med (Berl),* 93**,** 1213-1220.

WINSTANLEY, J., PEARSON, M. & RUDLAND, P. 2013. Staining for metastasis inducing proteins in early breast cancer lesions. *Association of Breast Surgery Annual Conference.* Liverpool.

WODITSCHKA, S., EVANS, L., DUCHNOWSKA, R., REED, L. T., PALMIERI, D., QIAN, Y., BADVE, S., SLEDGE, G., JR., GRIL, B., ALADJEM, M. I., FU, H., FLORES, N. M., GOKMEN-POLAR, Y., BIERNAT, W., SZUTOWICZ-ZIELINSKA, E., MANDAT, T., TROJANOWSKI, T.,

OCH, W., CZARTORYSKA-ARLUKOWICZ, B., JASSEM, J., MITCHELL, J. B. & STEEG, P. S. 2014. DNA double-strand break repair genes and oxidative damage in brain metastasis of breast cancer. *J Natl Cancer Inst,* 106, dju145.

WONG, C. S., CHU, T. Y. C. & MA, J. K. F. 2010. Peri-tumoural magnetic resonance spectroscopy to differentiate solitary primary intra-axial high-grade glioma and brain metastasis: a pilot study. *J Hong Kong College Radiologists,* 13.

YAMAMOTO, M., SERIZAWA, T., SHUTO, T., AKABANE, A., HIGUCHI, Y., KAWAGISHI, J., YAMANAKA, K., SATO, Y., JOKURA, H., YOMO, S., NAGANO, O., KENAI, H., MORIKI, A., SUZUKI, S., KIDA, Y., IWAI, Y., HAYASHI, M., ONISHI, H., GONDO, M., SATO, M., AKIMITSU, T., KUBO, K., KIKUCHI, Y., SHIBASAKI, T., GOTO, T., TAKANASHI, M., MORI, Y., TAKAKURA, K., SAEKI, N., KUNIEDA, E., AOYAMA, H., MOMOSHIMA, S. & TSUCHIYA, K. 2014. Stereotactic radiosurgery for patients with multiple brain metastases (JLGK0901): a multi-institutional prospective observational study. *Lancet Oncol,* 15**,** 387-95.

YOKOI, K., KAMIYA, N., MATSUGUMA, H., MACHIDA, S., HIROSE, T., MORI, K. & TOMINAGA, K. 1999. Detection of brain metastasis in potentially operable non-small cell lung cancer: a comparison of CT and MRI. *Chest,* 115, 714-19.

YOO, H., KIM, Y. Z., NAM, B. H., SHIN, S. H., YANG, H. S., LEE, J. S., ZO, J. I. & LEE, S. H. 2009. Reduced local recurrence of a single brain metastasis through microscopic total resection. *J Neurosurg,* 110**,** 730-6.

YUH, W. T. C., TALI, E. T., NGUYEN, H. D., SIMONSON, T. M., MAYR, N. A. & FISHER, D. J. 1995. The effect of contrast dose, imaging time, and lesion size in the MR detection of intracerebral metastasis. *Am J Neuroradiol,* 16.

YUSHKEVICH, P. A., PIVEN, J., HAZLETT, H. C., SMITH, R. G., HO, S., GEE, J. C. & GERIG, G. 2006. User-guided 3D active contour segmentation of anatomical structures: significantly improved efficiency and reliability. *Neuroimage,* 31**,** 1116-28.

ZAKARIA, R., DAS, K., BHOJAK, M., RADON, M., SLUMING, V., WALKER, C. & JENKINSON, M. D. 2014a. The reliability of routine clinical post-processing software in assessing potential diffusion-weighted MRI "biomarkers" in brain metastases. *Magn Reson Imaging,* 32**,** 291-6.

ZAKARIA, R., DAS, K., BHOJAK, M., RADON, M., WALKER, C. & JENKINSON, M. D. 2014b. The role of magnetic resonance imaging in the management of brain metastases: diagnosis to prognosis. *Cancer Imaging,* 14**,** 8.

ZAKARIA, R., DAS, K., RADON, M., BHOJAK, M., RUDLAND, P. R., SLUMING, V. & JENKINSON, M. D. 2014c. Diffusion-weighted MRI characteristics of the cerebral metastasis to brain boundary predicts patient outcomes. *BMC Med Imaging,* 14**,** 26.

ZAKARIA, R. & JENKINSON, M. D. 2014d. Using ADC maps with structural scans to improve intraoperative biopsy specimens in brain metastases. *Neuroradiol J,* 27**,** 422-4.

ZAKARIA, R. & JENKINSON, M. D. 2015. Selecting brain metastasis patients for neurosurgery: what are we getting wrong? *World Federation of Neurosurgical Societies.* Rome.